MASS. INST. OF TECHNOLOGY
JUN 23 1960
LIBRARY

OPTICAL AND ELECTRICAL PROPERTIES OF THIN BISMUTH DEPOSITS

by

John Piper

B.S., Trinity College

(1956)

Submitted in Partial Fulfillment of

the Requirements for the Degree of

DOCTOR OF PHILOSOPHY

at the

Massachusetts Institute of Technology

(1960)

Signature of author _____
Department of Chemistry, May 23, 1960

Certified by _____
Thesis Supervisor

Accepted by _____
Chairman, Departmental Committee on
Graduate Students

OPTICAL AND ELECTRICAL PROPERTIES OF THIN BISMUTH DEPOSITS

by

John Piper

Submitted to the Department of Chemistry

May 23, 1960

in partial fulfillment of the requirements for the

degree of Doctor of Philosophy

ABSTRACT

The infrared reflectance and transmittance of a series of thin vacuum deposits of bismuth were measured throughout the region 1.5 to 150 microns. The thicknesses of the deposits studied varied from 200 to 9000 Å. Hall effect measurements were also made on the same samples.

The experimental results were treated according to the band model of Abeles and Meiboom (2). The results indicate that the deposits were oriented with the (111) plane parallel to the substrate. The deposits were found from electron micrographs to be made up of crystallites approximately 2000 Å in diameter.

A classical theory was used to obtain an isotropic relaxation time for the electrons which corresponds to a value of 1.6×10^{-13} sec. for single crystals at room temperature. The ratio of conduction due to electrons to that due to holes was derived from reflection and transmission measurements for the deposits at room temperature and found to be 3.3. Effective masses of 0.0079 and 0.5 times the mass of the free electron were obtained for the conduction electrons in the plane perpendicular to the trigonal axis. The spread of values for the effective masses from sample to sample was, however, quite large, and the effective mass analysis was based on the assumption that the relaxation time for the holes is more than twice that for the electrons.

Deposits of less than 1000 Å thickness showed the effects of surface trapping which partially masked the free electron spectrum.

Thesis Supervisor: _____

Title: Associate Professor of Physical Chemistry

This doctoral thesis

has been examined by a committee

of the Department of Chemistry

as follows:

James A. Beattie, Chairman _____

Louis Harris, Research Supervisor _____

Frederick D. Greene _____

Lockhart B. Rogers _____

Walter H. Stockmayer _____

ACKNOWLEDGEMENTS

The author would like to thank Professor L. Harris for his advice and encouragement throughout the course of this investigation. This research has benefited from many discussions with Professor Harris.

The author is particularly grateful to Mr. E. R. Washwell who deposited the bismuth samples and carried out the chemical analyses reported here. He is also indebted to Mr. C. D'Agostino for preparing preliminary samples and cooperating in the deposited contact problem.

Many members of the Institute have materially aided in this research. The author is most grateful to Professor A. L. Loeb for making the optical computer program available and for his continued interest in this problem.

Dr. K. E. Hag contributed immeasurably to the early design and construction of the far infrared spectrometer.

Dr. A. J. Hodge took the electron diffraction and microscope photographs and Professor D. P. Shoemaker kindly made his x-ray equipment available to the author.

The M.I.T. Magnet Laboratory made proton resonance equipment available for calibration of the fluxmeter.

Computer time was provided by the M.I.T. Computation Center.

The author very much appreciates the personal assistance he has received from the Department of Chemistry in the form of Research and Teaching Assistantships, from the Union Carbide Corporation through the award of a Union Carbide Corporation Fellowship 1958-59, and from the National Science Foundation through the award of a Summer Fellowship 1959.

TABLE OF CONTENTS

Page

I. Introduction 1

II. Outline of Problem..... 4

III. Experimental Properties of Some Bismuth Deposits 7

A. Preparation of Samples..... 7
i Aluminum Oxide Substrates..... 7
ii Bismuth Deposits 8

B. The Physical Structure of the Deposits and Substrates.... 10
i Aluminum Oxide Substrates 10
ii Evaporated Bismuth Deposits..... 10
iii Thickness of the Bismuth Deposits..... 15

C. Galvanomagnetic Properties of the Bismuth Deposits..... 15
i Conductivity 15
ii Hall Coefficient 18
iii Magnetoresistance..... 24

D. Infrared Properties of the Bismuth Deposits 25
i Far Infrared Transmission and Reflection..... 25
ii Near Infrared Transmission and Reflection 28

IV. Application of Maxwell's Equations to a Thin Film System 31

A. Mathematical Treatment 31

B. Validity of Assumptions Introduced into Treatment 34

C. Anomalous Skin Effect 36

V. Theoretical Model for the Electronic Structure of the Bismuth Deposits.. 38

A. Orientation in Bismuth Deposits..... 38

B. Band Structure of the Bismuth Crystal..... 42

C. Conductivity of the Single Crystal in the (111) Plane.... 45

D. An Electronic Model for the Bismuth Deposits 48

VI. Application of the Oriented Film Theory to the Experimental Results... 50

TABLE OF CONTENTS (Cont'd)

		Page
VII.	Discussion	
	A. Some Remarks Concerning the Experimental Measurements....	60
	B. Experimental Properties of the Deposits.....	60
	C. Near Infrared Optical Characteristics of the Deposits ...	62
	D. Free Electron Effects	64
	E. Failures of the Theory	69
	F. Optical Characteristics of Thin Bismuth Deposits	71
VIII.	Suggestions for Future Work	72
	Appendices	
I.	Geometry of Samples and Methods of Mounting	74
II.	Details of the Preparation of the Bismuth Deposits	76
III.	Infrared Properties of Aluminum Oxide Films	78
IV.	Galvanomagnetic Measurements	82
	A. Hall Effect Measurements	82
	B. Resistance Measurements	87
V.	Some Magnetoresistance Measurements on Bismuth Films	88
VI.	Far Infrared Instrumentation and Measurements	89
	A. Design and Construction of the Spectrometer	89
	B. Operating Conditions	90
	C. Method of Making Measurements	91
VII.	Far Infrared Reflection and Transmission of Some Samples	96
VIII.	Near Infrared Spectrometer	100
IX.	Near Infrared Reflection and Transmission of Some Samples ...	101
X.	Solutions of Boltzmann's Equation	103
XI.	The Conductivity Matrix	105

TABLE OF CONTENTS (Cont'd)

Page

XII. The Hall Coefficient 107

XIII. Optical Constants of Samples 111

XIV. Calculation 122

XV. Parameters used in Figure VIIc 126

Bibliography 127

Biographical Note 131

LIST OF TABLES

Page

1. Conductivity of the Bismuth Deposits..... 17
2. Hall Coefficients of the Bismuth Deposits..... 20
3. Ratio of Reflectances from Deposit and Substrate Sides..... 25
4. Hall Coefficients of Single Crystals..... 39
5. Hall Coefficients of Deposits Compared to Single Crystals... 41
6. Conductivity Curve Fit Parameters..... 55
7. Relaxation Times, Individual Agreement..... 56
8. Transport Parameters, Individual Agreement..... 57
9. Relaxation Times..... 58
10. Increased Optical Conductivity of Very Thin Deposits..... 69
11. Optical Constants of Aluminum Oxide Films..... 80
12. Far Infrared Spectrometer - Operating Conditions..... 92

LIST OF FIGURES

Page

I. a) X-Ray Diffraction Photograph of Bismuth Deposit..... 12
b) X-Ray Diffraction Photograph of Bismuth Powder..... 12

II. a) Electron Diffraction Photograph of Bismuth Deposit..... 14
b) Electron Microscope Photograph of Bismuth Deposit..... 14

III. Field Dependence of the Hall Coefficient..... 21

IV. Far Infrared Reflectance and Transmittance of Some Bismuth Deposits..... 26

V. Near Infrared Reflectance and Transmittance of Some Bismuth Deposits..... 29

VI. Band Structure of Bismuth..... 43

VII. Conductivity as a Function of Wavelength

a) Samples: A, B, C, D..... 52
b) Samples: J, K..... 53
c) Samples: H, L, N, Q..... 54

VIII. Geometry of Samples and Holders..... 75

IX. Transmission and Reflection of Aluminum Oxide Films..... 79

X. Hall Voltage Measuring Circuit..... 86

XI. Optical Path, Far Infrared Spectrometer..... 95

XII. Conductivity as a Function of Frequency - Sample A.....124

XIII. Resistivity as a Function of Frequency - Sample A.....125

I. INTRODUCTION

While the study of the properties of thin metallic deposits is of considerable importance in the practical field of electronic device design, thin films also provide a suitable medium for the study of some of the fundamental characteristics of the parent material.

In the case of bismuth a considerable number of investigations have been made of the electronic properties of the bulk state. The galvanomagnetic effects have been studied (1-6) in some detail and considerable work has been performed on the oscillatory and resonant properties of the magneto-resistance (7,8,9), magnetic susceptibility (10,11), and cyclotron absorption (12-18). These experiments have resulted in the development (19,20) of an experimentally consistent band model for the material. The direct calculation of the band structure from quantum theory is extremely complicated, but the little work (21) that has been performed in this area is consistent with the experimental model.

The above studies permit the evaluation of the number and effective masses of the carriers and their mobilities - the ratio of the collision or relaxation time to the effective mass. There remains some doubt as to the magnitudes of the former and considerable doubt concerning the latter. These techniques do not, with the exception of cyclotron resonance line-broadening, allow the relaxation time to be observed directly.

The relaxation time may, however, be observed through the attenuation of the electrical conductivity at very high frequencies. At room temperature this attenuation occurs at frequencies in the far infrared part of the spectrum, and the conductivity may be obtained as a function of frequency by solving Maxwell's equations for electromagnetic radiation incident and within the metal. Since no simplifying assumptions such as those entailed in the Hagen-Rubens relation (22) are valid, it is generally necessary to experimentally determine two optical characteristics of the metal. These may be the reflectances of the metal surface for two directions of polarization, or the reflectance and transmittance of unpolarized light. Since the problem of obtaining sufficient monochromatic radiation to make quantitative measurements is considerable, the polarization of far infrared radiation is unfeasible. In order to measure a transmittance as well as a reflectance it is necessary to use very thin samples, hence the use of thin deposits.

Some optical measurements of the type described in this thesis were carried out in 1934 by Woltersdorff (23). However, two developments of the past decade permit measurements of this type to be quantitatively significant. The first is the development of the far infrared grating spectrometer (24-26) which, with sufficient filtering, may be used to make quantitative measurements at any frequency interval rather than a few <u>reststrahlen</u> wavelengths.

The second development is the use of the high speed digital computer as a means of data processing (27). While the solutions to Maxwell's equations for the optical problem are complicated and may only be solved by successive approximations, the computer is effectively capable

of generating complete conductivity curves, the uncertainty of which is determined only by the uncertainty in the original data.

II. OUTLINE OF THE PROBLEM

The specific problem that is examined in this thesis consists of essentially two parts: a) the determination of the relaxation time for the conduction electrons in a series of thin bismuth deposits, b) an investigation of the relationship between the properties of these deposits and those of single crystals of bismuth.

A relaxation time τ for electrons in a conducting medium may be defined on the basis of a hard sphere kinetic model as one half the mean time between collisions. In bismuth it has been reported to be $\sim 10^{-14}$ sec (49) at room temperature which corresponds to a period of oscillation for electromagnetic radiation of 20 microns wavelength. The contribution of the unbound electrons to the optical constants for a conductor is dependent (50) on a phase factor $(1 + 2\pi i\nu\tau)$, where ν is the frequency of the radiation.

The optical properties of the bismuth deposits may, thus, be expected to be strongly dependent on frequency in the far infrared region of the spectrum, and an analysis of the transmission and reflection spectra should yield a relaxation time for the deposits.

The evaluation of the relaxation time by this method introduces two experimental problems: the selection of suitable infrared transparent substrate material for the deposits, and the development of suitable instrumentation. In this case it was necessary to design and construct a far infrared spectrometer suitable for quantitative measurements.

In order to relate the relaxation time and other thin film parameters to the properties of single crystals, it is necessary to examine the relationship between the thin deposits and the single crystals. An investigation of this relationship may be carried out at two levels, that of the microscopic and that of the macroscopic properties.

Since the structure of the bismuth crystal is well-known a study of the bismuth deposits by x-ray and electron diffraction, and with an electron microscope was undertaken.

The galvanomagnetic effects which have been determined in single crystals (2,3), are particularly suitable as a means of studying the macroscopic relationship between the deposits and single crystals. The Hall coefficient in bismuth crystals is very sensitive to the orientation of the crystal and the conductivity is directly proportional to the relaxation time. Determination of these properties also allows the evaluation of some band structure parameters when taken in conjunction with the optical measurements and an applicable theory.

The measurement of these effects introduces the problem of making electrical contact to the deposits, and, in the case of the Hall effect, the measurement of a small transverse potential due to a longitudinal current and a perpendicular magnetic field.

Since the properties of thin deposits in general are dependent on the substrate and evaporation conditions used, it is necessary to make the different types of measurements on the same samples and to reproduce the evaporating conditions as closely as possible during the preparation of each member of a series.

The properties of films also change with thickness requiring measurements to be made on a series of deposits of different thicknesses. The range of thicknesses to be studied in the present case is limited by a requirement of a measurable infrared transmittance for the thickest films and by the thinnest deposits not being related to the single crystal.

Since the relaxation time decreases with increasing temperature, measurements at room temperature are completely adequate. In this investigation all temperature dependent measurements were made at, or corrected to, 294°K.

III. EXPERIMENTAL PROPERTIES OF SOME BISMUTH DEPOSITS

A. Preparation of Samples.

i Aluminum Oxide Substrates.

The choice of a substrate material to be used in this investigation was severely limited by mathematical as well as experimental considerations. The mechanical properties of the substrate had to be virtually independent of temperature at least to above 200°C so that a reasonably high annealing temperature could be used for the bismuth deposits. The substrate was required to retain a high degree of flatness to permit optical reflection measurements.

The extreme mathematical difficulties of treating optical data on films with absorbing substrates, limited the choice with a requirement of virtually complete transparency.

Most common substrates such as polyethylene, cellulose nitrate, glass, quartz, and sodium chloride were disqualified by preliminary optical measurements and bismuth depositions.

Thin aluminum oxide films prepared by the method of Harris (30) were found to be practically transparent in the far infrared (see Appendix III). They also had good heat stability and could be fairly easily made. Their main disadvantage was an absorption peak that reached a maximum at 15 microns wavelength.

The method of preparation described by Harris was used without alteration to prepare the substrates used in this investigation. The method consists of anodizing household aluminum foil in an ammonium citrate solution. The aluminum base is then dissolved away with hydrochloric acid leaving the suspended oxide film. The thickness of the oxide film is controlled by the anodizing voltage used. With the exception of one of the electron diffraction samples, 50 volt (corresponding to approximately 700 Å) films were used throughout. This thickness was determined by a compromise between a minimum infrared absorption and sufficient mechanical strength to survive a prolonged series of measurements.

The aluminum oxide substrates were mounted on glass rings and baked at 140-150° C for several days. Infrared reflection and transmission curves were obtained on each substrate as a quality control.

To permit electrical measurements, silver electrodes and probes were vacuum deposited on to the substrates. The geometry of the samples is shown in Appendix I. The deposited silver was approximately 1 micron thick and had a resistance of $\sim$ 0.02 ohms per square.

ii Bismuth Deposits

The geometry of the bismuth deposits was determined by the size of the focussed image in the far infrared spectrometer. The desire for the greatest beam intensity while maintaining a small angle of incidence precluded any optical condensing of the beam.

An effective sample size of 1.0 x 1.9 cm plus a 0.15 cm overlap on to each end electrode was used.

The bismuth with less than 10^{-4}% impurity * was vacuum deposited from an electron bombarded tantalum source through a mask on to the substrate. The details of the vacuum deposition are given in Appendix II. One deposition (preparation of Sample A) was carried out with "analytical" (10^{-2}% impurity) bismuth in order to observe any effects on the electrical properties due to the impurities.

After remaining without external heating during deposition, the film-substrate systems were annealed for several hours near 180°C before being removed from the vacuum.

The source to substrate distance (24 cm) in the evaporator was sufficient so that non-uniformity of the deposits due to geometry was negligible.

---

* According to J. E. Aubrey (16) there are approximately 10^{-4} conduction electrons per atom in bismuth. V. Heine (19) claims that acceptor impurities such as [redacted] Pb, Sn contribute in the order of one hole per atom.

B. The Physical Structure of the Deposits and Substrates.

i Aluminum Oxide Substrates

The aluminum oxide films appeared clear and colorless to the naked eye. A slight "grain" was visible with the aid of an optical microscope. The films gave no x-ray diffraction patterns indicating an amorphous state in agreement with other investigations (31,32) on similarly prepared films.

Hass and Kehler (31) report no structure to electron diffraction patterns: a condition that did not change on heating the aluminum oxide up to 500°C. Hass (32) mentions a transition to γ Al_2O_3 at 680°C.

Aluminum oxide films prepared by anodizing rolled aluminum foil have been reported to show no structure under an electron microscope unless the films are shadowed (33). Such films show a "grain" structure which is presumed to be due to the rolling of the parent foil.

ii Evaporated Bismuth Deposits

The bismuth deposits were bright with sharply defined edges. The aluminum oxide "grain" appeared on the bismuth as fine lines on the surface. This appearance was independent of deposit thickness. No relationship between the orientation of the "grain" and other properties of the deposits was observed. The resistances of deposits on aluminum oxide were equal to or less than similar deposits prepared adjacently on glass.

The outlines of the silver electrodes and probes were clearly visible on the undersides of the films. These outlines remained sharp and no visible indications of diffusion were observed on the present samples. Some other samples prepared by a different method showed signs of bismuth diffusion into the silver. The contact resistance between silver and bismuth

was found to be independent of the order in which the metals were evaporated *. The actual contact resistance was not determined but was shown experimentally to be small compared to 0.1 ohm.

The bismuth deposits were examined with x-ray and electron diffraction and with an electron microscope. Figure Ia shows an x-ray diffraction photograph of a 0.7 micron deposit (Sample C). Other films - from 0.1 to 1 micron thickness - showed the same general characteristics. Figure Ib is a corresponding photograph of bismuth powder on a fibre. The photographs were taken with a cylindrical camera with the perpendicular to the bismuth film oscillating between $\pm 7.5^{\circ}$ to the x-ray beam. The powder sample was rotated about the cylindrical axis. Chromium α radiation was used.

The powder and film photographs may both be indexed on the basis of the symmetry and bond lengths of bismuth crystals (34,35).

$\bar{3}^{2}/m$ symmetry, rhombohedral axes: $a_o = 4.746\text{Å}$

$\alpha = 57^{\circ}\ 14'$, two atoms per unit cell.

The uniformity of the circles in Figure Ia indicates no orientation of the crystallites in the plane of the substrate on the macro-scale of the x-ray beam ($\sim$ 0.5mm. diameter). The presence of all of the powder lines (with the possible exception of those from the (111) plane) indicates that the crystals of all orientations are present in the films. Note: the Chromium β lines also appear faintly in both photographs due to the long (48 hour) exposure time.

---

* According to Mr. C. D'Agostino.

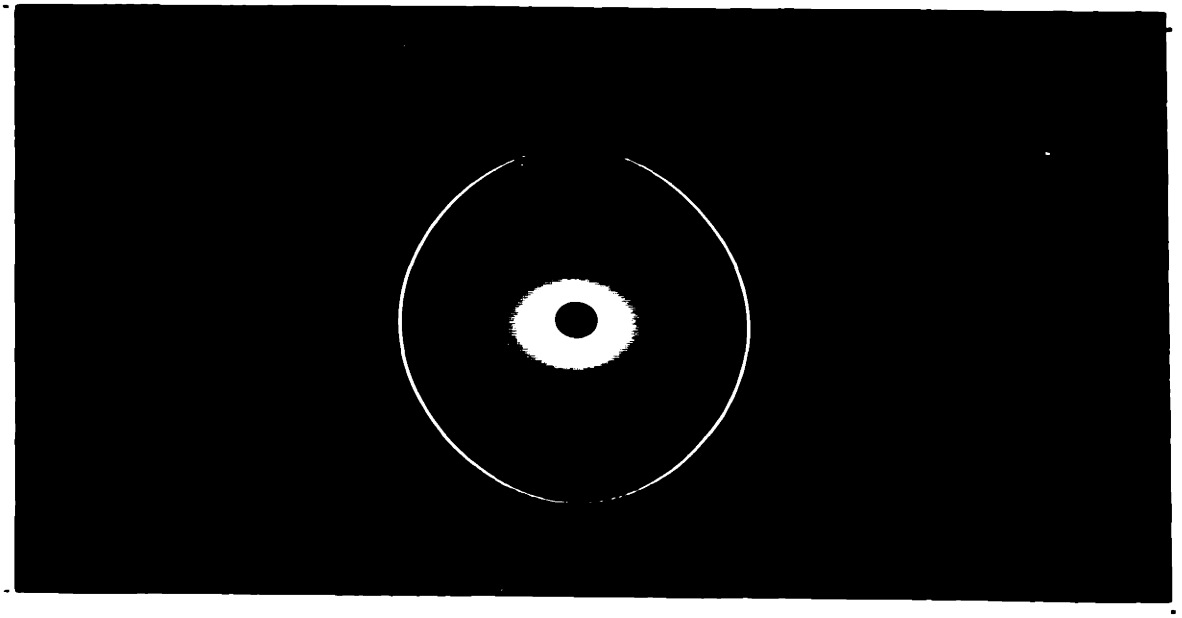

Figure I(a) X-Ray Diffraction Photograph of 7000 A Deposit

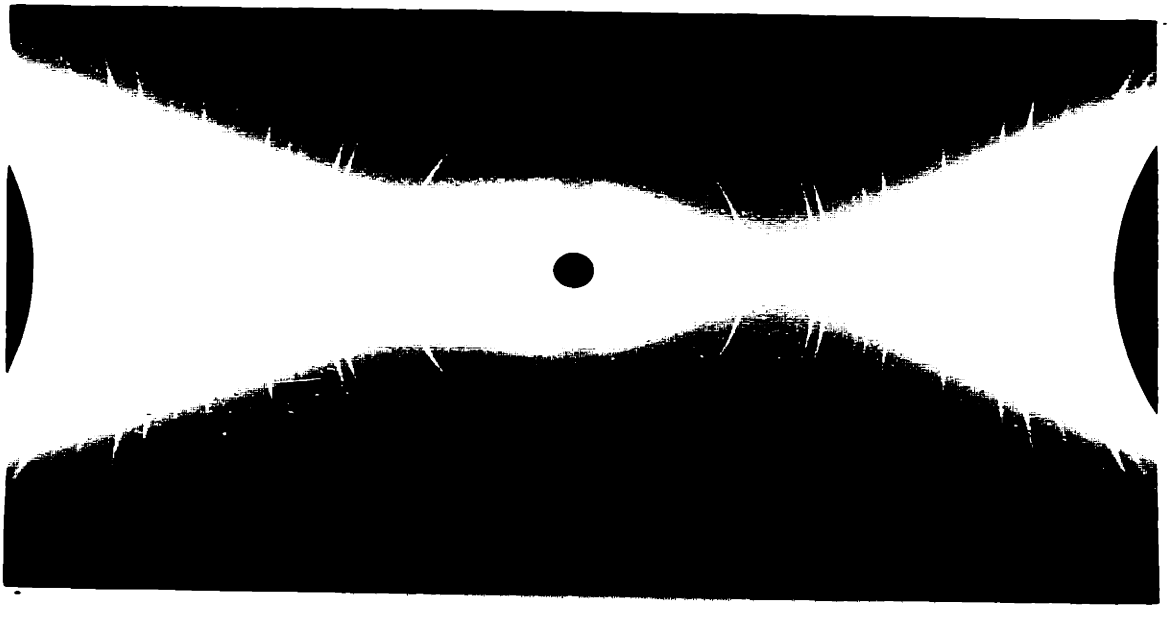

Figure I(b) X-Ray Diffraction Photograph of Bismuth Powder

A qualitative analysis of the intensities of the various lines is difficult due to the differences in geometry of the two samples and yields no unambiguous results concerning possible orientation in the plane perpendicular to the substrate. The very intense line in the photograph of the vacuum deposited bismuth corresponds to the (110) plane. Reflections from this plane may occur for orientations of the x-ray beam which make an angle greater than 5° with respect to the trigonal axis of the crystals. The intensity of this line is due at least in part to the small path length in bismuth traversed by the diffracted beam.

Figure IIa is an electron diffraction photograph of a 300 Å bismuth film on an approximately 200 Å Al_2O_3 substrate. Other than the substrate thickness, the method of preparation was identical to that described in Appendix II. The noticeable arcing of the diffraction circles indicates a degree of orientation in the plane of the substrate on the microscopic level of an electron diffraction probe ($\sim$10 micron diameter).

In view of the ambiguity of the x-ray intensity data, no interpretation of the intensities of this or other electron diffraction photographs was attempted. We have no reason to expect more information than that available from the x-ray work.

Figure IIb is an electron microscope photograph of the same bismuth film at 10,000 times magnification. The diameters of the crystallites range from 1000 to 4000 Å; most are about 2000 Å in diameter. A very slight texture of almost horizontal lines is visible. This appears to be due to the rolling texture of the substrate. It was also observed on a 600 Å bismuth film, but not on a bismuth film on a cellulose nitrate substrate. Other photographs taken indicated that the arcing in the diffraction patterns was not dependent on the presence of the rolling texture.

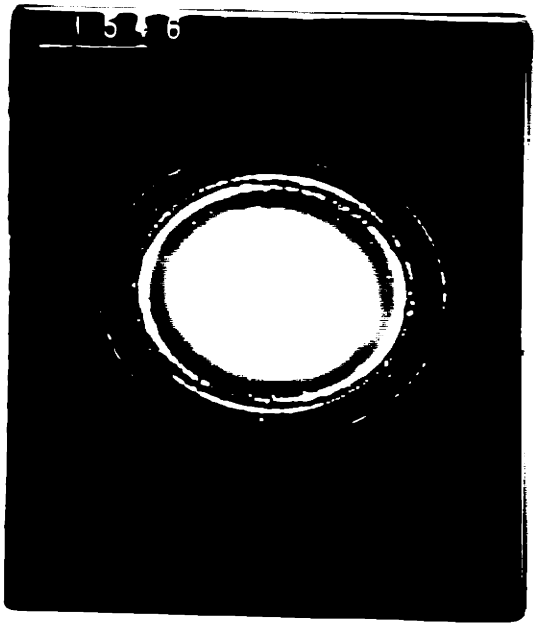

Figure II(a) Electron Diffraction Photograph 300 A Bismuth Film

Figure II(b) Electron Microscope Photograph 300 A Bismuth Film

10,000 X Magnification.

Although no systematic study of the effect of film thickness on crystallite size was made, no marked dependence was observed.

The electron microscope and diffraction photographs were taken with 80 kilovolt electrons and a current of approximately 10 microamps. No ordering or annealing of the films on aluminum oxide was observed when new sections of film were introduced into the beam, Such ordering was noticed, however, on a deposit with a cellulose nitrate substrate. The process took place in 1 or 2 seconds and appeared to leave the crystallite size unaltered.

iii Thickness of the Bismuth Deposits

The quantity of bismuth present in each sample was determined by a microchemical photometric technique. The method used employed dithizone as an extracting agent and was adapted from the method described by D. Hubbard (36). The total bismuth content of the films ranged from 60 to 2000 micrograms and was determined to better than ± 3%. A nominal thickness was calculated from the total bismuth content with the assumption of bulk density. Since the films were composed of crystallites with bulk structure and no obvious gaps were observed in the electron micrographs, this nominal thickness is probably accurate to within the meaning of thickness for a thin deposit.

C. Galvanomagnetic Properties of the Bismuth Deposits

i Conductivity.

Resistance measurements were made on the bismuth samples by mounting the films in a holder constructed with silver-tipped springs which made contact to the deposited silver electrodes on the substrate as described in Appendix I.

Two contacts were made to each end electrode and a potentiometric method was used to determine the resistance. Direct current was employed and the potentials across the film and across a resistance box in series were determined with a Leeds and Northrup microvolt amplifier. The details are given in Appendix IV. Primary currents which ranged from 4 to 100 microamps according to sample thickness were employed.

The conductivities and thicknesses of the series of films are listed in Table I.

TABLE 1 Conductivity of the Bismuth Deposits

Sample	Thickness	Conductivity
O	9000 Å	44.2×10^4 (ohm-meter)$^{-1}$
C	7400	32.5
A	6400	25.3
B	5300	30.3
K	4200	32.8
D	3800	34.5
J	1660	27.0
N	570	18.7
H	450	22.2
Q	347	12.3
L	220	15.7

The conductivity of a single crystal is 83.4×10^4 in the plane perpendicular to the trigonal axis and 66.7×10^4 (ohm - meter)$^{-1}$ in the direction of the axis (2) .

Experiments showed that the measured film conductivities were independent of the choice of current and potential probes and independent of the current over a range greater than a factor of 10 more than the currents used to measure the conductivity.

Early measurements on other samples showed no frequency dependence of the conductivity from d.c. to 16 kilocycles.

This method of resistance measurement fails to take the silver deposit to bismuth deposit resistance into account. However, as mentioned earlier, this was shown experimentally to be small compared to 0.1 ohm while the film resistances varied from 4.6 to 530 ohms. The temperature coefficient of resistance was negative and very small, $\sim 10^{-3}$ per degree, for some representative samples.

ii Hall Coefficient.

The Hall coefficient was determined as a function of magnetic field from approximately 1000 to 7500 gauss for each sample. Primary currents of between 50 and 1000 microamps depending on sample thickness were used. These values were sufficiently small so that the Hall voltage was a linear function of the current and no detectable heating occurred. The Hall voltages generated by these currents varied from 5 to 100 microvolts in accordance with the magnetic field strength.

The d.c. primary current was measured by determining the potential drop across a series resistor. The transverse Hall voltage caused by the perpendicular magnetic field was measured with a high impedance d.c.microvolt amplifier which permitted a minimum of 50 microvolts to be displayed full scale on a strip recorder.

A rotating-coil fluxmeter determined the magnetic field. The details of the method of measurement are given in Appendix IV.

The Hall coefficient R_H is defined as a proportionality constant.

$$R_H = \frac{V_y a}{I_x B_z} \qquad (1)$$

where

Ix is the primary current,

B_z the magnetic field in the medium,

V_y the voltage generated across an infinitely long rectangular slab of thickness a. The subscripts refer to the conventional (37) coordinate frame. In the case of bismuth the magnetic susceptibility is so small (10) that the permeability is effectively unity. In MKS units, then, the magnetic flux in the deposits is equal to the measured field in air. MKS units are used in the calculations presented here, however other units are used occasionally for convenience in the discussion.

Since the ratio of the length to width of the present samples was only 1.85, the measured Hall voltage had to be corrected for shorting by the end electrodes. The table and graph given by Isenberg (38) were used to make this correction. A proportional correction was also made for the intrusion of the Hall probes within the boundary of the film. The Hall coefficient of silver is approximately one fortieth of that of bismuth (39) so possible corrections due to the Hall effect in the electrodes were considered negligibl

Table 2 lists the Hall coefficients extrapolated to zero magnet field. The experimental field dependence of the Hall coefficient of all of the sample is plotted in Figure III. The values are normalized by dividing by the extrapolated zero field value in each case.

The Hall coefficients were positive in all cases except for Sample 0. All samples showed a decrease in the magnitude of the Hall coefficient with increasing magnetic field. This change increased with increasing thickness to give an 8% decrease for the thickest samples at 7500 gauss. Sample 0 showed a 30% decrease over the same range of magnetic field.

TABLE 2 Hall Coefficients of the Bismuth Deposits

Sample	Thickness	Hall Coefficient
U	9000 Å	-1.52×10^{-8} MKS
C	7400	5.40
A	6400	3.83
B	5300	4.82
K	4200	3.78
D	3800	4.21
J	1660	5.82
N	570	7.33
H	450	6.33
Q	347	9.09
L	220	7.99

Abeles and Meiboom (2) give the values for the zero field Hall coefficient in single crystals as 4.5×10^{-8} MKS for the magnetic field parallel to the trigonal axis and -135×10^{-8} MKS for the field perpendicular to the trigonal axis.

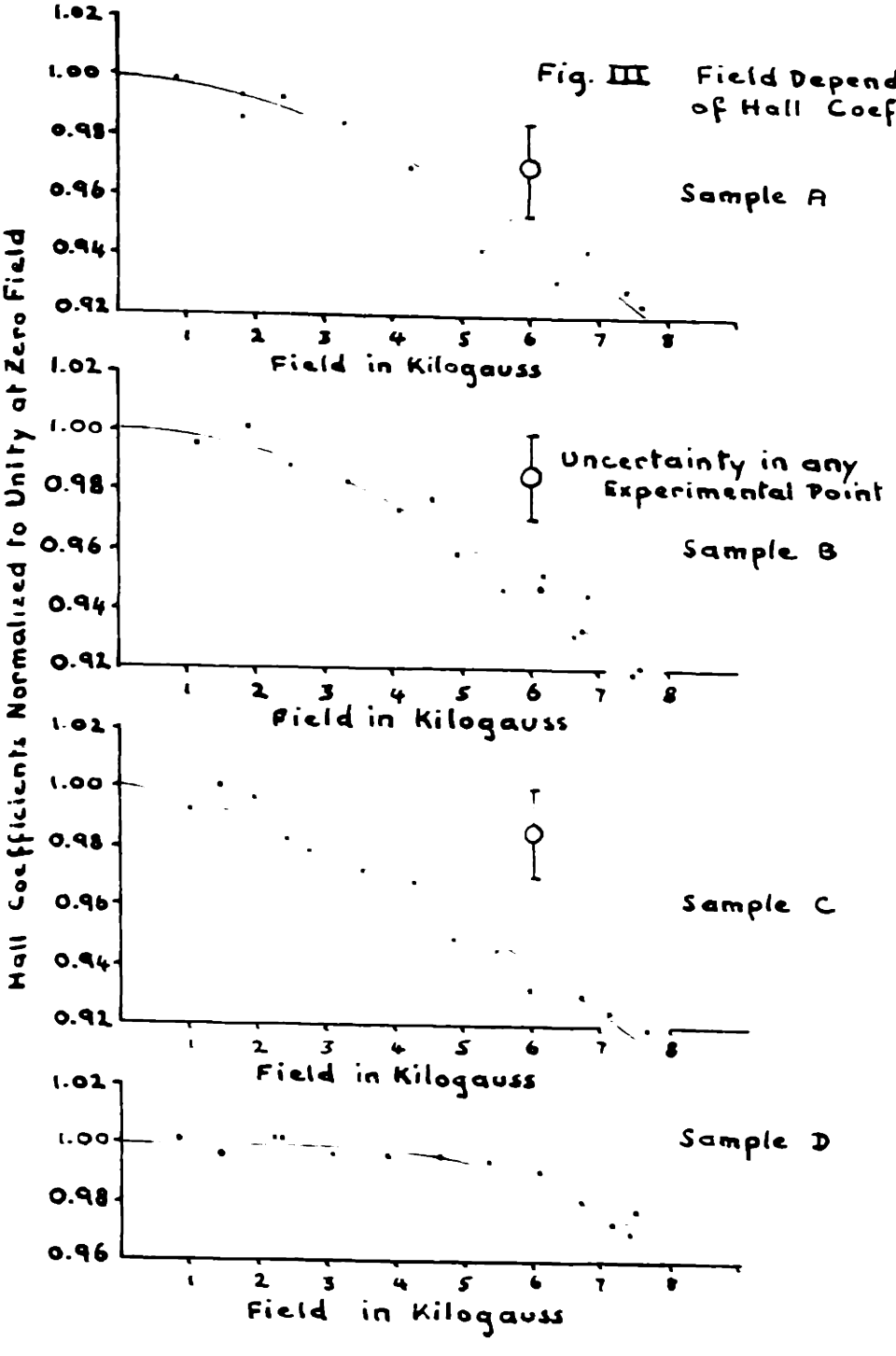

Fig. III Field Dependence of Hall Coefficient

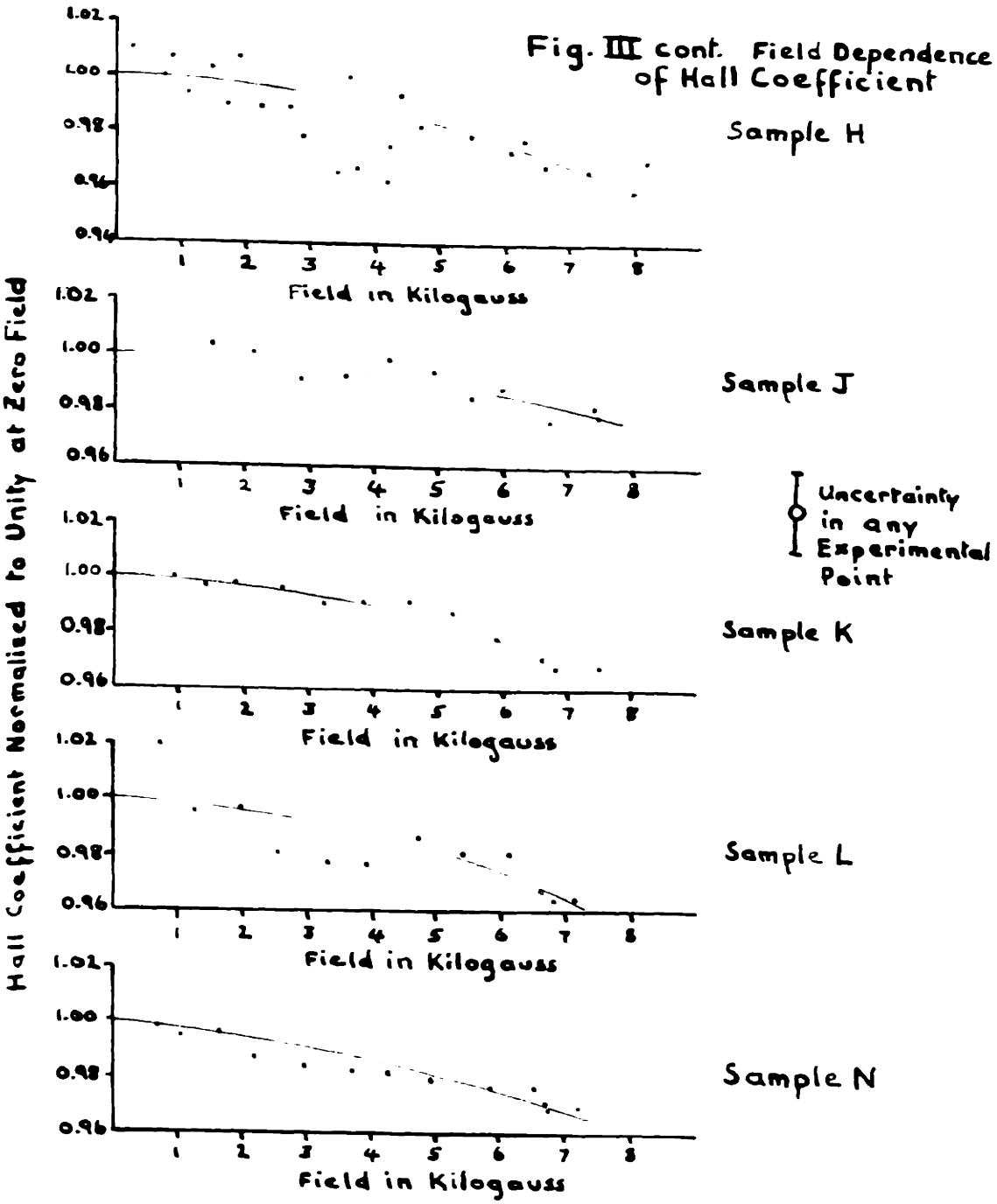
Fig. III cont. Field Dependence of Hall Coefficient
Sample H
Sample J
Sample K
Sample L
Sample N
Uncertainty in any Experimental Point
Hall Coefficient Normalised to Unity at Zero Field
Field in Kilogauss
1.02
1.00
0.98
0.96
1
2
3
4
5
6
7
8

Fig. III cont.

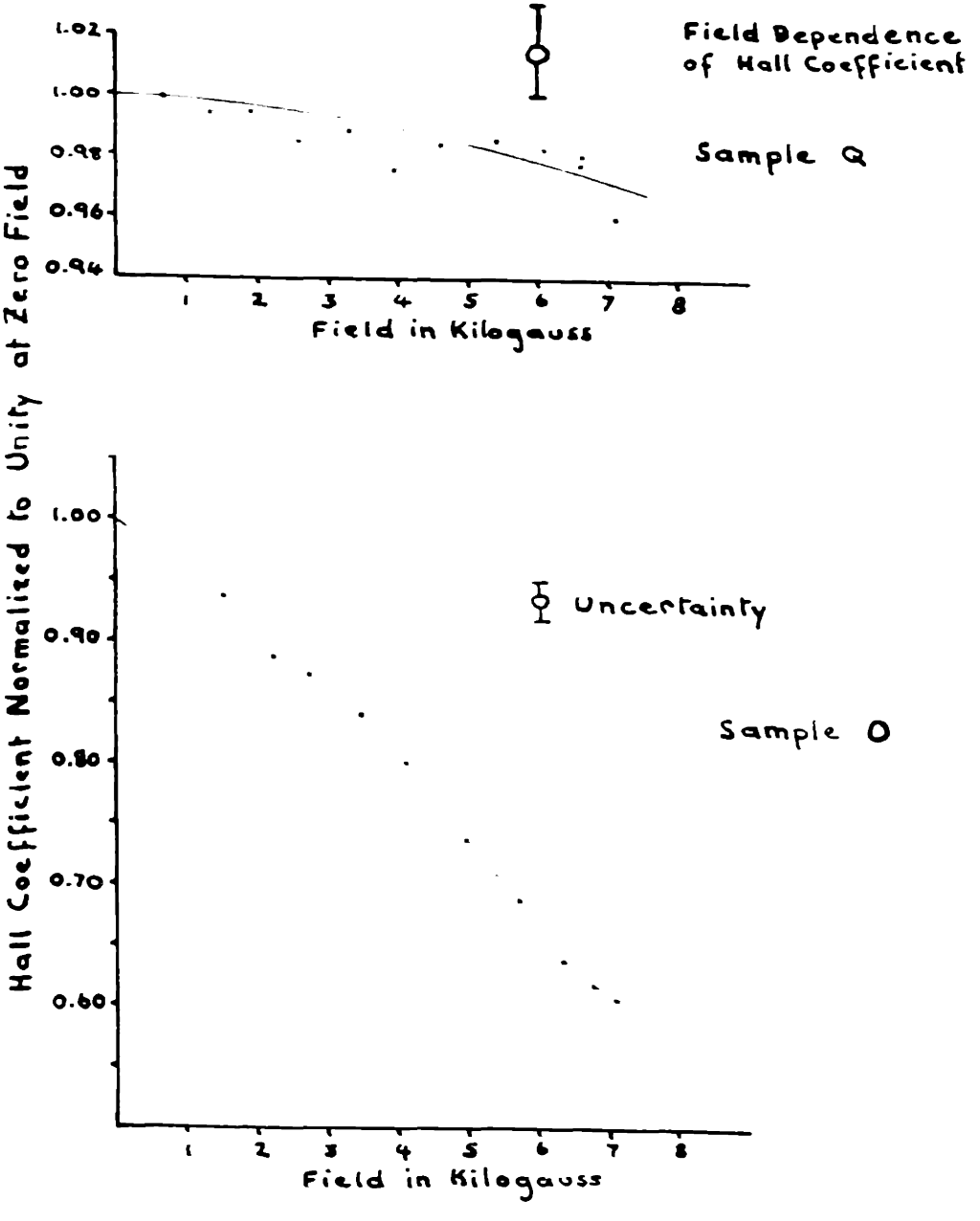
Field Dependence of Hall Coefficient
Sample Q
1.02
1.00
0.98
0.96
0.94
1
2
3
4
5
6
7
8
Field in Kilogauss
Hall Coefficient Normalized to Unity at Zero Field
Uncertainty
Sample O
1.00
0.90
0.80
0.70
0.60
1
2
3
4
5
6
7
8
Field in Kilogauss

iii Magnetoresistance.

A few magnetoresistance measurements were made on bismuth films with the magnetic field perpendicular and parallel to the substrates. Due to the limitation of a small magnet pole gap, these measurements were made on thin glass slides some of which were covered with aluminum oxide film.

An approximately two fold difference was observed in the magnetoresistance for the two orientations of the magnetic field. This result qualitatively corresponds with observations of Gross (51), Colombani and Huet (29), and Leverton and Dekker (52).

Since the samples used were not of the same quality or type as those whose other measurements are reported here, and the results are subject to a variety of interpretations, the data are reported in Appendix V without further comment.

D. Infrared Properties of the Bismuth Deposits

i Far Infrared Transmission and Reflection.

Infrared transmission and reflection measurements from 15-150 microns were made with unpolarized light using a grating spectrometer. The details of the design, construction, and operating conditions for the spectrometer are given in Appendix VI.

The transmissions were determined by introducing the samples into the monochromatic beam at a focus. The radiation consisting of a solid cone of angle 5.5° to the axis impinged normally on the transmission sample. The transmitted radiation within an equal cone was retained by the optics.

Reflection measurements were made at a focus with a rotating table which would introduce either a calibrated gold mirror or the sample into the optics. The optical axis made an angle of 7.5° to the normal from the sample. The incident radiation was contained within a cone of 5.5° to the optical axis

For both reflection and transmission measurements the incident beam impinged on the bismuth surface of the film. Occasional back reflection measurements were made. These showed little difference from the front reflections except in the region near 15 microns. Table 3 gives the ratio of front to back reflectance at several wavelengths for Sample K.

Table 3.
Ratio of Reflectances from Deposit and Substrate Sides - Sample K

Wavelength	Reflectance Ratio
15.5 micron	0.984 ± 0.016
26.0	0.996 ± 0.016
30.0	1.004 ± 0.016
35.0	1.007 ± 0.016
41.5	0.993 ± 0.016

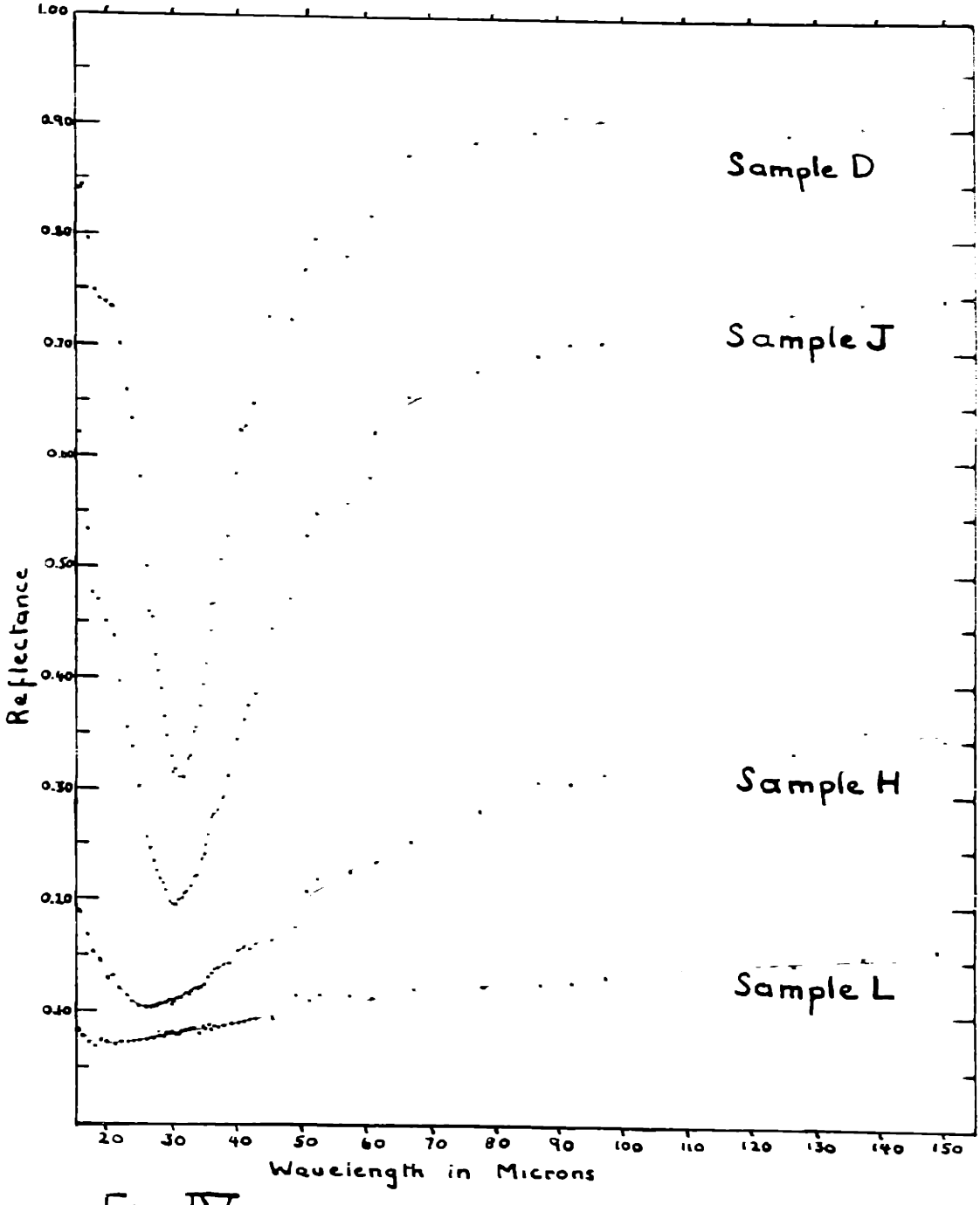

Fig. IV Far Infrared Reflectance

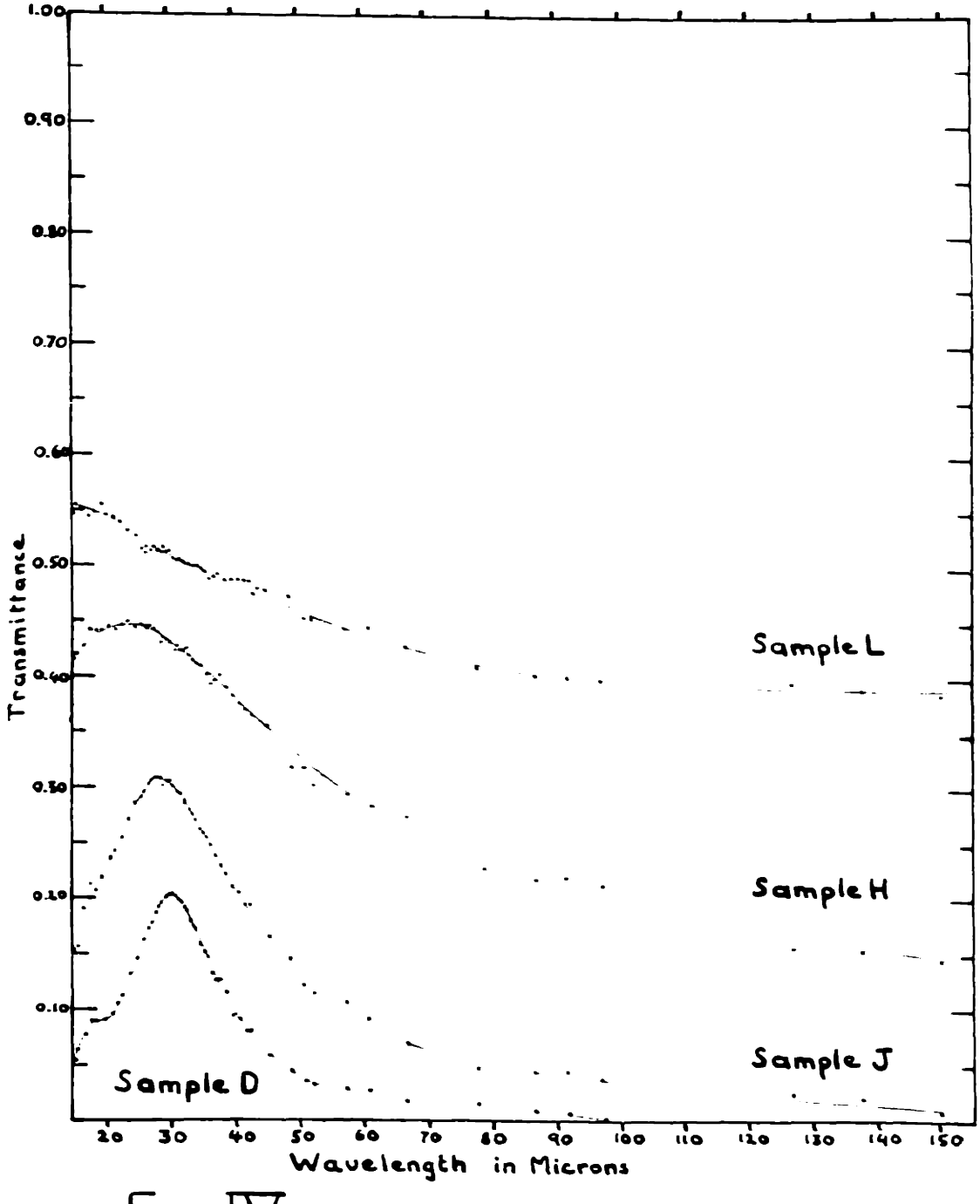

Fig. IV Far Infrared Transmittance

Reflection and transmission curves as a function of wavelength are given for a cross-section of the samples in Figure IV. The curves for the remainder of the samples are given in Appendix VII.

ii Near Infrared Transmission and Reflection.

Transmission and reflection measurements on the bismuth deposits were made in the near infrared using a Perkin-Elmer model 12B sodium chloride prism spectrometer. The transmission samples were inserted in front of the entrance slits of the monochromator section. The source section had previously been modified with a rotating table for reflection measurements. The beam geometry was approximately the same as that in the far infrared spectrometer with the exception that the transmission samples were before the monochromator and somewhat displaced from the focus.

The operating conditions for the instrument are given in Appendix VIII. The transmission and reflection spectra of several of the samples are given in Figure V. Those for the remaining samples are given in Appendix IX. No data are given for Sample H which broke during near infrared measurements.

The interesting spectrum is due to interference caused by the large index of refraction of the deposits at these wavelengths.

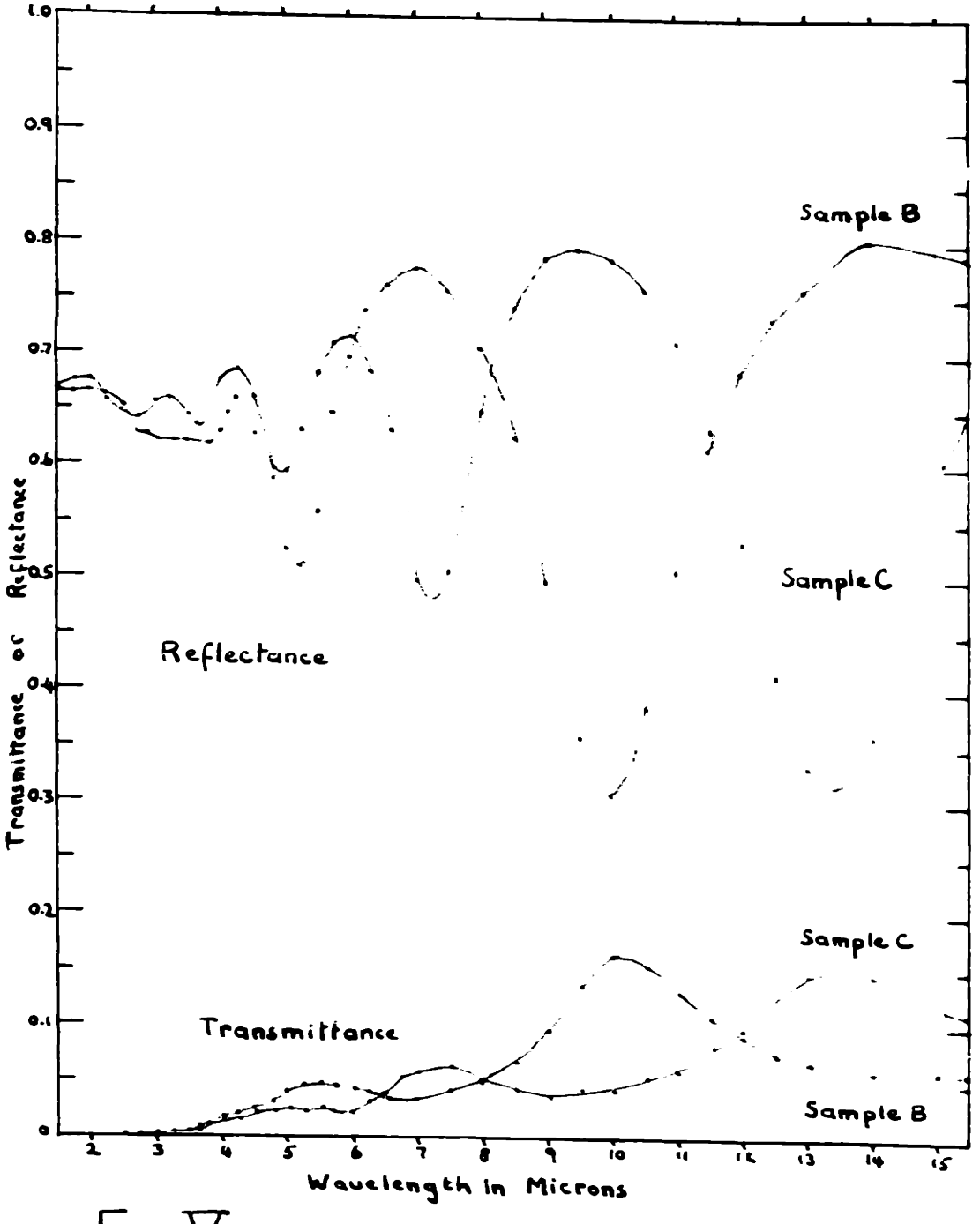

Fig. V Near Infrared Transmittance and Reflectance

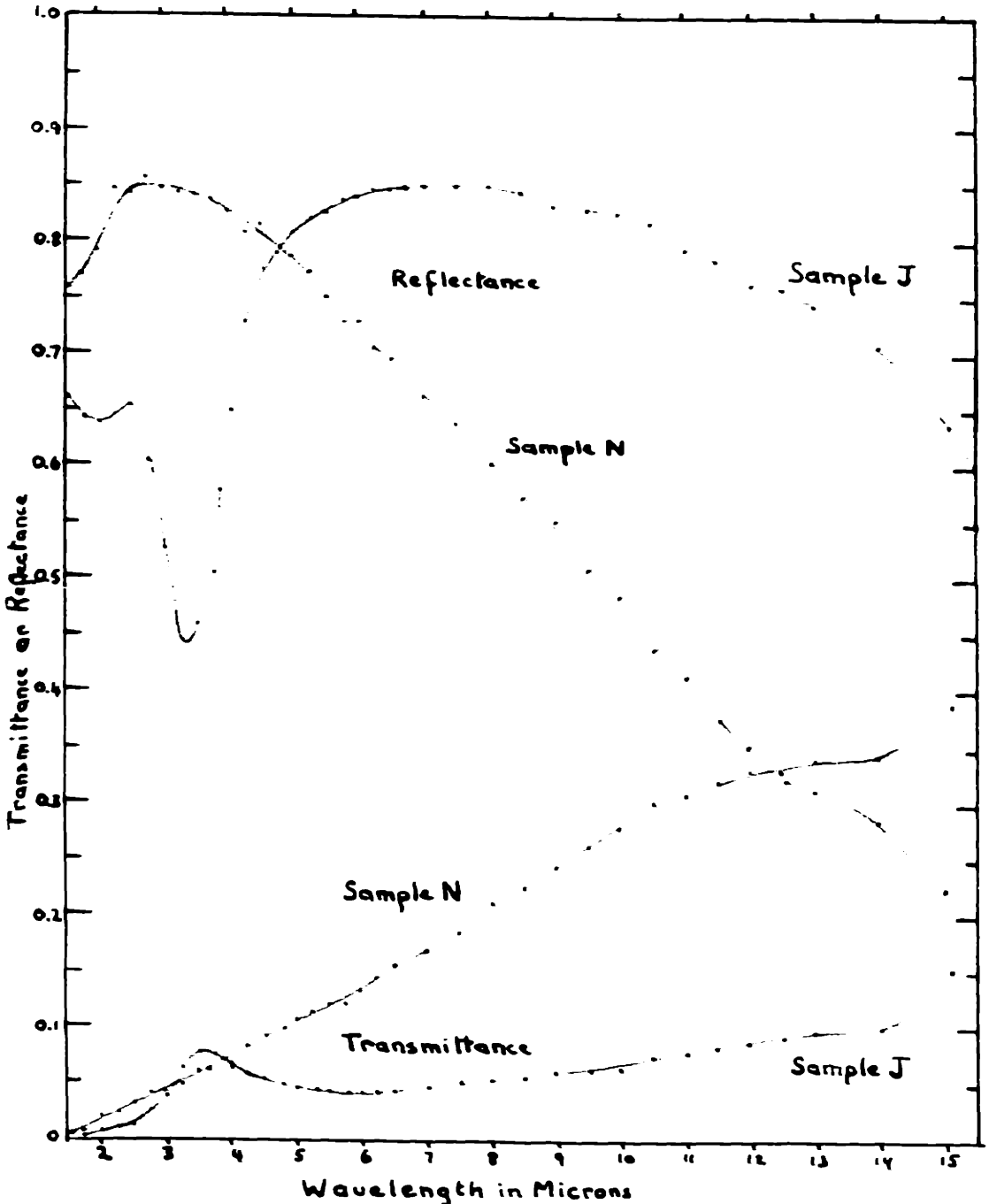

Fig. V Near Infrared Transmittance and Reflectance

IV. APPLICATION OF MAXWELL'S EQUATIONS TO A THIN FILM SYSTEM WITH INCIDENT MONOCHROMATIC RADIATION.

A. Mathematical Treatment

In order to examine the theoretical implications of the infrared spectra of the bismuth films it is desirable to express these properties in terms of parameters which afford a more simple theoretical interpretation. The index of refraction n and absorption coefficient k and their physical counterparts the conductivity and dielectric constant are suitable parameters.

The solutions of Maxwell's equations for electromagnetic radiation falling on thin conducting films are readily obtained (46,47) when certain simplifying assumptions are made. The method of solution is briefly reviewed below so that the validity of these assumptions and, therefore, the validity of the solutions themselves may be examined.

Let us consider the case of an electromagnetic wave traveling in the z - direction through a medium which is isotropic in the xy - plane. Maxwell's equations (48) are

$$\vec{\nabla}\cdot\vec{D} = \rho \qquad \vec{\nabla}\cdot\vec{B} = 0 \qquad (2)$$

$$\vec{\nabla}\times\vec{E} = -\frac{\partial\vec{B}}{\partial t} \qquad \vec{\nabla}\times\vec{H} = \vec{J} + \frac{\partial\vec{D}}{\partial t}$$

where

$\vec{\mathcal{E}}$ is the electric vector

$\vec{B}$ the magnetic flux

$\vec{D}$ the electric displacement

$\vec{H}$ the magnetic field

$\vec{J}$ the current density. -

If we accept Poynting's Theorem, i.e.

$$\vec{S} = \vec{\mathcal{E}} \times \vec{H} \tag{3}$$

where $\vec{S}$ is the energy flow per unit area, without derivation $\vec{\mathcal{E}}$ and $\vec{H}$ are required to lie in the xy - plane. We may write, then

$$\begin{aligned} \vec{B} &= \mu \vec{H} \\ \vec{D} &= \epsilon \vec{\mathcal{E}} \end{aligned} \tag{4}$$

where μ is the magnetic permeability and ϵ dielectric constant, each in the xy - plane.

Thus

$$\begin{aligned} \vec{\nabla} \times \vec{\mathcal{E}} &= -\frac{\partial \vec{B}}{\partial t} = -\frac{\partial}{\partial t}(\mu \vec{H}) \\ \vec{\nabla} \times \vec{\nabla} \times \vec{\mathcal{E}} &= -\frac{\partial}{\partial t}(\vec{\nabla} \times \mu \vec{H}) = -\mu \frac{\partial}{\partial t}\left(\vec{J} + \frac{\partial \vec{D}}{\partial t}\right) \\ &= -\mu \frac{\partial}{\partial t}\left(\vec{J} + \epsilon \frac{\partial \vec{\mathcal{E}}}{\partial t}\right) \end{aligned} \tag{5}$$

If we now assume Ohm's Law, i.e.

$$\vec{J} = \sigma \vec{\mathcal{E}}$$

where σ is the conductivity in the xy-plane, and that the charge density is not spatially dependent, i.e.

$$\nabla \rho = 0$$

we may expand $\vec{\nabla} \times \vec{\nabla} \times \vec{\mathcal{E}}$ to obtain

$$\nabla^2 \vec{\mathcal{E}} - \mu \epsilon \frac{\partial^2 \vec{\mathcal{E}}}{\partial t^2} - \sigma \mu \frac{\partial \vec{\mathcal{E}}}{\partial t} = 0 \tag{6}$$

If we assume $\vec{\mathcal{E}}$ to vary sinusoidally with frequency $\omega/2\pi$ and be spatially dependent on z only, we may obtain a solution to Maxwell's equations of the form

$$\vec{\mathcal{E}} = \vec{\mathcal{E}}_0 \exp\left(i(Kz-\omega t)\right) \tag{7}$$

where

$$K = \pm\sqrt{\omega^2\mu\epsilon + i\omega\mu\sigma} = \frac{2\pi}{\lambda}(n+ik) \tag{8}$$

and

$$n^2 - k^2 = \frac{\mu\epsilon}{\mu_0\epsilon_0}, \quad nk = \frac{\lambda}{4\pi}\mu c\sigma$$

On the assumption that $\mu=\mu_0$ at infrared frequencies, a condition that even holds for ferrites (53), we have

$$n^2-k^2 = \frac{\epsilon}{\epsilon_0} \qquad nk = \frac{\lambda}{4\pi}\mu_0 c\sigma \tag{9}$$

where n and k are the familiar optical constants, and λ is the wavelength of the radiation in a vacuum.

A similar expression to equation (7) may be obtained for $\vec{H}$.

If one considers an electromagnetic wave with $\vec{\mathcal{E}}$ and $\vec{H}$ vectors of the form given by equation (7) impinging normally on a thin parallel slab of material with optical constants n and k, the following expressions may be obtained from satisfaction of boundary conditions. (The derivation is given by Harris, Beasley, and Loeb (46), the equations below correspond to their equations (18) and (19)).

$$R = \frac{\left|\left(\frac{n_0}{n+ik} - \frac{n+ik}{n_0}\right)\sin\frac{2\pi a}{\lambda}(n+ik)\right|^2}{\left|2\cos\frac{2\pi a}{\lambda}(n+ik) - i\left(\frac{n_0}{n+ik} + \frac{n+ik}{n_0}\right)\sin\frac{2\pi a}{\lambda}(n+ik)\right|^2} \tag{10}$$

$$T = \frac{4}{\left|2\cos\frac{2\pi a}{\lambda}(n+ik) - i\left(\frac{n_0}{n+ik} + \frac{n+ik}{n_0}\right)\sin\frac{2\pi a}{\lambda}(n+ik)\right|^2} \tag{11}$$

where

$$R = \left|\frac{\vec{S}_R}{\vec{S}_I}\right| \qquad T = \left|\frac{\vec{S}_T}{\vec{S}_I}\right|$$

$\vec{S}$ is Poynting's vector. Subscripts I, R, and T correspond to incident, reflected and transmitted. n_o is the index of refraction of air.

Expressions (10) and (11) permit evaluation of the complex index of refraction, $n + ik$, for the bismuth films as a function of wavelength, and the physically meaningful conductivity and dielectric constant may be calculated from expression (9).

A computer program to carry out the above calculation was described by Harris and Loeb (49). This program has been converted for use with the IBM 704 by A.L. Loeb and Phil Friend. In effect, the computer substitutes successive n and k values into expressions (10) and (11) until R and T are reproduced to a given degree of accuracy. The details of the program are given by Loeb and Denman (27).

B. Validity of Assumptions Introduced into the Mathematical Treatment.

To determine how applicable the above treatment is to the present experimental system the following assumptions which were made must be examined.

1. Radiation consisting of monochromatic plane waves.
2. Radiation at normal incidence to the sample.
3. Negligible influence of the substrate.
4. Medium isotropic in the plane of the substrate.
5. Validity of Ohm's Law.

The validity of using amplitude addition of plane waves in derivations of this type has been discussed by Harris, Beasley, and Loeb (46) in some detail and will, therefore, not be re-examined. They also discuss the effect of angle of incidence on the reflection and transmission and find practically no change between 0° and 30° for an example with unpolarized

light. The mean angle of incidence of 7.5° used for reflection measurements in the present investigation should produce little error even with the relatively large index of refraction of the metal films (see Appendix XIII

Criteria for ignoring the contribution of the backing to the optical properties of thin film systems have been discussed by Harris and Loeb (49,54) and Harris, Beasley, and Loeb (46). Qualitatively these criteria amount to a requirement of almost 100% transmission by the substrate. This condition is well satisfied for 50 volt aluminum oxide films from 3 to 10 microns and beyond 30 microns wavelength (Appendix III). In the absorbing region from 10 to 30 microns the use of this treatment is not physically correct.

The optical constants for aluminum oxide have been evaluated and are given in Appendix III so that a rigorous treatment of the optical data may be made for the 10 to 30 micron region when a suitable program becomes available.

The above solution of Maxwell's equations assumes that the film is isotropic in the plane of the substrate. Figure IIb indicates that the crystallites of which the film is composed are very small compared to the wavelength of the radiation used. The electron diffraction photograph (Figure IIa) suggests, however, that there may be some orientation within the plane of the substrate over dimensions comparable to the shortest wavelengths used. As is discussed in Section V the Hall effect data strongly suggest an orientation of the individual crystallites such that their properties would be isotropic in the plane of the substrate.

The question of the validity of Ohm's Law introduces the concept of the anomalous skin effect and is discussed below.

C. The Anomalous Skin Effect

A common view of the mechanism of electronic conduction in a metal (55) is that a velocity distribution of the charge carriers is somewhat perturbed by an impressed electric field giving a resultant current. Thus an electron may move a considerable distance during the perturbation of its velocity by an impressed electric field. Ohm's Law states that the current density at a given point is proportional to the electric field at that point. Clearly if an electron moves out of the vicinity of the electric field Ohm's Law breaks down.

The application of this concept of the anomalous skin effect to the optical properties of isotropic conductors is discussed by Reuter and Sondheimer (56) and by Dingle (57). Its application to anisotropic thin films is considerably more difficult so the effect is only considered qualitatively here.

A carrier may move out of the influence of the electromagnetic field if the distance it moves during one period of the radiation is comparable to either the wavelength or the penetration depth of the radiation.

While mean free paths in bismuth have been reported from 0.02 to 7 microns (58,59,60) it is most doubtful that the mean free path in bismuth deposits composed of 2000 Å crystallites is of the same order of magnitude as the wavelength of the infrared radiation used in this investigation.

The penetration depth δ of the radiation may be defined using equation (7).

$$|\vec{\mathcal{E}}_0 \exp[i(K\delta-\omega t)]|^2 = |\vec{\mathcal{E}}_0|^2 \exp[-1]$$

so that

$$\delta = \frac{\lambda}{4\pi k} \qquad (12)$$

where λ is the wavelength of the radiation,

k the absorption coefficient.

The curves for the real and imaginary parts of the complex index of refraction given in Appendix XIII show that $\delta \sim 0.3$ micron in the far infrared increasing to 0.6 micron at 30 microns wavelength. When the thickness of the film is small compared to δ the charge carriers cannot move beyond the influence of the electromagnetic field and Ohm's Law holds. However, in the case of the thicker films carriers would be able to move in or out of the field if the distance moved perpendicular to the film surface during one period of the field was larger than the penetration depth. If ℓ is the mean free path of the carriers and τ their relaxation time the requirement for Ohm's Law amounts to

$$\frac{\ell}{\omega\tau} < \delta \tag{13}$$

for thick films. Since there is some question of whether electrons are specularly or diffusely reflected from the air-bismuth interface (61), ℓ is difficult to determine. However, it is probably not longer than 0.2 microns (16) in single crystals and even less in thin deposits so that inequality (13) provides a method of determining the validity of the optical theory.

Failure of this condition means that fewer charge carriers are taking part in the conduction process (62) and would result in a decrease in the observed conductivity.

V. THEORETICAL MODEL FOR THE ELECTRONIC STRUCTURE OF THE BISMUTH DEPOSITS

In order to examine the relationship between thin deposits and bismuth single crystals on a quantitative basis it is desirable to construct a model for the deposits in terms of the bulk properties. Treatment of the experimental film properties in terms of this model should then make a comparison with bulk single crystal parameters possible.

Quite generally the thin vacuum-deposit state of a solid is very complicated and to describe the properties in terms of a simple model represents a gross oversimplification. The present case is no exception. However, the results of the simple model developed here do appear to be theoretically significant and aid in understanding the nature of the deposits

A. Orientation in the Bismuth Deposits.

The problem of simply describing the bismuth deposits is greatly complicated by the large anisotropy of some of the electrical properties of the single crystals. The orientation of the deposited crystallites, therefore, becomes most important.

Several investigators have reported that bismuth deposits prepared on various substrates in a similar way to the ones described here have their (111) planes parallel to the substrate. Lane (63) and Büssem, et al. (64) carried out x-ray analyses with the beam oriented at a glancing angle to the substrate to emphasize the reflections from the (111) plane. With

thicker films (~ 2 microns) this orientation may become less pronounced (64,65). Drumheller (66) from electron microscope work reports 80% of crystallites oriented in films of comparable resistivity to those reported here.

The x-ray and electron diffraction work of the present investigation fails to indicate orientation. The design of the experiments, i.e. the use of a large beam of monochromatic x-radiation oriented perpendicular to the sample and little movement of the deposit, would tend to emphasize the disorder since the disordered crystallites present planes at Bragg angles to the beam for a larger fraction of the exposure time.

A strong indication of orientation, however, is given by the sign of the Hall coefficients for the deposits. T. Okada (3) and Abeles and Meiboom (2) have measured the Hall coefficient of bismuth single crystals with the magnetic field parallel and perpendicular to the trigonal axis. They obtain the results give in Table 4.

Table 4. Hall Coefficients of Single Crystals

	R (H parallel)	R (H perpendicular)
Okada	6×10^{-8} MKS (0°C)	-169×10^{-8} MKS (0°C)
A. and M.	4.5×10^{-8} (23°C)	-135×10^{-8} (23°C)

The results of the present investigation compare closely with the values for the magnetic field parallel to the axis for all deposits except Sample O. The Hall coefficients were given in Table 2. The ratio of deposit Hall coefficient to that measured by Abeles and Meiboom for the magnetic field parallel to the trigonal axis is given in Table 5 for each sample with a positive Hall coefficient.

Okada's (3) measurements as a function of angle would crudely suggest that the coefficient changes sign with less than 20° angle between the field and the trigonal axis.

Bismuth deposited on to a very cold substrate, i.e. in a manner that would appear to favor disoriented growth, has been reported always to give a negative Hall coefficient ($\sim -10 \times 10^{-8}$ MKS) (67,68).

A result of our own structure study was, however, to determine that the individual crystallites had the bismuth single crystal structure. A reasonable model for the deposits would, therefore, be a thin film composed of many bismuth single crystals with their trigonal axes perpendicular to the substrate. The degree of orientation within the plane of the substrate is unimportant here, since the crystals are isotropic in that plane. Such a model cannot, however, be applied to Sample O which, on the basis of its Hall coefficient, appears to have little orientation.

To obtain theoretical expressions for the electronic properties of this model, it is necessary to examine the band structure of the single crystal and the electronic properties such a structure predicts both for a single crystal and a composite.

TABLE 5

Hall Coefficients of Deposits Compared to Single Crystals

Sample	R (Deposit) /R * (H parallel)
A	0.85
B	1.07
C	1.20
D	0.94
H	1.41
J	1.29
K	0.84
L	1.78
N	1.63
Q	2.02

* Value taken from Abeles and Meiboom (2)

B. Band Structure of the Bismuth Crystal.

As mentioned earlier a variety of investigations have been made into the band structure of bismuth. While there remains some doubt (16) about the magnitudes of the parameters involved and many of the details, a fairly consistent general picture has evolved.

The band structure has been described in two review articles (69,70) and will only be briefly discussed here as it applies to a theoretical model for the deposits.

If the interatomic binding in bismuth crystals were non-directional the crystal would be a face centered cubic insulator. The fifth Brillouin zone would be completely filled with electrons, the next empty. The covalent nature of the binding, however, slightly distorts the cubic structure changing the bond angle from 60° to 57° 14' (35). This distortion creates a slight overlap between the fifth Brillouin zone and the next higher. Due to the $\bar{3}m$ symmetry of the crystal and consequent similar symmetry of the reciprocal lattice, a band structure like that represented in Figure VI is indicated. With suitable translations the surfaces of constant energy at the Fermi level may be approximated by three ellipsoids located at the edges of the Brillouin zone in a manner that retains the 3-fold symmetry, and one ellipsoid of revolution about the principal axis. Smith (61) has suggested a model consisting of 6 and 2 ellipsoids, however, the present experiments would not distinguish between these models and the former is more widely used. The ellipsoid of revolution is probably warped (7) to some degree.

Such a model is capable of explaining most galvanomagnetic (2), magnetic susceptibility (10,20), and cyclotron resonance (18) measurements to date. The ellipsoids at the edges of the Brillouin zone appear

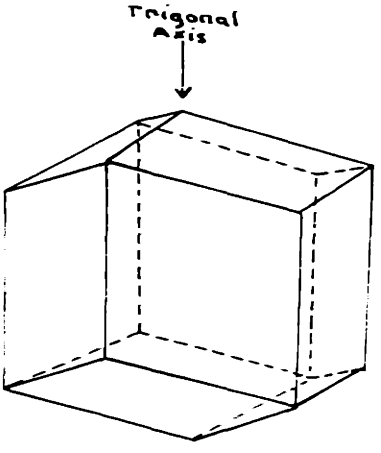

Brillouin Zone

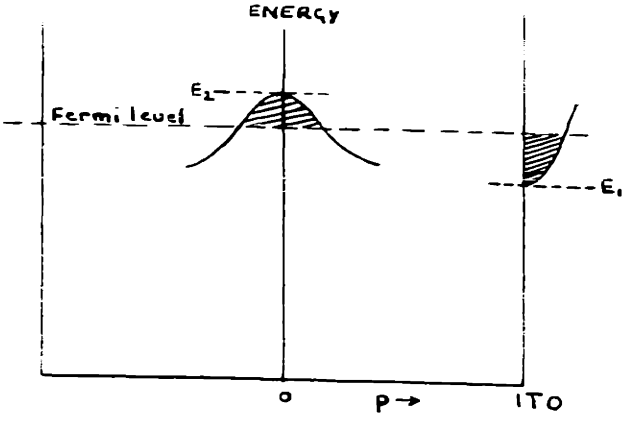

Energy vs Momentum in 1TO Direction

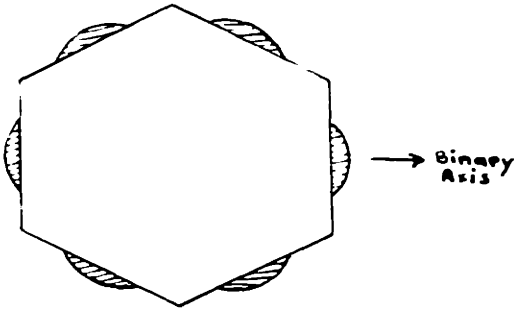

Cross Section of Brillouin Zone Perpendicular to Trigonal Axis

Fig. VI

Band Structure of Bismuth

[after Mott and Jones "The Theory of the Properties of Metals and Alloys" Oxford: Clarendon Press, 1936, and B. Lax, Rev. Mod. Phys. 30, 122 (58)]

to be tilted approximately 6° (10,7). However, since this tilt does not appear to affect the galvanomagnetic properties at low fields (2), and is small compared to the uncertainty of the orientation of the crystallites in the deposits, it will be neglected in this discussion.

In the terminology of electrons and holes (70), there are N electrons per unit volume equally distributed into 3 constant energy surfaces in momentum space, each described by

$$E_F - E_1 = \frac{1}{2m_0} (\alpha_1(\Delta p_1)^2 + \alpha_2(\Delta p_2)^2 + \alpha_3(\Delta p_3)^2) \tag{14}$$

where E_1 is the energy of the bottom of the conduction band or higher Brillouin zone.

E_F is the Fermi energy of the electrons,

m_0 the mass of the free electron,

$\alpha_1, \alpha_2, \alpha_3$ are the axial parameters of the ellipsoid: subscript 3 refers to the axis parallel to the 3-axis, 1 to the axis perpendicular to the edge of the Brillouin zone and 2 to the axis parallel to the edge.

$\Delta p_1, \Delta p_2, \Delta p_3$ are the differences in position in momentum space between the electron and the bottom of the band, referred to the ellipsoid axes.

There are also P holes, where N = P for a perfect crystal, in the valence ellipsoid described by

$$E_2 - E_F = \frac{1}{2m_0} (\beta_1 (p_1^2 + p_2^2) + \beta_3 p_3^2) \tag{15}$$

where E_2 is the energy of the top of the valence band, β_1, β_3 the axial parameters for the ellipsoid of revolution. p_1, p_2, p_3 are the components of momentum of the hole: 1, 2, and 3 are mutually perpendicular with the 3-direction parallel to the trigonal axis.

Above $0^{\circ}K$ the carriers exist in an energy distribution about the energy E_F, given by the Fermi distribution expression

$$N(E) = \frac{2}{\exp\left((E-E_F)/kT\right)+1} \qquad (16)$$

where E is the actual energy of an electron or hole.

C. Conductivity of the Single Crystal in the (111) Plane.

If the electrons and holes of the preceding section are subject to an external electromagnetic field, their Fermi distribution will be perturbed and a net flow of charge will result. If the assumption is made that transitions between ellipsoids are rare (2) each ellipsoid may be treated separately and the resultant current summed.

Boltzmann's equation may thus be solved for each ellipsoid to determine the perturbation to its Fermi distribution and the resulting current.

Boltzmann's equation for the distribution **function** f has the form

$$\frac{\partial f}{\partial t} + \vec{v}\cdot\overrightarrow{\mathrm{grad}}_{\vec{r}}\, f + \vec{F}\cdot\mathrm{grad}_{\vec{p}}\, f = \left.\frac{df}{dt}\right]_{\text{collisions}} \qquad (17)$$

where $\vec{v}$ is the velocity of an electron (or hole),

$\vec{F} = \mp(\vec{\mathcal{E}} + \vec{v} \times \vec{H})e$ is the force due to an electric field $\vec{\mathcal{E}}$ and magnetic field $\vec{H}$. $\vec{p}$ represents the momentum of the carrier.

Assuming that the distribution f may be written as a perturbation f_1 of the Fermi distribution f_o, we may write

$$f = f_o + f_1\,(p,t) \qquad (18)$$

Strictly, at optical frequencies f_1 is a function of position also; neglecting this dependence amounts to ignoring the anomalous skin effect (56).

If we assume, on removal of the applied field, that the perturbation will exponentially decay due to collisions of the electrons with phonons or lattice imperfections we may write

$$\left.\frac{df}{dt}\right]_{\text{collisions}} = \frac{-(f - f_o)}{\tau} \qquad (19)$$

where τ is designated a relaxation time. We will assume

here that τ is a constant, independent of energy and momentum. This assumption is discussed in the next paragraph.

With these assumptions equation (17) may be now written

$$\frac{\partial f_1}{\partial t} - e(\vec{\mathcal{E}} + \vec{v} \times \vec{H}) \cdot \mathrm{grad}_{\vec{p}} f_0 = -\frac{f_1}{\tau} \qquad (20)$$

which may be solved with the aid of equations (14), (15), and (16) to provide expressions for the conductivity and Hall coefficient.

The relaxation time parameter as introduced into equation (20) is in general an average value of a complicated function of energy and momentum (72). The scattering of electrons in a bismuth deposit is mainly due to contributions from phonons and lattice imperfections. To the electron these present approximately the same type of scattering center - namely a localized deformation of the lattice (73). To a first approximation the dependencies of the relaxation time in a film will be the same as those in bulk.

Since the relaxation time is an average of momentum as well as energy, it is generally a function of direction in momentum space.

While no specific study of τ anisotropy has been made in single crystals, comparison of the effective mass and the mobility anisotropy indicates that the dependence, if any, is small (16). This view is certainly reasonable since the applied fields only produce small perturbations to the Fermi distribution which should not materially change the distribution of collisions.

Equation (20) may be solved to give expressions for the current produced by an applied electric and magnetic field. The details are given in Appendix X. By considering a sinusoidal electric vector and summing the current contributions due to each band edge ellipsoid, a matrix expression

for the conductivity σ of a bismuth single crystal as a function of frequency $\omega/2\pi$ is obtained.

$$\sigma = \begin{vmatrix} \varphi_\omega\left(\frac{\alpha_1+\alpha_2}{2}\right) + \chi_\omega\beta_1 & 0 & 0 \\ 0 & \varphi_\omega\left(\frac{\alpha_1+\alpha_2}{2}\right) + \chi_\omega\beta_1 & 0 \\ 0 & 0 & \varphi_\omega\alpha_3 + \chi_\omega\beta_3 \end{vmatrix} \qquad (21)$$

where

$$\varphi_\omega = \frac{Ne^2\tau_n}{m_0(1+i\omega\tau_n)} \qquad \chi_\omega = \frac{Pe^2\tau_p}{m_0(1+i\omega\tau_p)}$$

α_i, β_i are the energy band edge ellipsoid parameters .

N and P are the number of electrons and holes respectively, τ_n and τ_p their relaxation times, e the charge on the electron. The details of the derivation are given in Appendices X and XI.

It is clear from expression (21) that the conductivity is isotropic in the plane perpendicular to the trigonal axis.

Equation (20) may also be solved for the Hall coefficient R_H . In the case where the magnetic field is parallel to the principal axis, the Hall coefficient is independent of the direction of the current within the (111) plane. In the limit of a small magnetic field

$$R_0 = \frac{-\mathcal{E}x}{jy\ H_z} = \frac{\mathcal{E}y}{jx\ H_z} = \frac{Pe\nu_1^2 - Ne\mu_1\mu_2}{\left(Ne\left(\frac{\mu_1+\mu_2}{2}\right) + Pe\nu_1\right)^2} \qquad (22)$$

where

$$\mu_i = \frac{e\tau_n\alpha_i}{m_0} \qquad \nu_i = \frac{e\tau_p\beta_i}{m_0}$$

j is the current density.

When the assumption that N = P is valid R_H as a function of magnetic field is given by

$$R_H = \frac{1}{Ne}\,\frac{[\nu_1^2-\mu_1\mu_2][1+\mu_1\mu_2 H_z^2]}{\left[\nu_1+\frac{\mu_1+\mu_2}{2}\right]^2 + \left[\mu_1\mu_2 + \nu_1\left(\frac{\mu_1+\mu_2}{2}\right)\right]^2 H_z^2} \qquad (23)$$

for the magnetic field parallel to the 3-axis. The details of the derivations are given in Appendix X and XII. The equations (22) and (23) above are identical to those given by Abeles and Meiboom (2).

D. An Electronic Model for the Bismuth Deposits.

If the assumption is made that the bismuth deposits are largely made up of crystallites with their 3-fold axes perpendicular to the substrates, the expressions derived above may be applied to the deposits.

In the case of the conductivity, orientation, or lack of it, in the plane of the substrate only changes the scattering of the electrons, or the relaxation time. The conductivity within the plane of the substrate is isotropic and given by

$$\sigma_\omega = Ne\frac{\mu_1+\mu_2}{2(1+i\omega\tau_n)} + Pe\frac{\nu_1}{(1+i\omega\tau_p)} \tag{24}$$

as a function of frequency with the d.c. value given by

$$\sigma_{d.c.} = Ne\frac{\mu_1+\mu_2}{2} + Pe\nu_1 \tag{25}$$

The problem of summing the Hall voltage contributions of the various crystallites in a deposit has been examined by Volger (74). A result of his analysis is that the Hall coefficient of the layer will be the same as that of the constituent crystallites when the distance between the crystallites is very small compared to the crystallite size. The assumption is made that the area between the crystallites, if any, is of high resistivity so that the individual crystals are not short-circuited.

Both of these conditions are well satisfied for the present samples and the expressions (22) and (23) may be directly applied to the films. The substitution of equation (25) into equation (22) gives the useful relation

$$R_0\sigma_{dc}^2 = Pe\nu_1^2 - Ne\mu_1\mu_2 \tag{26}$$

It is to be noted that none of the above expressions permit the differentiation between the 1 and 2 directions. In the following sections it will be assumed that $\alpha_1 > \alpha_2$ in accordance with the single crystal parameters (16).

VI. APPLICATION OF THE ORIENTED FILM THEORY TO THE EXPERIMENTAL RESULTS

If the mathematical treatment outlined in Section IV is applied to the optical data of Figure IV and Appendix VII in the far infrared region where the substrate absorption is small, the experimental points in Figure VII are obtained for the conductivity at each wavelength. These points represent values of the conductivity that will reproduce the experimental reflectance and transmittance to within ± 0.005. This value was used as it lies comfortably within the experimental tolerance (See Appendix VI) and yet may be usually obtained with a reasonable number of approximations (between 1 and 20 depending on film thickness and wavelength). The values of the optical constants for this far infrared region have been calculated under the same conditions and are given in Appendix XIII.

There are a few experimental points in Figure IV and Appendix VII whose conductivities and optical constants have not been evaluated. This is due to a very low transmittance on some thick deposits producing a large degree of uncertainty, or lack of convergence in the mathematical determination of n and k.

For the same reason the optical conductivities for Sample O are not given. Evaluation of the reflection and transmission data for this sample can only be made for a small region of the far infrared spectrum, and within this region the uncertainty of the results is too large to permit a meaningful analysis. The optical constants, however, are given in Appendix XIII for the cases where evaluation is possible since the results do have qualitative significance.

The uncertainties in Figure VII are calculated on the assumption that the conductivity may be approximated (49) by

$$\sigma_\omega \sim \frac{1}{\mu_0 c a} \frac{1-R-T}{T} \tag{27}$$

where $\mu_0 c$ = 377 ohms and a is the thickness of the film. R and T are the reflectance and transmittance respectively. The uncertainties in R and T given in Appendix VI are used.

In the application of equation (24) to the optical conductivity data we shall assume that the relaxation time for the holes is long compared to the period of oscillation of the infrared electromagnetic field. This assumption is necessary in bismuth single crystals to relate the large mobility of the holes from Hall effect measurements (2) with the results of cyclotron resonance and electronic heat capacity measurements (16,18,19). The optical treatment gives only the real part of the conductivity, since the imaginary part is incorporated with the dielectric constant (c.f. equation (8)). Equation (24) becomes

$$\sigma_\omega = Ne \frac{\mu_1 + \mu_2}{2(1+\omega^2\tau^2)} \tag{28}$$

where μ_1, μ_2 are the axial components of the mobility and $\omega/2\pi$ is the frequency in the infrared region of the spectrum. The experimental conductivity results in Figure VII should, therefore, satisfy equation (28). The abscissa in Figure VII is linear in ω^2. If we write the low frequency limit of equation (28) as σ_0, the mobility of the holes ν_1 is given by

$$\sigma_{d.c.} - \sigma_0 = Pe\nu_1 \tag{29}$$

where $\sigma_{d.c.}$ is the measured d.c. electrical conductivity.

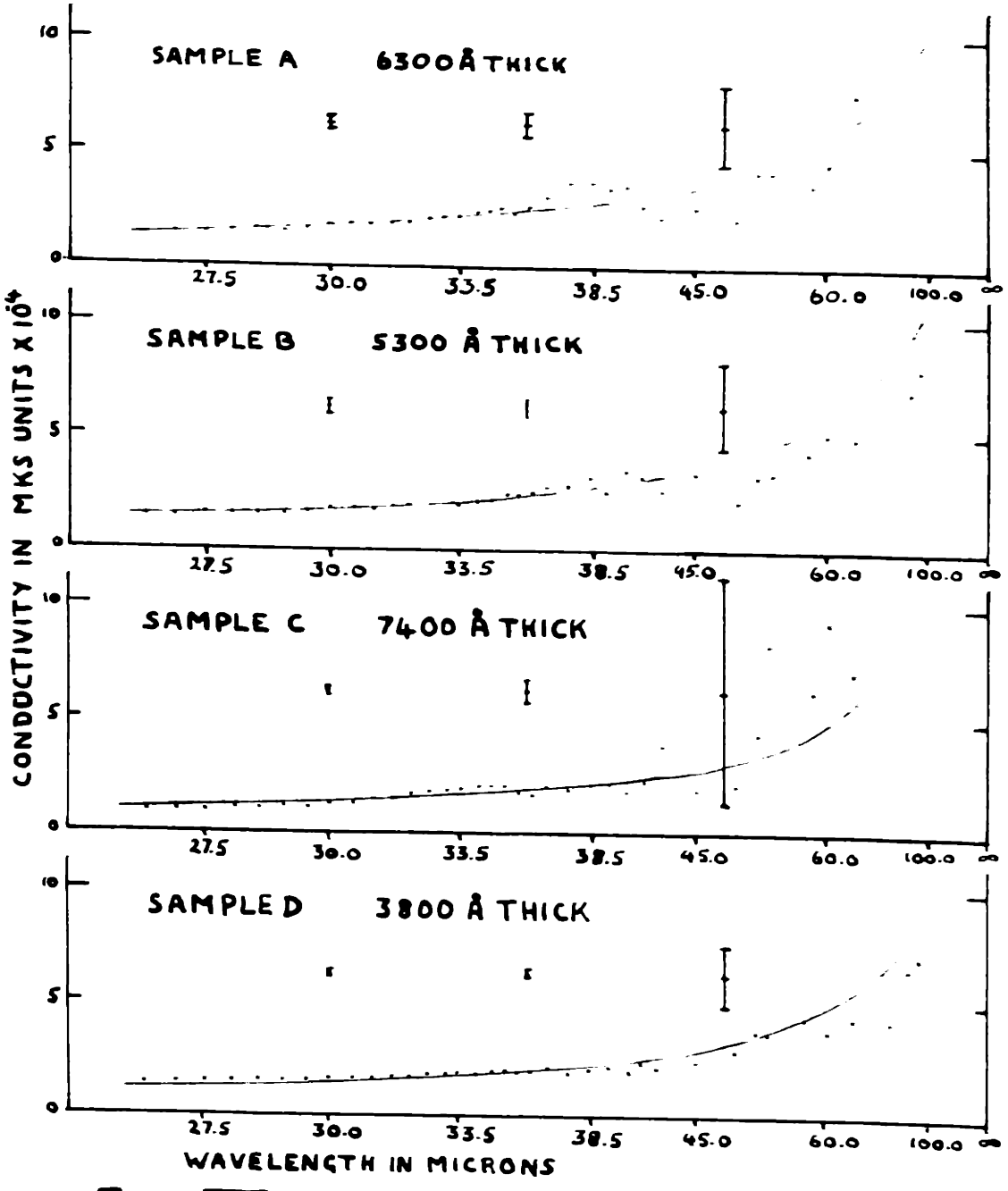

Fig. VIIa Conductivity as a Function of Wavelength

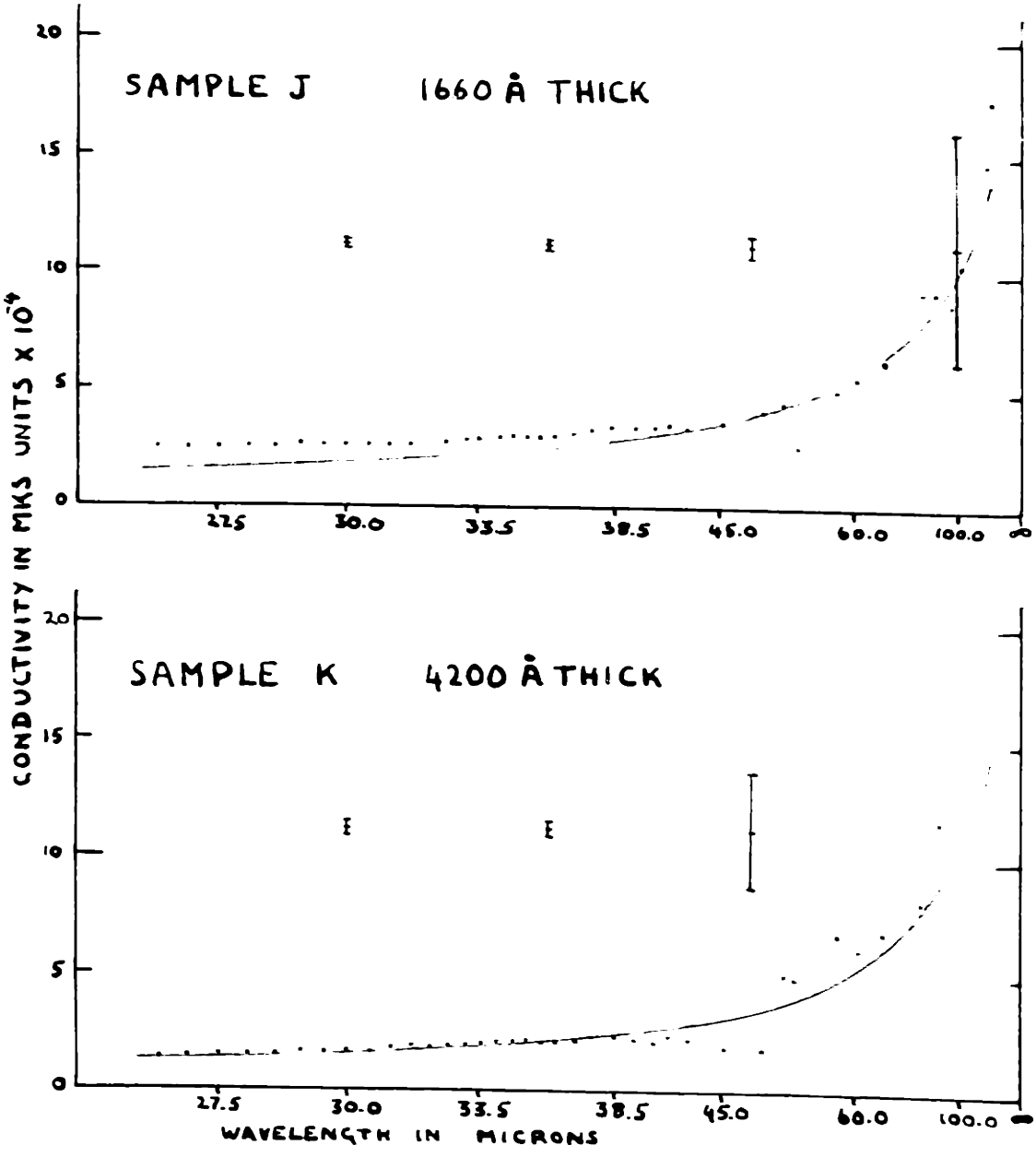

Fig. VII b Conductivity as a Function of Wavelength

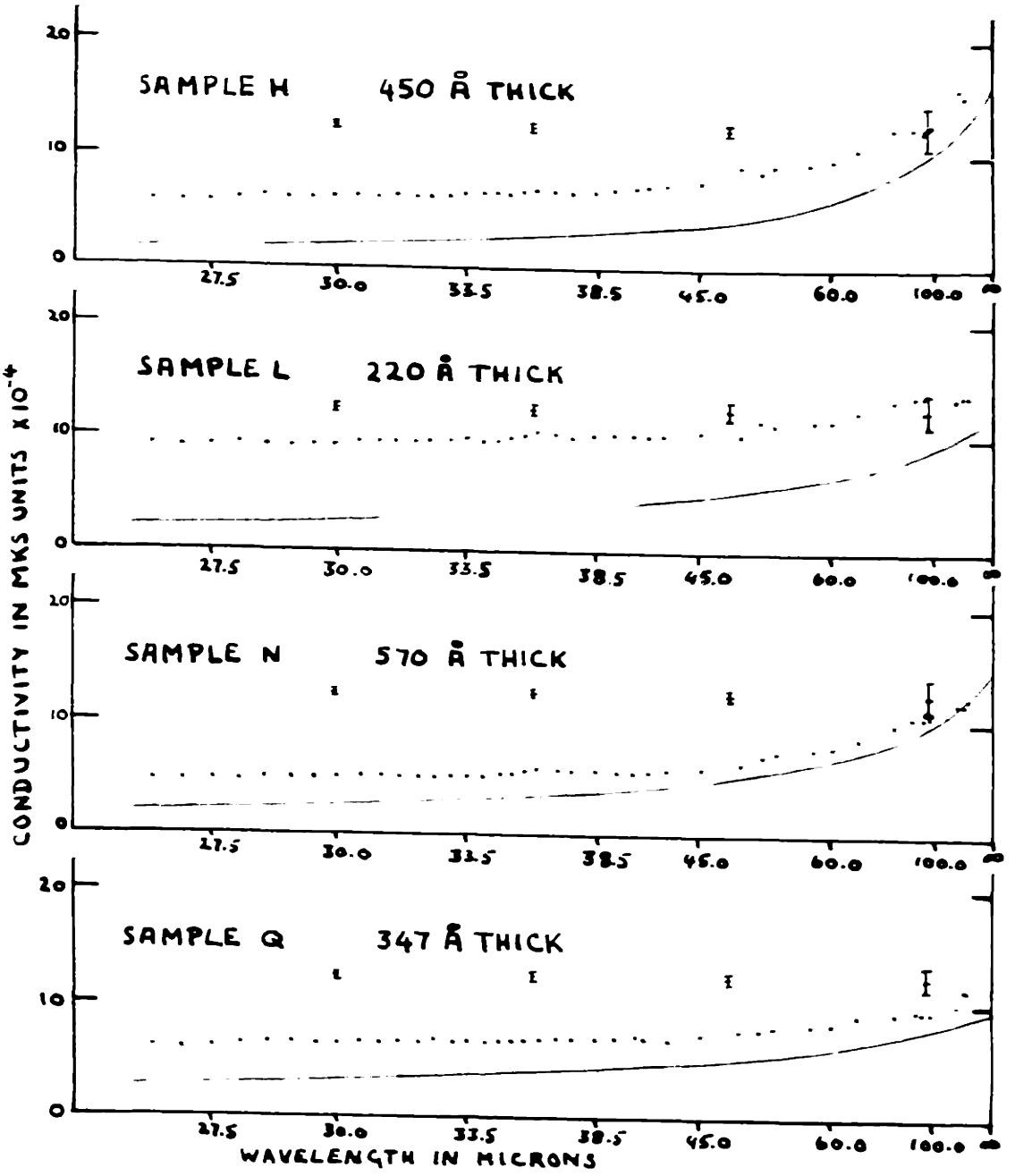

Fig. VII c Conductivity as a Function of Wavelength

Equation (29) may also be inverted to give the form of a straight line

$$\frac{1}{\sigma_\omega} = \frac{1}{A} + \frac{B}{A}\omega^2 \qquad (30)$$

where

$$A = Ne\left(\frac{\mu_1 + \mu_2}{2}\right) \qquad B = \tau_n^2$$

The parameters A and B were obtained for the six thickest samples (omitting O) by fitting the equation (28) to the experimental points and by plotting reciprocal conductivities and drawing the best straight line.

A sample calculation is given in Appendix XIV. The results for the individual "best fits" are given below in Table 6.

TABLE 6 - Conductivity Parameters

Sample	Parameters using Eg.(28) A	$4\pi^2 B$	Parameters using Eg.(30) A	$4\pi^2 B$
A	21×10^4 MKS	0.12×10^{-24}	$(19 - 21) \times 10^4$ [a]	$(0.10 - 0.11) \times 10^{-2}$
B	22[a]	0.12	20 - 25[a]	0.11 - 0.14
C	27[a]	0.10	------*	
D	21[a]	0.13	27[b]	0.21
J	20[a]	0.10	20[b]	0.09
K	26[a]	0.15	26[a]	0.15

a. Data beyond 28.5 microns used to obtain parameters.
b. Data beyond 37.0 microns used to obtain parameters
* Scatter of points too great to obtain meaningful parameters
A, B are defined in equation (30)

The uncertainty in determining the parameter B was somewhat less than $\pm 0.02 \times 10^{-24}$. The disagreement in Sample D is due to the inclusion of the data from 28.5 to 37 microns into the curve fitting. It is hard to assign an uncertainty to the parameter A. Some indication is given by a comparison of the results from the two methods of curve fitting. An "absolute"

uncertainty based on the possible uncertainty of the raw optical data and the range of curves falling within this uncertainty would be very large indeed. For this reason both methods of obtaining the parameters are given here.

The relaxation times may be calculated directly from the parameter B in Table 6. They are given in Table 7.

TABLE 7.- Relaxation Times

Sample	Relaxation Time of Electron
A	$(0.50 \text{ to } 0.55) \times 10^{-13}$ sec
B	$(0.53 \text{ to } 0.60) \times 10^{-13}$
C	0.50×10^{-13} *
D	$(0.58 \text{ to } 0.73) \times 10^{-13}$
J	$(0.48 \text{ to } 0.50) \times 10^{-13}$
K	0.62×10^{-13} *

* Uncertainty $\pm 0.05 \times 10^{-13}$ unless spread is given.

If it is now assumed that the number of electrons and the number of holes are equal for the thicker samples, the Hall coefficients may be related to the optical results. Since no independent determination of the number of electrons has been made in this investigation, we will assume the value of 2.2×10^{24} per cubic meter. This value has been obtained independently from galvanomagnetic measurements (2) and from magnetic susceptibility work (16) on single crystals. With these assumptions equation (26) becomes

$$\frac{R_0 \sigma_{dc}^2}{Ne} = \nu_1^2 - \mu_1 \mu_2 \tag{31}$$

where ν_1 may be obtained from equation (29). Solving equation (31)

gives two sets of parameters of interest: the ratio of the axial constants $\alpha_1 : \alpha_2$, and the ratio of the conduction due to the electrons to that due to the holes. The values of these parameters are given in Table 8. It may be noted that the magnitude of the left hand side of equation (31) varies from 0.2 to 0.5 of ν_1^2 so the value taken for N is not very critical here.

TABLE 8 - Transport Parameters

Sample	α_1/α_2 (1)		$(\mu_1+\mu_2)/2\nu_1$ (2)	
	Curve Fit	Straight Line	Curve Fit	Straight Line
A	140	36 - 140	4.6	2.8 - 4.6
B	36	16 - 200	2.7	1.9 - 4.7
C	230	----	4.7	---
D	9	66	1.6	4.7
J	44	44	2.9	2.9
K	83	83	3.6	3.6

(1) Ratio of axial parameters for an electron band edge ellipsoid in plane perpendicular to the trigonal axis.

(2) Ratio of conductivity due to electrons to that due to holes.

The spread of values in Table 8 is due to the sensitivity with which they depend on the curve fitting parameters.

To a first approximation one might expect the ratio of the contributions of the holes and the electrons to the conductivity to change little from film to film. This essentially implies that the degree of orientation and the ratio of the relaxation times of the two types of carriers do not change from sample to sample. Since the Hall coefficient which is orientation dependent and the conductivity which is relaxation time dependent are roughly constant, within the precision of this analysis this assumption is probably valid.

On this basis we may search for a single such ratio of contributions to the conductivity which will satisfy the experimental curves for all of the six samples. Since the frequency dependence of the conductivity is very sensitive to the relaxation time, we are not justified in holding τ_n constant. Thus holding $(\mu_1 + \mu_2)/2\nu_1$ constant and varying τ_n to give a satisfactory fit of the experimental points in Figure VII a, b for each of the six thick samples, the values in Table 9 are obtained.

TABLE 9 - Relaxation Times

$$\frac{\mu_1 + \mu_2}{2\nu_1} = 3.3 \pm 0.3$$

Sample	τ_n sec	σ_{dc} MKS
A	5.0×10^{-14}	25.3×10^{4}
B	5.5	30.3
C	5.6	32.3
D	5.8	34.5
J	5.0	27.0
K	5.2	32.8

The uncertainty in τ_n is $\pm$ 0.5×10^{-14}

The solid curves in Figure VII a, b are based on the parameters in Table 9.

The thin samples - H, L, N, and Q - do not fit into the same type of analysis as the thick. The solid curves in Figure VIIc which clearly do not fit the data, are based on the thick film parameters assuming the relaxation times to be proportional to the conductivities. The parameters used are given in Appendix XV.

Substitution of the values in Table 9 into the expression for the field dependence of the Hall coefficient - equation (23), predicts only a very slight decrease with increasing field. The decrease is approximately quadratic and less than 1% at 10,000 gauss, with little variation from sample to sample.

The optical constants for the deposits, with the exception of Sample H, were calculated for the near infrared region (3 to 10 microns). The results are plotted in Appendix XIII. Due to the sensitivity with which the optical constants depend on the reflectance and transmittance, the values are quite uncertain as the spread in successive points indicates. The conductivities in the same spectral region are also uncertain and since they do not contribute to the free electron problem they are not presented. The conductivities may, of course, be obtained immediately from the data in Appendix XIII with the use of equation (9).

If the optical data in the region from 10 to 30 microns are treated with the assumption of a non-absorbing substrate, the optical constants change their values smoothly to join the near and far infrared constants as they are given in Appendix XIII. The results are not presented here, however, as they are not mathematically correct and no valid simple approximate correction for the aluminum oxide absorption can be made (41). When the results in Table 9 are taken in conjunction with the Hall coefficients, the electronic band ellipsoid parameters may be obtained. The six samples give values of α_1 between 118 and 133, α_2 between 1.9 and 2.

VII. DISCUSSION

A. Some Remarks Concerning the Experimental Measurements

With the exception of the Hall effect on Sample H, no difficulty in reproducing either optical or electrical measurements was encountered. During the first few Hall effect measurements on Sample H, intermittent failure of the Hall probe balancing potentiometer occurred. Since some of the measurements made at that time appear satisfactory, all have been reported.

In Figure VII a, b the correspondence between the solid curves based on the parameters of Table 9 and the results of the transmission and reflection measurements may be materially improved for the thick samples at long wavelengths by the use of the smooth curves rather than the individual points of Figure IV. This procedure has not been used, however, since it tends to obscure the true uncertainty of the data.

The reason for the negative Hall coefficient of Sample O is uncertain. The sample was prepared at a slightly slower rate than the other thick samples. The other parameters of preparation remained unchanged. A result of the slower evaporation rate may have been to heat the substrate more by a longer exposure to radiation from the electron bombardment filamer

B. Experimental Properties of the Deposits.

The experimental reflection and transmission curves given in Figure IV and Appendix VII correspond in form and magnitude quite closely with the values reported by Woltersdorff (23). Since his sample thick-

nesses are not identical to those given here, no comparison on a sample to sample basis may be made.

The Hall effect measurements of Table 2 lie somewhat below the value of 7.1×10^{-8} MKS obtained by Leverton and Dekker (28) for deposits more than 1000 Å thick. Impurities have been observed, however, to give large increases in the Hall coefficients of thin deposits of bismuth (75) and Leverton and Dekker used only 99.8% pure bismuth. The field dependence of their measurements, however, corresponds closely with that presented here.

An extensive series of galvanomagnetic measurements on thin Bi_2O_3-Bi-Bi_2O_3 sandwiches has recently been reported by Colombani and Huet (29). Their deposits were annealed above the melting point of bismuth and the Hall coefficients, while positive, do not agree in magnitude with the ones reported here. They determine the thicknesses of their deposits from the resistivity in the molten compared to the solid state. This method of thickness determination is at best doubtful, and may explain some of the discrepancy between their measurements and the ones presented here.

The conductivities of the thickest deposits given in Table I lie below the range of 47 to 76×10^4 MKS given by Harris (76) for bismuth deposits 7300 to 15,800 Å thick. The Harris method of preparation which involves a radiation heated substrate was unsuccessful with thin aluminum oxide substrates. The resulting deposits had an amorphous or droplet structure and high resistance. It is interesting to note that our own Sample O, during the preparation of which the substrate may have become heated, has a conductivity almost comparable to Harris. It also has a negative Hall coefficient; unfortunately, no Hall effect information is available for the Harris deposits.

The characteristics of the "analytically pure" Sample A seem quite comparable with those of Samples B and C which have similar thicknesses. In fact the impurity sensitive Hall coefficient is lowest for Sample A. Thus, it would appear that the purity of all the samples is more than adequate to eliminate impurity effects in the electronic properties.

C. Near Infrared Optical Characteristics of the Deposits.

The optical constants, n and k, for the series of deposits are given in Appendix XIII. The uncertainty in the optical constants in the regions of wavelength and thickness where interference is occurring is very large, probably in the order of a factor of 2. Beyond the interference, i.e. at longer wavelengths, the optical constants are more accurate.

The characteristics of the near infrared part of the spectrum correspond closely to those reported by Markov and Lindstrem (77). An increase in the absorption coefficient k is starting to occur on some samples at the very short wavelengths. This undoubtedly corresponds to the absorption band reported by Hodgson (78) who suggests that the cause is an electronic transition between the valence and conduction bands. Too little is known about the constant energy surfaces away from the Fermi level, however, to confirm this point of view.

Beyond this absorption other investigators (Markov, Schulz(79), Hodgson) and the present research agree; there is a region of low absorption before the free electron absorption starts in the far infrared. These characteristics, it is interesting to note, are quite similar to those of a relatively pure semiconductor but occur at shorter wavelengths.

Some overlap between the near infrared interband absorption and that due to the free electrons may occur. An approximate upper limit may be put

on the contribution of the transition to the conductivity beyond 30 microns. If, for example, Sample J is examined - this sample is chosen as it is sufficiently thin to give good optical results in the near infrared - the optical conductivity from equation (9) is found to be 3×10^4MKS at 5 microns wavelength. The contribution of electronic transitions to the conductivity at long wavelengths compared to the transition falls off approximately as the square of the frequency (50). Thus only $\sim 0.08 \times 10^4$MKS of a total conductivity of 2.5×10^4MKS at 30 microns could be due to this transition.

It is perhaps relevant to note that values of n and k near 3 microns have been reported by Schulz (79) and Markov and Lindstrem (77) each to an accuracy of $\sim \pm 20\%$. The disagreement between their values is much larger. While some of this discrepancy is probably due to the different samples used, it has been suggested (41), however, that this is partly due to the large values of $\partial n/\partial R$, $\partial n/\partial T$, etc. Since the only requirement that has been placed on the optical results of this investigation is that they reproduce the experimental reflectances and transmittances to $\pm$ 0.005, i.e. to comfortably within experimental tolerance, it is probable that the wide spread of some of the results reported here does not imply any greater absolute uncertainty than in other reported results.

D. Free Electron Effects.

A classical optical theory has been used to calculate the conductivity in the far infrared region of the spectrum. This has meant that any anomalous skin effect is ignored. In Section IV this proved to be a satisfactory assumption for the thinnest samples and held for the thickest when

$$\frac{\ell}{\omega\tau} < 0.3 \text{ microns}$$

where ℓ is the mean free path. $\omega\tau$, according to the relaxation time obtained, is equal to 1 at 100 microns wavelength. The best estimates of ℓ at room temperature are in the order of 0.02 to 0.2 micron (16) for single crystals. The lower conductivity of the present deposits would suggest that ℓ for the films is a factor of 3 smaller. Accordingly, the inequality may not be large at the longest wavelengths but will be sufficient to make the anomalous skin effect small compared to the experimental uncertainty at those wavelengths.

The relaxation times are given for the 6 thick deposits in Table 9. It is noteworthy that there is a very close correspondence between the relaxation time of the elctron and the d.c. conductivity of each of these samples. This is, of course, to be expected if 77% of the conduction is due to electrons. These relaxation times are between 4 and 6 times longer than those values obtained by Harris and Loeb (49) using the data of Wottersdorff for deposits of similar resitivity.

It should be noted that the values obtained for the relaxation time are virtually independent of any assumptions concerning the orientation of the deposits. They are, however, dependent on the assumpton that perturbations to the electron Fermi distribution will decay exponentially on the removal of the perturbing force, and that the decay constant, τ, will be independent of the direction of the perturbing force.

The determination of the other parameters is, however, strictly dependent on the validity of the model developed in Section V. The axial parameters, α_1 and α_2 can be calculated from the results in Table 9. The six samples give $\alpha_1 = 126 \pm 8$, $\alpha_2 = 2.1 \pm 0.2$, where the limits represent the spread for the six samples. The best values obtained from cyclotron resonance are probably $\alpha_1 = 168$, $\alpha_2 = 2.0$, $\alpha_3 = 100$ based on the same axes but including a $5^\circ 45'$ tilt of the ellipsoids (16,18). The values $\alpha_1 = 114$, $\alpha_2 = 0.56$, $\alpha_3 = 43$, have also been reported (80) from other cyclotron resonance results.

This agreement may be fortuitous. Certainly, in order to explain a positive Hall coefficient together with a conductivity which is largely due to electrons, a high degree of anisotropy of the constant energy surfaces is required. However, the uncertainty for the individual samples shown in Table 8 is very large. Also, there is little reason to expect the deposits to be so well oriented. Disorder, according to the cyclotron resonance parameters above, should increase the value α_2. Unfortunately there is no way with the present model to evaluate α_3 using thin deposits.

The values of α for the present samples are strictly dependent on the value assumed for the number of electrons. A higher value would lower α_1 and α_2 and increase the ratio of α_1/α_2. However, the number of electrons appears reasonably well established (16) and the present investigation determines the relaxation time quite accurately, so the absolute magnitudes of the α's are probably quite good. Most of the uncertainty is reflected in the ratio α_1/α_2. An estimate of the uncertainty of this ratio is given by the spread in the average values for each sample from Table 8 i between 38 and 230.

A possible second explanation for the positive Hall coefficient woul be the trapping of electrons on the surfaces of the deposits. This certainly occurs to some extent and appears to be important with the thinnes samples. However, to obtain a positive Hall coefficient with a high degree of disorder would require so much trapping that there would be insufficient electrons left to explain the far infrared observations. This, of course, results from the very large negative Hall coefficient for the magnetic field perpendicular to the trigonal axis. One would also expect to see an appreciable change in the properties with thickness for the thick films, if surface trapping were important. Such changes only exhibit themselves strongly with the four thinnest samples.

Other assumptions as to the band structure and the relative lengths of the relaxation times for the hole and electrons may completely change the analysis of the anisotropy of the ellipsoids. Falt and his co-workers (30) have reported a light effective mass for the holes in bismuth from cyclotron resonance work. This would suggest a smaller differential between the relaxation times of the holes and the electrons with the result that the contribution to the conductivity from the holes may not be entirely damped out at the infrared frequencies. Due the τ^2 dependence of the optical conductivity, $\tau_p < 2\tau_e$ would be required to change the above analysis of the energy band ellipsoid anisotropy appreciably. If this inequality were to hold, the true anisotropy α_1/α_2 would decrease for the deposits. The ratio of conduction due to electrons to that due to holes would also decrease from the value of 3.3 determined in this investigation. In this connection it is interesting to note that Abeles and Meiboom (2) obtain a value for this ratio of 2.1 from d.c. galvanomagnetic measurements and an anisotropy α/α_2 of 40.

A model consisting of two valence bands, one with a light effective mass and one heavy, has been suggested (81,61) to reconcile the Galt light effective mass with specific heat (82) and low temperature resistivity data. The experiments of this investigation, however, have obviously too little resolution to permit speculation on such band structures. It should be noted that neither a very light effective mass for the holes nor a more complex valence band will change the main results of this investigation which are the directly observed relaxation time for the electrons and the apparent high degree of orientation of the deposits.

Before examining the relationship between the relaxation times in the films and in single crystals, it is valuable to examine the available information concerning the mean free paths in bismuth. Aubrey and Chambers (16) have calculated a mean free path for the electrons of 0.02 to 0.2 microns and for the holes 0.5 to 1 micron from resistivity data on single crystals at room temperature. The experimental work reported here appears in conflict with these values. The increased scattering evident from the higher resistance of the deposited bismuth would be expected to reduce the hole mean free path more than that of the electrons and make observation of a large positive Hall coefficient impossible. It may be reasonable to expect (89) that the holes, being in an almost filled band with few empty states to be scattered into, would be relatively insensitive to scattering centers. However, the small effective mass m_0/α_1 would have the same effect on the electrons by giving the electron waves an unusually long wavelength. Indeed, microwave measurements on single crystals (61) indicate specular rather than the usual diffuse scattering of other metals (83) occurs at the surfaces.

The hole mean free path is probably similar or somewhat smaller than that of the electrons. It cannot, however, be much smaller without making the negative Hall coefficients of the high resistance films of Buckel (67,68) hard to interpret.

With this in mind, it appears reasonable to assume that the mean free paths of the electrons and holes are approximately equal and that they are affected by scattering centers in a similar way. This implies that $\sigma_{dc} \propto \tau_n$ where σ_{dc} is the conductivity of the film or single crystal bismuth, τ_n the electronic mean free time of the sample.

On this basis the electronic relaxation time for a pure bismuth crystal is 1.6×10^{-13} sec. at room temperature. This is quite comparable with the value of 1.0×10^{-13} sec. estimated from conductivity and cyclotron resonance measurements on single crystals (16). It should be emphasized that while there is some uncertainty in the value determined in this investigation due to the extrapolation from deposit to single crystal, this value is considerably more dependable due to its origin in direct observation rather than as a function of other parameters whose values are still in doubt.

The effective masses for the electrons in the plane parallel to the substrate are given by the reciprocal values of α_1 and α_2, i.e. $0.0079m_0$ and $0.5m_0$ where m_0 is the mass of the free electron.

In summary it may be said that the transport parameters for the electrons in bismuth derived from far infrared optical measurements on thin vacuum deposited films are in very good agreement with those derived from other measurements on single crystals. The observed relaxation time is in close agreement with the previous estimated value.

For the valence band the agreement is not so complete. There is good evidence that the mean free path of the holes is shorter by about a factor of 5 from previous estimates. Neither the relaxation time nor the effective mass of the holes has been determined.

E. Failures of the Theory.

Other than the x-ray and electron diffraction study, two effects have defied quantitative interpretation. These are the magnetic field dependence of the Hall coefficient and the optical conductivity of the very thin deposits.

Figure VII c shows that the experimental conductivity is considerably more than that expected from a free electron model indicated by the solid curves. This may be summarized by Table 10. Two characteristics are apparent.

TABLE 10

Increased Optical Conductivity of Very Thin Deposits

Sample	Thickness Å	Incremental Conductivity (MKS) 30 microns	50 microns
N	570	3.5	1.5
H	450	4	3.7
Q	347	3.2	2.2
L	220	5.2	5

First is that the contribution to the conductivity increases with decreasing thickness, and secondly that there is only a small decrease with increasing wavelength. The anomaly of Sample Q will be discussed presently. The first of these characteristics suggests that the effect is independent of thickness and implies a surface absorption. The second,

namely the small decrease with increasing wavelength, defies explanation in terms of a single transition. Since kT at room temperature corresponds to approximately 40 microns wavelength, the effect appears to be due to a series of very shallow surface states capable of trapping electrons.

The small values for Q in Table 10 may result from the assumed relaxation time used to give the solid curve. If this relaxation time were actually longer, i.e. the low conductivity of Q not being entirely due to a small relaxation time, larger values in Table 10 would result. In turn, this suggests that part of the high resistivity of Sample Q is due to a reduction in the number of electrons by surface trapping. Such surface trapping can easily explain the poor curve fit of Sample J at the short wavelengths and the increased Hall coefficients of the thin samples.

These surface states are probably quite similar to those observed in semiconductors (84), however, the higher electron concentration of a metal makes their effects generally less evident.

The failure of the theory to predict quantitatively the field dependence of the Hall coefficient is disappointing. The good agreement between the field dependence observed by Leverton and Dekker (20) and that reported here indicates that the problem is theoretical. While accurate Hall effect measurements for single crystals are scarce in the region 5 - 10 kilgauss, the theory presented here is not satisfactory at higher fields (2) for single crystals. The observed changes may be due to the small dimensions of the samples, but this is doubtful since the effects diminish, not increase, with decreasing thickness (85). Another possible cause may be a quantization of the energy bands by the magnetic field producing changes in the ellipsoidal anisotropy (15).

F. Optical Characteristics of Thin Bismuth Deposits

The infrared spectrum of the bismuth deposits may be broken into four regions. In the far infrared there is a region of high metallic reflection rather like that encountered in a metal such as gold in the near infrared. As the wavelength decreases the finite relaxation time causes a decrease in the conductivity and, therefore, in the reflection. The dielectric constant (n^2-k^2) changes sign from negative which is characteristic of a metal to positive. This change in sign displays itself in the form of the reflection minimum near 30 microns. At shorter wavelengths the optical properties are determined by electronic transitions rather than free electrons. Some absorption is caused by surface states, and eventually the interband transition of the very near infrared becomes predominant. Interference patterns exhibit themselves with samples which are sufficiently thick.

It is noteworthy that the negative Hall coefficient Sample 0 has the same infrared characteristics including the reflection dip at 30 microns which is in accord with an isotropic relaxation time.

VIII. SUGGESTIONS FOR FUTURE WORK

The need for better structure determination work is most obvious. Similar experiments to those carried out by Lane (63) or Büssem and co-workers (64) may not be the answer. While the x-ray work reported here tends to emphasize any disorder, their experiments would similarly emphasize the ordered crystallites. A possible solution would be a series of quantitative intensity measurements. Movement of the deposit in the plane of the substrate during exposure would tend to give a better sampling of the crystallites. A comparison of intensities with those from the usual spherical single crystals would be difficult but not impossible. The planar shape of the deposits should be simple enough to permit analytical comparison with a spherical crystal.

Infrared measurements at elevated and low temperatures would give interesting information concerning the surface states. It is doubtful, however, that sufficiently high temperatures could be reached to ionize most of the surface states and permit a clear examination of the free electrons in very thin deposits.

It would be of great interest to use a similar analysis to that reported here to examine the relaxation time for the holes in bismuth. The validity of the assumption of a long relaxation time for the holes made in the present analysis of the electronic enery band anisotropy could be

determined. Information on the veracity of the Galt light effective mass for the holes (80) would also be forthcoming. The influence of the holes on the conductivity may be increased by the doping of the deposits with an acceptor impurity such as tin. Since the relaxation time for the holes is probably longer than that for the electrons, it may be necessary to extend any optical measurements beyond the 150 micron maximum of the present work.

Similar work on bismuth deposits using lead as an acceptor is already in progress (75).

The uncertainties in Figure VII demonstrate the need for more accurate measurements at long wavelengths. While larger optics (24,87) have been shown to give some improved accuracy at these wavelengths, it is uncertain whether substantial improvement can be made with conventional techniques. New instrumentation such as that developed by Genzel (88) may be adaptable to quantitative spectroscopy and allow substantially better measurements.

APPENDIX I

Geometry of Samples and Methods of Mounting

Except for the film thicknesses, the geometry of the series of samples used for optical and Hall effect measurements was kept constant.

The aluminum oxide substrates were mounted on Pyrex rings 25 mm o.d., 22 mm. i.d., approximately 4 mm deep. The silver electrodes and then bismuth were deposited through masks with the geometry shown in Figure VIII. The edges of the masks were bevelled and the masks mounted approximately 0.1 mm. from the surface of the substrate.

The films were mounted for optical measurements in circular apertures in brass plates as shown in cross-section in Figure VIII.

For Hall effect and resistance measurements the films were placed in a lucite holder. Contact was made to the silver electrodes and probes by means of phosphorbronze springs on which silver contacts were soldered. After mounting each film in the holder the contacts were lowered on to the top of the glass frame where the aluminum oxide and silver of the deposited electrodes overlapped the glass. Contacts made in this manner had very low resistances ($\sim$ 0.01 ohms) and no case of failure was experienced. Since the resistance of the films was measured by a four probe technique (see Appendix IV) and the Hall voltmeter had a 12 megohm input impedance, the contact resistances were immaterial.

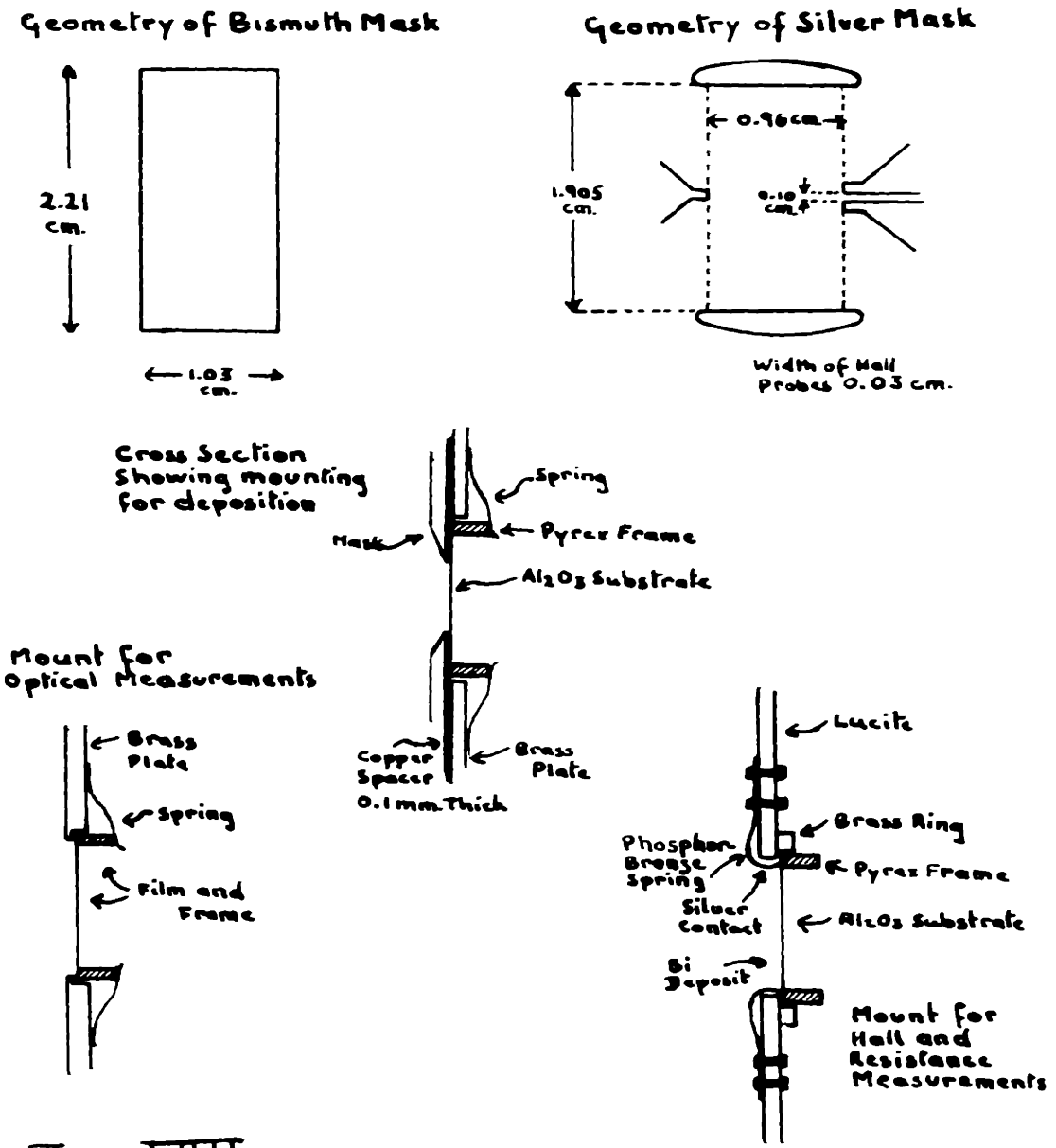

Fig. VIII

Geometry of Samples and Holders

APPENDIX II

Details of the Preparation of the Bismuth Deposits

The bismuth used in this investigation was "spectroscopically pure" and supplied by the Cerro De Pasco Copper Corporation, 40 Wall Street, New York 5, N.Y. According to the laboratory report (#67500) the batch was prepared by numerous recrystallizations of commercially pure bismuth (less than 0.001% impurity) and it is "very probable that the total metallic impurities do not exceed 0.0001%." The sulfur impurity was claimed to be less than 0.0001%.

This bismuth was recrystallized under vacuum.

The vacuum deposition equipment used to prepare the samples has been described by D. Metzger (40). The bismuth was premelted in a tantalum boat heated by electron bombardment. An electronic feed-back control gave a constant evaporation rate. After an initial increase in pressure due to degassing in the vacuum system, a shutter was opened exposing the substrate to the evaporation source. Evaporation rates of between 300 and 500 Å /minute were used depending on the sample.

A vacuum of better than 10^{-5} mm Hg was maintained with the use of a liquid nitrogen trap during the deposition. After the time of controlled evaporation required to provide a given thickness, the shutter was closed and evaporation stopped.

The films were then heated *in situ* to 175 to 180° C over a period of two hours. They were maintained at this temperature for two hours before cooling slowly.

APPENDIX III

Infrared Properties of Aluminum Oxide Films.

The mathematical treatment of the optical data given in Section IV was based on the assumption that the substrate was non-absorbing and thin compared to the wavelength of the radiation.

The transmission and reflection spectra displayed in Figure IX show that this assumption is quite good for a 50 volt Al_2O_3 film throughout most of the spectrum but becomes poor in the region near 15 microns.

Since the mathematical problem of a computer program for two or more layers of absorbing thin films is at present being considered (41), it appears desirable to have the optical constants of the substrate material available. An accurate computation of the film properties in the region of 15 microns may thus be feasible.

The transmission and reflection spectra together with the optical constants computed from them have been reported by Harris (30) for the near infrared region. Figure IX and the computed optical constants in Table 11 effectively extend this work into the far infrared. The thicknesses used to compute the optical constants are based on the assumption of bulk density and a proportionality constant of 14 Å per volt (30).

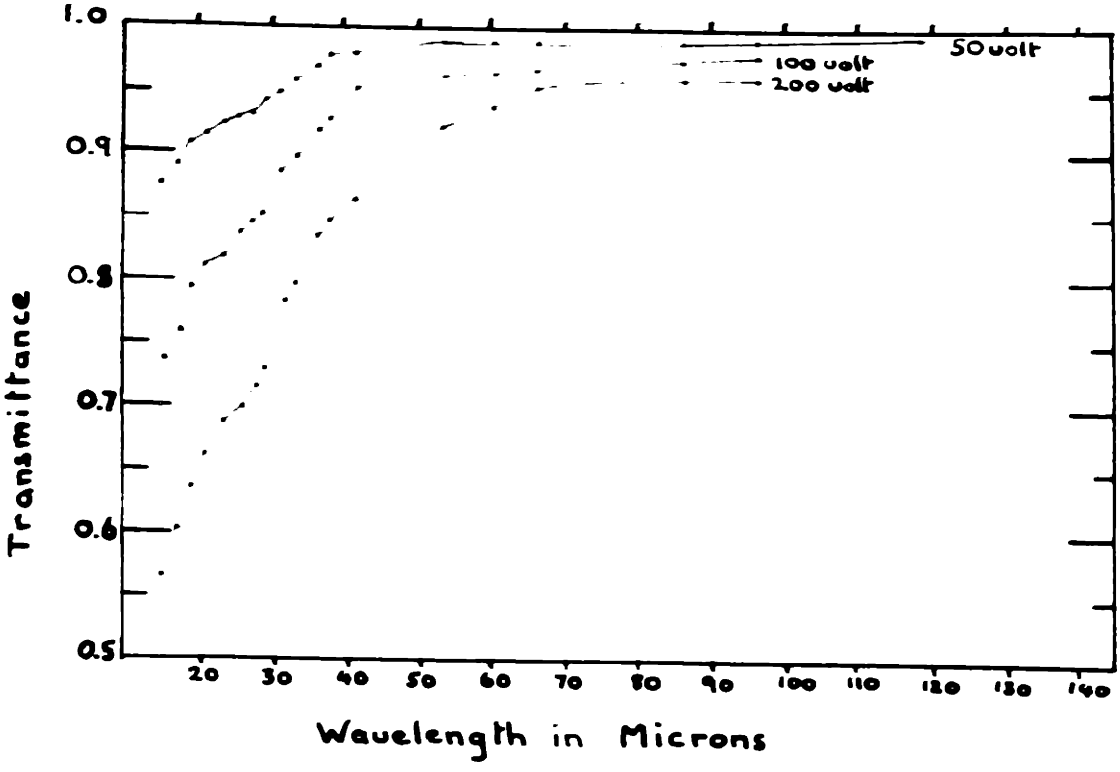

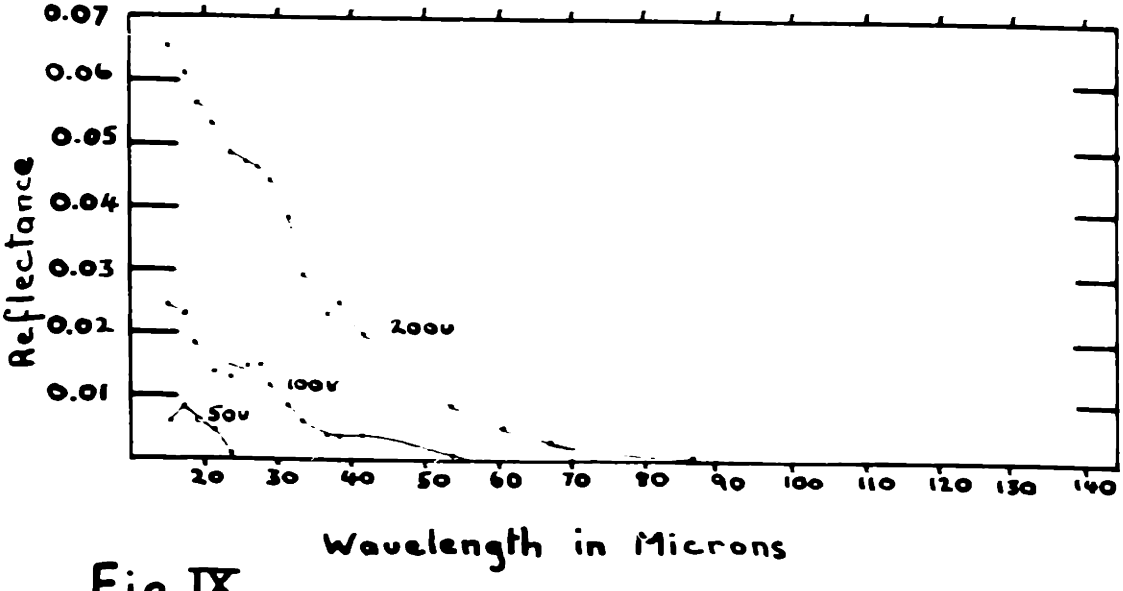

Fig. IX

Transmission and Reflection of Aluminum Oxide Films

TABLE 11.

Optical Constants of Al_2O_3 Films

Wavelengths	50 volt		100 volt	
(microns)	n	k	n	k
15.1	1.93 ± 1.0	1.21 ± 0.8	1.95 ± 0.3	1.42 ± 0.3
17.2	2.40 ± 0.7	0.94 ± 0.4	2.14 ± 0.3	1.32 ± 0.3
19.1	2.35 ± 0.8	0.88 ± 0.4	2.12 ± 0.4	1.21 ± 0.3
21.1	2.34 ± 1.0	0.92 ± 0.5	2.05 ± 0.5	1.29 ± 0.4
23.7			2.15 ± 0.5	1.29 ± 0.4
25.9			2.46 ± 0.4	1.06 ± 0.3
27.8			2.58 ± 0.4	1.0 ± 0.2
29.0			2.97 ± 0.3	0.62 ± 0.2
31.6			2.38 ± 0.6	0.86 ± 0.3
33.5			2.14 ± 0.8	0.97 ± 0.5
36.8			2.01 ± 1.0	0.86 ± 0.6
38.3			2.08 ± 1.0	0.77 ± 0.5

TABLE 11 (cont)

Wavelength (microns)	Optical Constants of Al_2O_3 Films 200 volt	
	n	k
15.1	1.78 ± 0.2	1.55 ± 0.3
17.2	1.98 ± 0.1	1.37 ± 0.2
19.1	2.08 ± 0.1	1.26 ± 0.1
21.1	2.19 ± 0.1	1.16 ± 0.1
23.7	2.27 ± 0.1	1.13 ± 0.1
25.9	2.39 ± 0.1	1.12 ± 0.1
27.8	2.48 ± 0.1	1.06 ± 0.1
28.0	2.25 ± 0.1	0.98 ± 0.1
31.0	2.53 ± 0.1	0.81 ± 0.1
33.5	2.39 ± 0.2	0.07 ± 0.1
36.8	2.35 ± 0.2	0.74 ± 0.1
38.3	2.48 ± 0.2	0.66 ± 0.1
41.5	2.42 ± 0.2	0.65 ± 0.1
53.5	2.20 ± 0.5	0.53 ± 0.2
60.6	1.96 ± 0.9	0.53 ± 0.3
66.6	1.77 ± 1.2	0.48 ± 0.5

APPENDIX IV

Galvanomagnetic Measurements

A. Hall Effect Measurements

As indicated in equation (1), the Hall voltage is generally directly proportional to the current. Since the present samples were mounted on very thin, and therefore low thermal mass substrates, heating effects become appreciable at quite low currents. It is, of course desirable to work with current densities well below of this range. In consequence the Hall voltages were quite small and required measuring equipment capable of accurately determining potentials as small as 5 microvolts.

Two experimental methods of making Hall effect measurements were evaluated. Each had some desirable as well as undesirable attributes.

1 An A. C. Method of Measurement

A simple a.c. Hall voltmeter was constructed using a two stage preamplifier (a 12AX7 tube) and a General Radio Model 736A wave analyzer. The latter served as a narrow band (4 cycle band width) amplifier. The primary current for the Hall voltage measurements was supplied by a Hewlett-Packard Model 200 AR audio-oscillator and controlled by a General Radio type 546-B microvolter.

This system had the advantage of high sensitivity (a noise level of approximately ± 0.025 microvolts) and freedom from the effects of stray thermal emfs. The main disadvantage was the non-linearity of the measuring circuit. The wave analyzer was linear to only about ± 2%, the preamplifier

to approximately ± 1%. Another disadvantage was the comparatively low input impedance of the preamplifier which introduced a correction term into the measured voltage on high resistance samples.

ii A.D.C. Method of Measurement

A d.c. circuit employing a Leeds and Northrup type 9835A stabilized d.c. microvolt amplifier was used for the Hall effect measurements reported here. The output of the amplifier was displayed on a Leeds and Northrup Speedomax G strip chart recorder. This resulted in a "floating zero" d.c. voltmeter with scales permitting the display of 50 up to 2000 microvolts full scale on the recorder. The limit of error of the amplifier is specified by the manufacturer as ± 0.4% of the reading, and the recorder uses a potentiometric method of measurement. This circuit was considerably more linear than the a.c. circuit described above. Also the input impedance of the meter was 12 megohms. The circuit was, however, subject to any stray thermal effects.

Since the measurements were made as a function of magnetic field and the variations were in the order of a few percent, the need for a linear circuit was the most important consideration. The effect of noise and drift could be largely eliminated by making a series of measurements and displaying them on a continuous chart.

Within the sensitivity of each set of equipment, the measured Hall effects were the same with a.c. and d.c., and were independent of audio-frequency and, within the limits of damaging the film, of current.

iii The Magnet

The magnetic field was supplied by an electromagnet with 2 inch pole faces and a variable gap width. The field was uniform to ± 0.7% over a 3.5 cm. diameter, and uniform to ±0.5% over the sample area. The magnetic field was varied by changing the magnet coil current.

iv Measurement of the Magnetic Field

A rotating coil fluxmeter was constructed using an a.c. synchronous electric motor. A split ring commutator rectified the output of the rotating coil. The filtered output was measured with a General Radio type 1230-A d.c. amplifier. An amplifier input impedance of 1 megohm proved adequate to yield negligible any resistance changes in the commutator-brush section. The d.c. amplifier and galvanometer were accurate to better than ±1% of full scale on the ranges used with the fluxmeter. Tests of the reproducibility of the fluxmeter system indicated that the accuracy of the meter was the limiting value.

The fluxmeter was calibrated with nuclear magnetic resonance devices to nearly 10,000 gauss. A slight fall off in the number of volts per gauss occurred at the higher fields according to the calibration.

v. Measurement of the Hall Effect

The circuit in Figure X was used to measure the Hall effect and resistance of the samples. The current through the sample was measured as an emf. drop across a peg box resistance (accurate to ± 0.5%) and displayed on the strip recorder.

The Hall voltage was determined by a "3-probe" method which introduces a potentiometer into the Hall probe circuit as shown in Figure X. Adjustment of this potentiometer reduces the "IR" drop caused by probes not being

located on equipotentials, until it is small compared to the Hall voltage. After the balancing of this potentiometer, the signal from the Hall probes consists mainly of the Hall voltage with a minor contribution due to thermal effects and the "IR" drop. As shown by Lindberg (42) the Hall voltage may be separated from other effects by making a total of four measurements changing the directions of the current and the magnetic field. Since the measuring circuit had a floating zero it was theoretically possible to determine the Hall voltage from only two measurements - the increases in signal when the current is pulsed through the sample with the magnetic field in the positive and negative directions. Practically this was found to introduce slight errors, so all four measurements were made.

The Hall coefficient in the films was a function of temperature as well as magnetic field. In order to express the results as a function of field only, it was necessary to determine the change in Hall coefficient as a function of temperature over the few degrees range in environmental temperature encountered during measurements. A copper-constantin thermocouple was placed approximately 1 mm from the surface of the film and a reference junction was set next to a thermometer in a heat reservoir. The thermal emf was measured on the Hall voltmeter.

The sample and pole gap were shielded to prevent air currents.

Noise and drift in the system were usually only a few tenths of a microvolt during a Hall determination. Generally the Hall voltages ranged from 5 to 100 microvolts and the primary current densities from 1 to 2×10^5 amp./m^2. The change in Hall effect with temperature was under 1% per degree for all except the thickest samples. The samples changed about 2^oC in temperature during a series of measurements, never more than 4^oC.

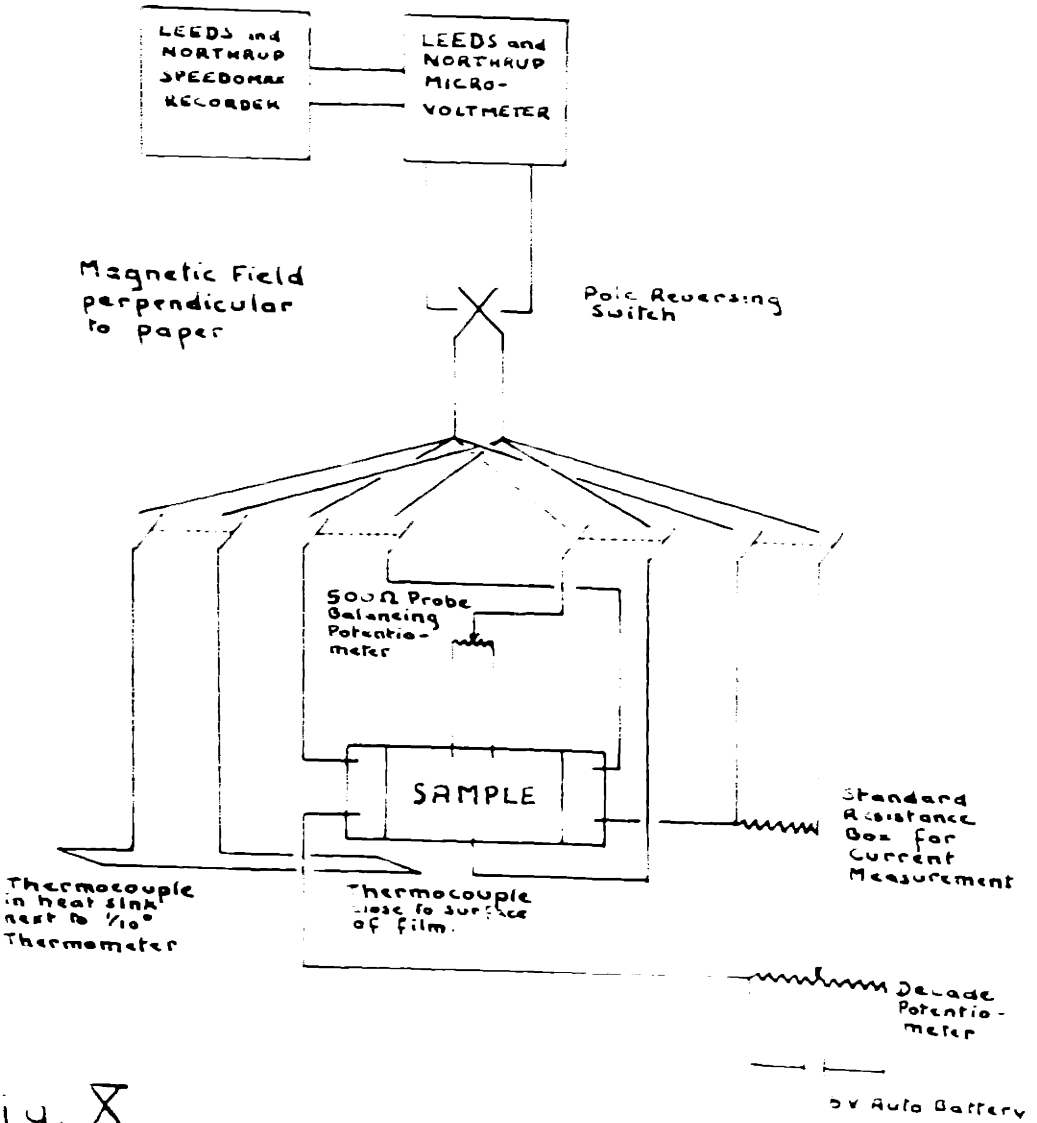

Fig. X

Hall Voltage Measuring Circuit

3. Resistance Measurements

The resistances of the samples were measured by a "4 probe" potentiometric technique. The circuit in Figure X was employed with the current passing through the standard resistance box and the sample in series. The emf drop between the two current electrodes on the sample was measured with a separate pair of probes.

By adjusting the resistance box so that the emfs across the box and the sample were almost equal, non-linearities in the voltmeter circuit were minimized and the sample resistance was given by the product of the box reading and the ratio of the two voltages.

Primary currents from 4 to 100 microamps were used to give potential drops in the order of 1 millivolt.

APPENDIX V

Some Magnetoresistance Measurements on Bismuth Films

Type of Substrate	Thickness	$\Delta\rho_{\parallel}/\Delta\rho_{\perp}$ (a)
Glass	2000 Å	2.14
	2500	1.97
	5000	1.04
	15,000	1.94
Glass with Al_2O_3(b)	2000	1.70

(a) Ratio of increases in resistance with field parallel and perpendicular to substrate at 10 kilogauss.

(b) Glass with aluminum oxide film placed on top, resultant surface was not very flat.

APPENDIX VI

Far Infrared Instrumentation and Measurements

A. Design and Construction of the Spectrometer.

The grating spectrometer used to make the infrared measurements beyond 15 microns was constructed around a Perkin-Elmer model 98 G monochromator base in a manner similar to that described by Lord and McCubbin (25).

The model 98 G is a single pass system converted for use with a diffraction grating. The wavelength drive was modified to permit 52° of rotation of the grating instead of the original 11°. The slit mechanism was changed to allow the slits to open to 6.0 mm rather than the customary 2 mm.

The optical path of the spectrometer is shown in Figure XI.

A source section was constructed to allow the use of two reflection filters and a crystal or metal shutter and chopper as desired.

The design of the detector section permits reflection and transmission measurements to be made on the samples with monochromatic radiation at foci.

This layout minimizes heating of the samples by the beam and permits the use of the smallest samples consistent with the aperture of the system. The image was 15 mm. high and from 3 to 6.5 mm. wide depending on slit width.

A transmission sample holder moves the sample in and out of the beam at normal incidence. A reflection sample table rotates with stops reproducing its position every quarter of a turn. A comparison of signals from a standard mirror and from a given reflection sample may thus be made.

The Golay cell detector and the reflection sample are at the near and far foci of a large elliptical mirror. The properties of the ellipse are such that small changes in the positions of the reflection sample do not affect the focussing of the system, and the beam image is condensed to one-fourth of the source size allowing most of the energy to enter the 3.2 mm window of the detector.

The detection system used to make the measurements reported here consisted of the 10 cycle metal chopper, Golay cell, and synchronous amplifier manufactured by the Eppley Laboratory, Inc. The amplifier output was displayed on a Leeds and Northrup Speedomax G strip recorder.

For all measurements at wavelengths beyond 50 microns the entire optical system was flushed with nitrogen to reduce atmospheric water vapor absorption.

B. Operating Conditions: Resolution and Filtering.

Since the properties of metals in the far infrared change relatively slowly with wavelength, there are no stringent resolution requirements for this type of spectroscopy in contrast with those for molecular studies. The measurements, however, are quantitative requiring a relatively large signal to noise ratio and very little stray radiation.

With these factors in mind the set of operating conditions given in Table 12 was developed. Two sources were used for the work described here. In the range 15 to 90 microns the source consisted of a platinum wire spiral coated with Sauereisen resistor cement. The cement surface was coated with tantalum pentoxide powder. Beyond 90 microns the quartz mercury arc section of a General Electric H 100-L4 lamp was used.

All of the gratings mentioned in Table 12 were obtained from the Bausch and Lomb Co. and have blaze angles of 26° 45'. The reststrahlen plates have ground surfaces to scatter visible and near infrared radiation. The ground mirrors consist of "flat" glass plates ground with carbide grit of the size indicated and vacuum coated with aluminum.

The filtering was evaluated by making reflection and transmission measurements on a variety of materials (salt plates, gold blacks, etc.) whose characteristics were such as to accent the presence of unwanted higher or lower order radiation.

The calibration of the wavelength drum for each of the gratings was made using the water vapor absorption lines given by W. Benedict (43) and those of Randall (44).

The agreement between the observed lines and those from the literature indicated that the calibration did not err by more than 0.2 microns anywhere.

C. Method of Making the Measurements.

Transmission measurements were made by measuring the output of the detector with the sample in and out of the infrared beam. The ratio of the outputs gave the transmittance directly.

Reflection measurements consisted of determining the ratio of the signals reflected from standard gold mirrors and bismuth samples. The reflection standards were the samples described by Fowler (45) who determined their reflection to 0.1 to 0.2%. A correction for the finite absorptance of these gold mirrors was made.

No correction was made for the substrate absorption in any spectral region.

TABLE 12

Spectrometer - Operating Conditions

Spectral Region (microns)	Radiation Source	Diffraction Grating	Order	Slit Width	Wave Length Equivalent ** (microns)
15-25	Ta_2O_5	20L/mm.	1	3.0 mm.	0.5
25-34	Ta_2O_5	20L/mm.	1	3.0 mm.	0.5
34-45	Ta_2O_5	20L/mm.	1	4.5 mm.	0.65
45-48	Ta_2O_5	20L/mm.	1	4.5 mm.	0.65
48-50	Ta_2O_5	20L/mm.	1	4.5 mm.	0.65
50-62	Ta_2O_5	8L/ mm.	2	6.0 mm.	0.95
62-80	Ta_2O_5	8L/ mm.	1	6.0 mm.	1.9
80-90	Ta_2O_5	8L/ mm.	1	6.0 mm.	1.9
90-100	Quartz Hg Arc	8L/mm.	1	6.0 mm.	1.9
beyond 100	Quartz Hg Arc	8L/ mm.	1	6.0 mm.	1.9

** Corresponds to twice the half-width of the wavelength spread of the monochromatic beam. Resolution would be substantially better.

TABLE 12 (cont'd)

Spectrometer - Operating Conditions

Filter Combinations

Spectral Region (microns)	Trans-mission	Rest-strahlen	Zero Order Grating	Ground Mirrors (grits)
15-25	sooted poly-ethylene	LiF	300L/mm.	400 320
25-34	"	NaF	"	"
34-45	"	"	"	"
45-48	"	NaCl	"	"
48-50	1mm. quartz sooted	"	"	"
50-62	"	"	"	"
62-80	"	KCl	"	"
80-90	"	KBr	"	"
90-100	"	KI	"	"
beyond 100	3mm. quartz sooted	KRS-5	20L/mm.	"

TABLE 12 (cont'd)

Spectrometer - Operating Conditions

Spectral Region (microns)	Uncertainty in Measurements *
15-25	±0.8 **
25-34	±0.8
34-45	±0.8
45-48	±1.0
48-50	±1.0
50-62	±1.3
62-80	±1.3
80-90	±1.3
90-100	±1.3
beyond 100	±2.0

* Based on amount of detected impurity in beam, noise level, linearity of detection equipment, etc.

** e.g. (30±0.8)%

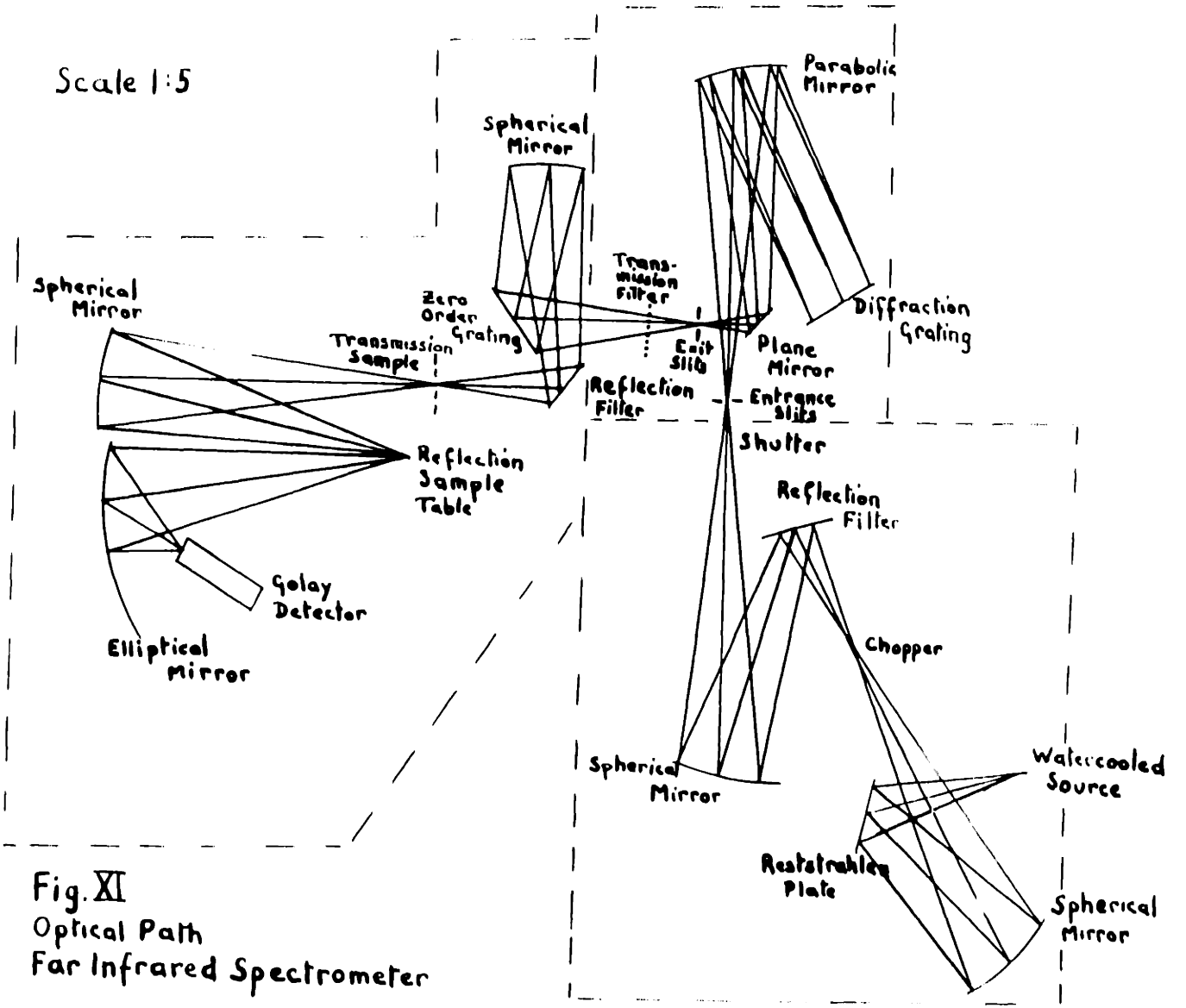

Fig. XI
Optical Path
Far Infrared Spectrometer

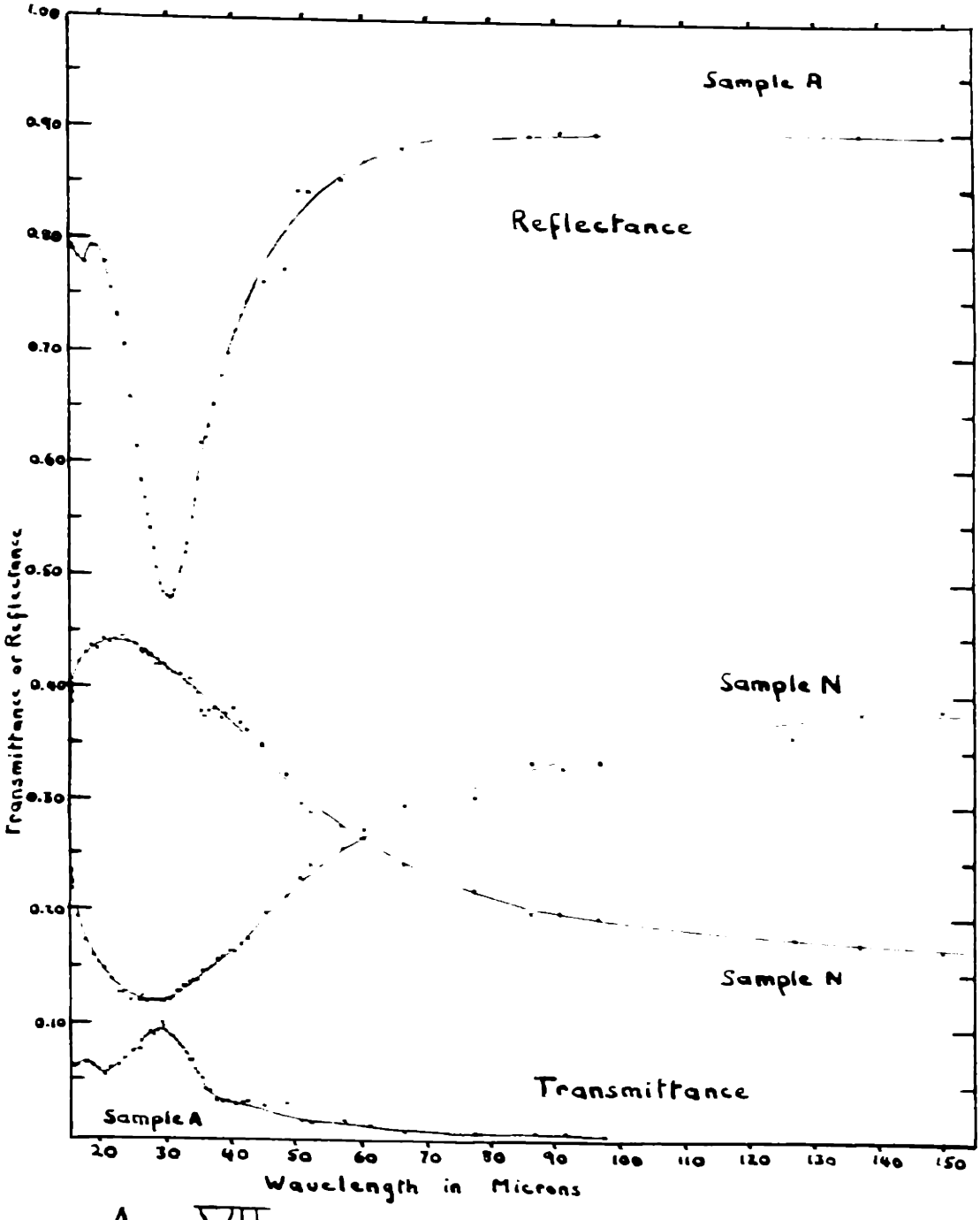

App. VII Reflectance and Transmittance - Samples A, N

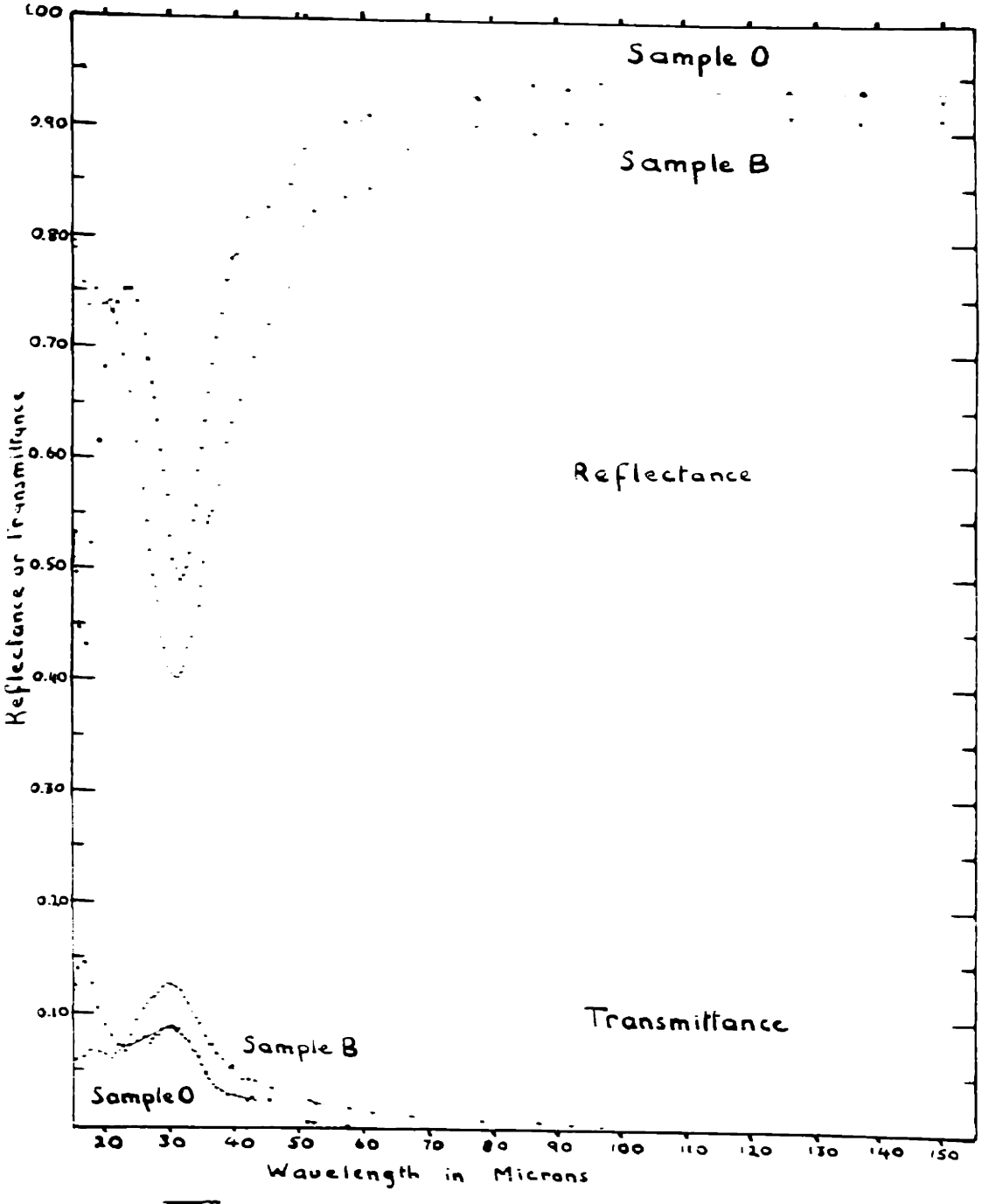

App. VII cont. Transmittance and Reflectance - Samples B, O

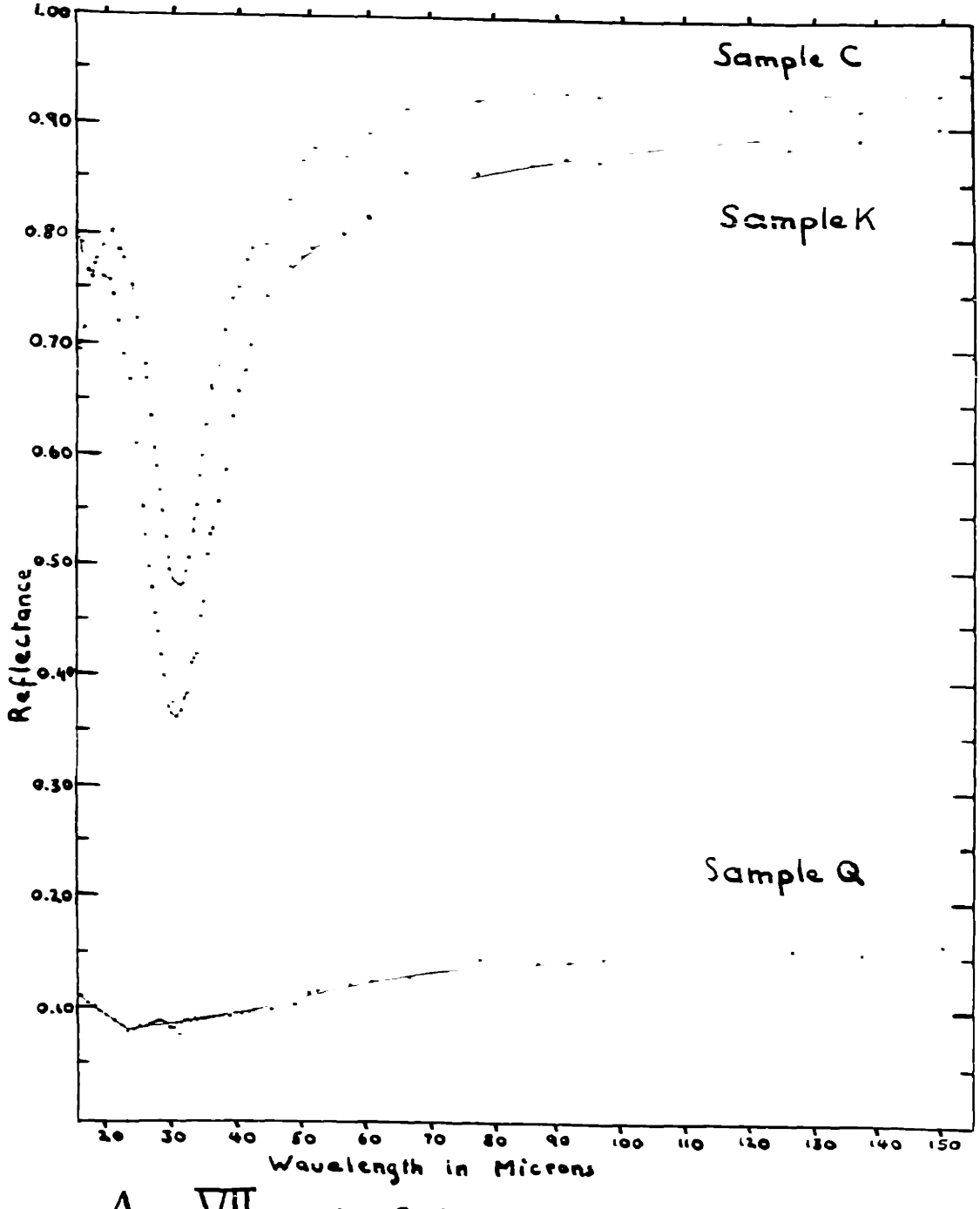

App. VII cont. Reflectance of Samples C, K, Q

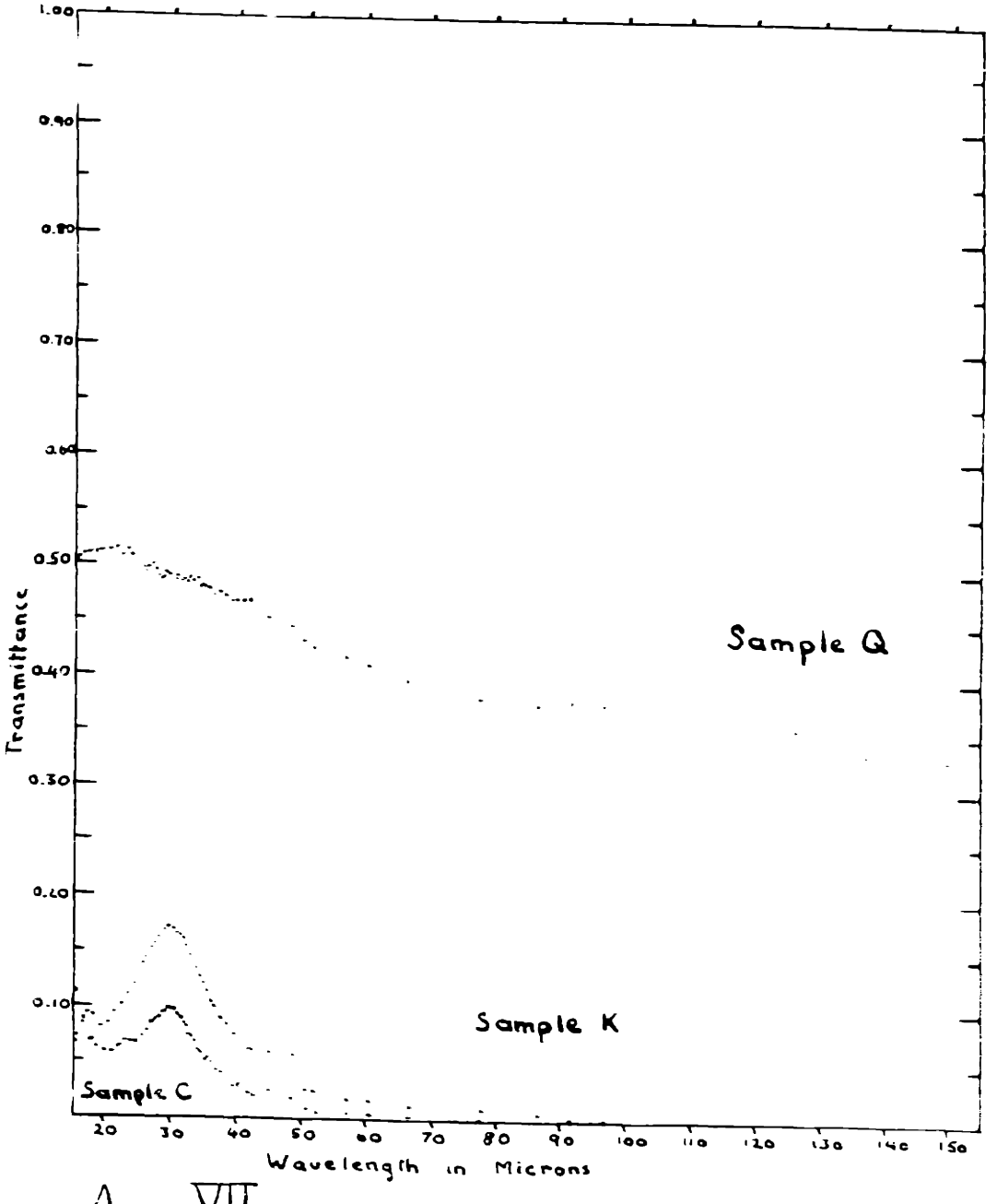

App. VII cont Transmittance of Samples C, K, Q

APPENDIX VIII

Operating Conditions: Near Infrared Spectrometer

The optical measurements between 1.5 and 14 microns were made with a standard Perkin-Elmer Model 12B sodium chloride prism monochromator. The wavelength drum was recalibrated with H_2O, CO_2 and NH_3 spectra as described in the Perkin-Elmer instruction manual for the instrument, 1956 edition.

A metal shutter was used throughout the range. The radiation was pure except for 2% and 3% scattered 4 micron radiation at 13 microns and 14 microns respectively.

Slit Widths Used

Wavelength Range	Slit Width
1.5 - 4.9 microns	0.3 mm
5.0 - 5.9	0.4
6.0 - 6.9	0.5
7.0 - 7.9	0.6
8.0 - 8.9	0.7
9.0 - 9.9	0.8
10.0 - 10.9	0.9
11.0 - 11.9	1.0
12.0 - 12.9	1.1
13.0 - 14.0	1.2

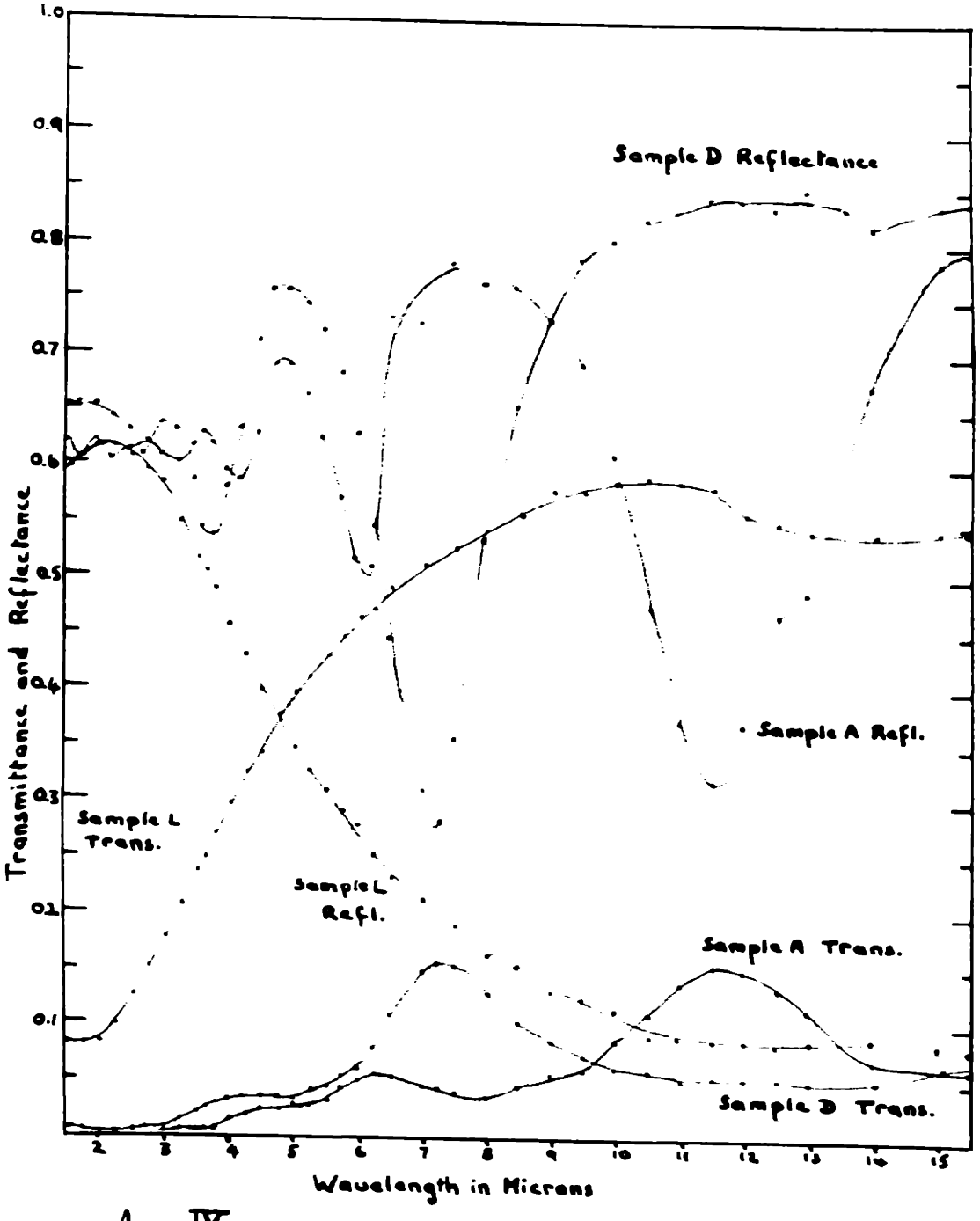

App. IX Near Infrared Transmittance and Reflectance Samples A, D, L

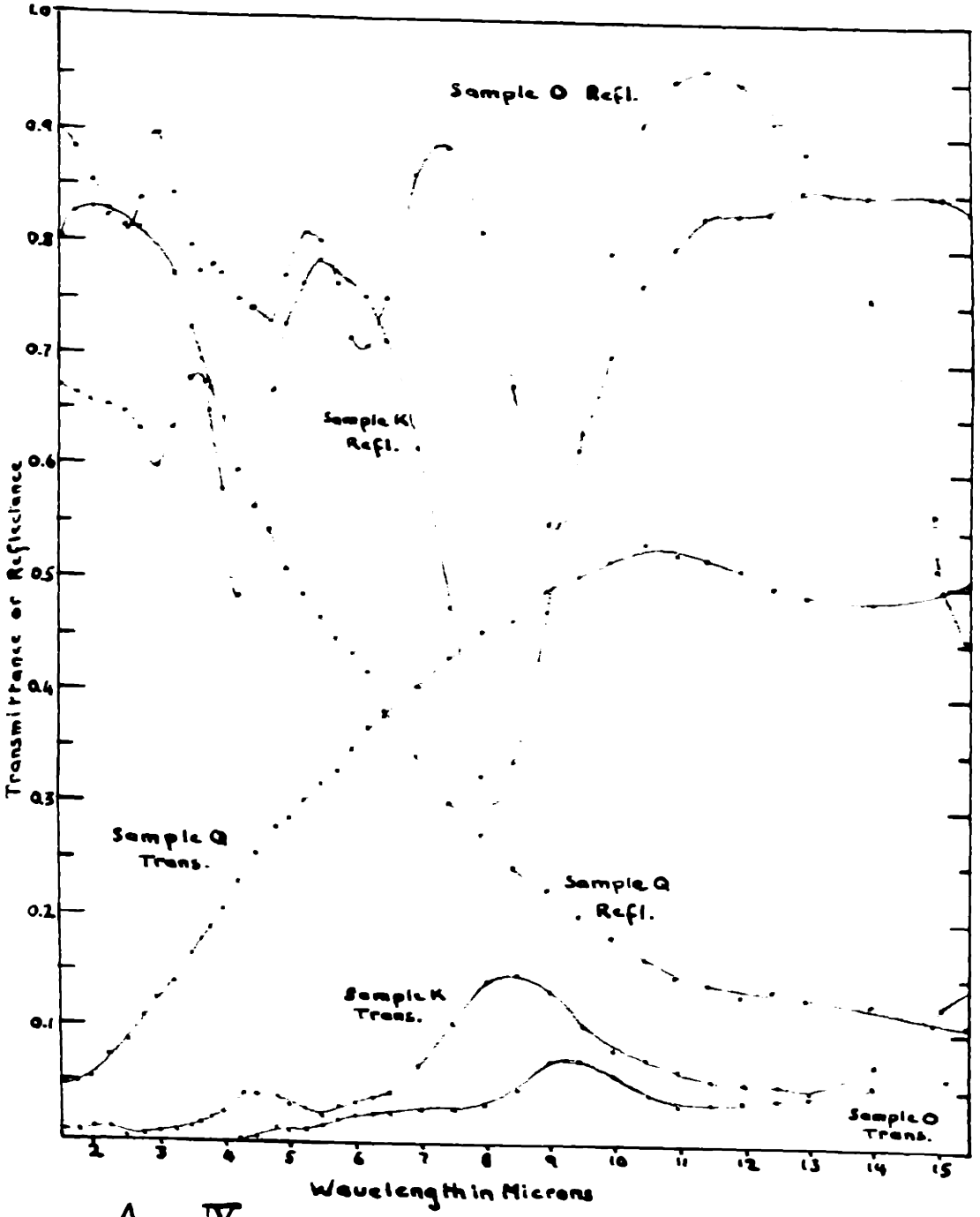

App. IX cont. Near Infrared Transmittance and Reflectance Samples K, O, Q

APPENDIX X

Solutions of Boltzmann's Equation

$$\frac{\partial f_1}{\partial t} - e\left(\vec{\mathcal{E}} + \vec{v} \times \vec{H}\right) \cdot \overrightarrow{\text{grad}}_{\vec{p}}\, f_0 = -\frac{f_1}{\tau} \qquad \text{(A-1)}$$

Equation (A - 1) above was derived in Section V. Two solutions to this equation are of interest here.

A. The Current Resulting from the Action of a Sinusoidal Electric Field on a Single Energy Band Ellipsoid.

This corresponds to the case of infrared frequencies when the negligible contribution of the $\vec{H}$ vector is ignored.

Writing $\vec{\mathcal{E}} = \vec{\mathcal{E}}_0 \exp(i\omega t)$ and assuming a similar time dependence for f_1, equation (A - 1) becomes

$$i\omega f_1 - e \exp(i\omega t)\vec{\mathcal{E}}_0 \cdot \overrightarrow{\text{grad}}_{\vec{p}}\, f_0 = -\frac{f_1}{\tau} \qquad \text{(A-2)}$$

$$f_1 = \frac{e\tau \exp(i\omega t)}{1 + i\omega\tau}\, \vec{\mathcal{E}}_0 \cdot \overrightarrow{\text{grad}}_{\vec{p}}\, f_0 \qquad \text{(A-3)}$$

Now the current density $\vec{J}$ is given by (90)

$$\vec{J} = -e \int n \vec{v} f_1 \, dp \qquad \text{(A-4)}$$

where n is the number of carriers in the ellipsoid.

Since $\vec{v} = \overrightarrow{\text{grad}}_{\vec{p}} E$ we may use equations (14) and (16) and integrate equation (A - 4) in the manner of Wilson (90) (Chapter 8) to give

$$\vec{J} = \frac{n e^2 \tau_n \exp(i\omega t)}{m_0(1 + i\omega\tau_n)} \begin{vmatrix} \alpha_1 & 0 & 0 \\ 0 & \alpha_2 & 0 \\ 0 & 0 & \alpha_3 \end{vmatrix} \begin{vmatrix} \mathcal{E}_1 \\ \mathcal{E}_2 \\ \mathcal{E}_3 \end{vmatrix} \qquad \text{(A-5)}$$

where $\mathcal{E}_1$, $\mathcal{E}_2$, and $\mathcal{E}_3$ are the components of $\vec{\mathcal{E}}_0$ referred to the axes on the ellipse.

A similar expression may be obtained for the valence band ellipsoid

$$\vec{J} = \frac{p e^2 \tau_p \exp(i\omega t)}{m_0(1 + i\omega\tau_p)} \begin{vmatrix} \beta_1 & 0 & 0 \\ 0 & \beta_1 & 0 \\ 0 & 0 & \beta_3 \end{vmatrix} \begin{vmatrix} \mathcal{E}_1 \\ \mathcal{E}_2 \\ \mathcal{E}_3 \end{vmatrix} \tag{A-6}$$

3. The Current Resulting from a Constant $\vec{\mathcal{E}}$ and $\vec{H}$ Field on a Single Ellipsoid

In this case $\frac{\partial f_1}{\partial t} = 0$ so equation (A-1)

becomes

$$-e(\vec{\mathcal{E}} + \vec{v} \times \vec{H}) \cdot \overrightarrow{\text{grad}}_p f_0 = -\frac{f_1}{\tau} \tag{A-7}$$

$$f_1 = e\tau(\vec{\mathcal{E}} + \vec{v} \times \vec{H}) \cdot \overrightarrow{\text{grad}}_p f_0 \tag{A-8}$$

we may again substitute into equation (A-4) and integrate. This integration is fairly involved and is given in Wilson (90) pages 224-225. Neglecting terms in H^3 and higher the following result is obtained (2).

$$\vec{J} = \frac{n e^2 \tau_n}{m_0} \begin{vmatrix} \alpha_1 & 0 & 0 \\ 0 & \alpha_2 & 0 \\ 0 & 0 & \alpha_3 \end{vmatrix} \left| \vec{\mathcal{E}} + \frac{1}{ne} \vec{J} \times \vec{H} \right| \tag{A-9}$$

APPENDIX XI.

The Conductivity Matrix

Expressions (A-5) and (A-6) in Appendix X represent the contributions to the conductivity of single energy ellipsoids. To determine the total current, the contributions of all four ellipsoids must be added. If we arbitrarily take the axes of a single conduction band ellipsoid as a frame of reference, the other two ellipsoids in that band must be transformed by a similarity matrix $\underline{S}$.

$$\underline{S} = \frac{1}{2}\begin{vmatrix} -1 & \sqrt{3} & 0 \\ -\sqrt{3} & -1 & 0 \\ 0 & 0 & 2 \end{vmatrix} \qquad \text{(A-10)}$$

The current contribution of the holes will be

$$\vec{J}_p = \frac{pe^2\tau_p}{m_0(1+i\omega\tau_p)}\begin{vmatrix} \beta_1 & 0 & 0 \\ 0 & \beta_1 & 0 \\ 0 & 0 & \beta_3 \end{vmatrix}\vec{\mathcal{E}} \qquad \text{(A-11)}$$

from equation (A-6), and the contributions from the 3 electron energy band edge ellipsoids

$$\vec{J}_1 = \frac{N}{3}\frac{e^2\tau_n}{m_0(1+i\omega\tau_n)}\begin{vmatrix} \alpha_1 & 0 & 0 \\ 0 & \alpha_2 & 0 \\ 0 & 0 & \alpha_3 \end{vmatrix}\vec{\mathcal{E}} \qquad \text{(A-12)}$$

$$\vec{J}_2 = \frac{N}{3}\frac{e^2\tau_n}{m_0(1+i\omega\tau_n)}\underline{S}\begin{vmatrix} \alpha_1 & 0 & 0 \\ 0 & \alpha_2 & 0 \\ 0 & 0 & \alpha_3 \end{vmatrix}\underline{S}^{-1}\vec{\mathcal{E}} \qquad \text{(A-13)}$$

$$\vec{J}_3 = \frac{N}{3}\frac{e^2\tau_n}{m_0(1+i\omega\tau_n)}\underline{S}^{-1}\begin{vmatrix} \alpha_1 & 0 & 0 \\ 0 & \alpha_2 & 0 \\ 0 & 0 & \alpha_3 \end{vmatrix}\underline{S}\,\vec{\mathcal{E}} \qquad \text{(A-14)}$$

Adding expressions (A-12, 13, and 14) we obtain

$$\vec{J}_n = \frac{Ne^2\tau_n}{m_0(1+i\omega\tau_n)} \begin{vmatrix} \frac{\alpha_1+\alpha_2}{2} & 0 & 0 \\ 0 & \frac{\alpha_1+\alpha_2}{2} & 0 \\ 0 & 0 & \alpha_3 \end{vmatrix} \vec{\mathcal{E}} \tag{A-15}$$

(A-11) and (A-15) may be added to give a conductivity matrix

$$\sigma = \begin{vmatrix} \varphi_\omega\left(\frac{\alpha_1+\alpha_2}{2}\right) + \chi_\omega\beta_1 & 0 & 0 \\ 0 & \varphi_\omega\left(\frac{\alpha_1+\alpha_2}{2}\right) + \chi_\omega\beta_1 & 0 \\ 0 & 0 & \varphi_\omega\alpha_3 + \chi_\omega\beta_3 \end{vmatrix} \tag{A-16}$$

where

$$\varphi_\omega = \frac{Ne^2\tau_n}{m_0(1+i\omega\tau_n)} \qquad \chi_\omega = \frac{Pe^2\tau_p}{m_0(1+i\omega\tau_p)}$$

APPENDIX XII.

The Hall Coefficient

The following derivation is similar to that given by Abeles and Meiboom (2) and is presented here for the sake of completeness.

Rewriting equation (A-9) of Appendix X we obtain

$$\vec{J}_1 = ne \begin{vmatrix} \mu_1 & 0 & 0 \\ 0 & \mu_2 & 0 \\ 0 & 0 & \mu_3 \end{vmatrix} \left[\vec{\mathcal{E}} + \frac{1}{ne} \vec{J} \times \vec{H} \right] \tag{A-17}$$

where

$$\mu_i = \frac{e\tau_n}{m_0} \alpha_i$$

Similarly for the valence band

$$\vec{J}_p = Pe \begin{vmatrix} \nu_1 & 0 & 0 \\ 0 & \nu_1 & 0 \\ 0 & 0 & \nu_3 \end{vmatrix} \left[\vec{\mathcal{E}} + \frac{1}{Pe} \vec{J} \times \vec{H} \right] \tag{A-18}$$

where

$$\nu_i = \frac{e\tau_p}{m_0} \beta_i$$

Solving (A-17) for $\vec{\mathcal{E}}$ gives

$$ne \begin{vmatrix} \mu_1 \mathcal{E}_1 \\ \mu_2 \mathcal{E}_2 \\ \mu_2 \mathcal{E}_3 \end{vmatrix} = \begin{vmatrix} 1 & -\mu_1 H_3 & \mu_1 H_2 \\ \mu_2 H_3 & 1 & -\mu_2 H_1 \\ -\mu_3 H_2 & \mu_3 H_1 & 1 \end{vmatrix} \begin{vmatrix} J_1 \\ J_2 \\ J_3 \end{vmatrix} \tag{A-19}$$

where $\mathcal{E}_i$, H_i, and J_i are the components of $\vec{\mathcal{E}}$, $\vec{H}$, and $\vec{J}$ in the ith direction referred to the axis of a single conduction band edge ellipsoid. (A-19) may be solved for $\vec{J}$ assuming $H_1 = H_2 = 0$ since the field in the 3-direction is

the case of interest.

$$\begin{vmatrix} J_1 \\ J_2 \\ J_3 \end{vmatrix} = \underline{M}^{-1}\, ne \begin{vmatrix} \mu_1 \mathcal{E}_1 \\ \mu_2 \mathcal{E}_2 \\ \mu_3 \mathcal{E}_3 \end{vmatrix} \tag{A-20}$$

where

$$\underline{M} = \begin{vmatrix} 1 & -\mu_1 H_3 & 0 \\ \mu_2 H_3 & 1 & 0 \\ 0 & 0 & 1 \end{vmatrix}$$

and rewriting

$$\begin{vmatrix} J_1 \\ J_2 \\ J_3 \end{vmatrix} = en \begin{vmatrix} \mu_1 & \mu_1\mu_2 H_3 & 0 \\ -\mu_1\mu_2 H_3 & \mu_2 & 0 \\ 0 & 0 & \mu_3(1+\mu_1\mu_2 H_3^2) \end{vmatrix} \Bigg/ (1+\mu_1\mu_2 H_3^2) \begin{vmatrix} \mathcal{E}_1 \\ \mathcal{E}_2 \\ \mathcal{E}_3 \end{vmatrix} \tag{A-21}$$

We want to sum over the current contributions from each energy band edge ellipsoid. Taking the axes of one conduction band ellipsoid as a frame of reference, relating x , y, and z to 1, 2, 3 respectively, the current contributions of the valence band ellipsoid and the first conduction band ellipsoid are obtained directly.

$$\vec{J}_p = pe \begin{vmatrix} \nu_1 & \nu_1^2 H_2 & 0 \\ -\nu_1^2 H_2 & \nu_1 & 0 \\ 0 & 0 & \nu_3(1+\nu_1^2 H_2^2) \end{vmatrix} \Bigg/ (1+\nu_1^2 H_2^2)\ \vec{\mathcal{E}} \tag{A-22}$$

and

$$\vec{J}_1 = \frac{N}{3} e \begin{vmatrix} \mu_1 & \mu_1\mu_2 H_2 & 0 \\ -\mu_1\mu_2 H_2 & \mu_2 & 0 \\ 0 & 0 & \mu_3(1+\mu_1\mu_2 H_2^2) \end{vmatrix} \Bigg/ (1+\mu_1\mu_2 H_2^2)\ \vec{\mathcal{E}} \tag{A-23}$$

Writing (A-23) in the form

$$\vec{J}_1 = \frac{N}{3} e\, \underline{C}\, \vec{\mathcal{E}}$$

the current contributions of the other two conduction band ellipsoids are obtained by applying the similarity matrix $\underline{S}$ defined in equation (A-10)

$$\vec{J}_2 = \frac{N}{3} e\, \underline{S}\, \underline{C}\, \underline{S}^{-1}\, \vec{\mathcal{E}} \tag{A-24}$$

$$\vec{J}_3 = \frac{N}{3} e\, \underline{S}^{-1}\, \underline{C}\, \underline{S}\, \vec{\mathcal{E}} \tag{A-25}$$

Defining $\underline{s}' = \underline{S}\ \underline{C}\ \underline{S}^{-1}$

and $\underline{s}'' = \underline{S}^{-1}\ \underline{C}\ \underline{S}$

then

$$\underline{s} = \frac{\begin{vmatrix} (\mu_1 + 3\mu_2) & \pm\sqrt{3}(\mu_1 - \mu_2) + 4\mu_1\mu_2 H_z & 0 \\ \pm\sqrt{3}(\mu_1 - \mu_2) - 4\mu_1\mu_2 H_z & (3\mu_1 + \mu_2) & 0 \\ 0 & 0 & (1 + \mu_1\mu_2 H_z^2)\,4\mu_3 \end{vmatrix}}{4(1 + \mu_1\mu_2 H_z^2)}$$

where the upper sign refers to $\underline{s}'$ and the lower to $\underline{s}''$.

Adding the contributions to the total current from (A-22), (A-23), (A-24), (A-25) we obtain

$$\vec{J} = \{ Q_{ij} \} \vec{\mathcal{E}} \qquad \text{(A-26)}$$

where

$$Q_{11} = Q_{22} = Neg\left(\frac{\mu_1 + \mu_2}{2}\right) + Peh\nu_1$$

$$Q_{33} = Neg\mu_3(1 + \mu_1\mu_2 H_z^2) + Peh\nu_3(1 + \nu_1^2 H_z^2)$$

$$Q_{21} = -Q_{12} = Neg\mu_1\mu_2 H_z - Peh\nu_1^2 H_z$$

$$Q_{13} = Q_{31} = Q_{23} = Q_{32} = 0$$

and $g = (1 + \mu_1\mu_2 H_z^2)^{-1}$

$n = (1 + \nu_1^2 H_z^2)^{-1}$

e, ν_i, μ_i are absolute values.

To obtain an expression for the Hall coefficient, equation (A-26) must be solved for $\vec{\mathcal{E}}$

$$\vec{\mathcal{E}} = \{ Q_{ij} \}^{-1} \vec{J} = \{ T_{ij} \} \vec{J} \qquad \text{(A-27)}$$

Two cases are of interest here:

1) The value of Ey for a given Jx

2) The value of -Ex for a given Jy.

T 21 and T 12, therefore, need to be evaluated.

$$T21 = \frac{Q_{12}}{Q_{11}\,Q_{22} - Q_{12}\,Q_{21}} = -T_{12} \tag{A-28}$$

$$= \frac{H_z\left[Peh\nu_1^2 - Neg\mu_1\mu_2\right]}{\left[Neg\left(\frac{\mu_1+\mu_2}{2}\right)+Peh\nu_1\right]^2+\left[Peh\nu_1^2-Neg\mu_1\mu_2\right]^2 H_z^2} \tag{A-29}$$

In the limit of small fields

$$T_{21} = \frac{H_z\left[Pe\nu_1^2 - Ne\mu_1\mu_2\right]}{\left[Ne\left(\frac{\mu_1+\mu_2}{2}\right) + Pe\nu_1\right]^2} \tag{A-30}$$

For the case N = P, from equation (A-29)

$$T_{21} = \frac{-H_z}{Ne}\,\frac{\left[\nu_1^2 - \mu_1\mu_2\right]\left[1 + \mu_1\mu_2 H_z^2\right]}{\left[\nu_1 + \frac{\mu_1+\mu_2}{2}\right]^2 + \left[\mu_1\mu_2 + \nu_1\left(\frac{\mu_1+\mu_2}{2}\right)\right]^2 H_z^2} \tag{A-31}$$

From the definition of the Hall Coefficient R_H

$$R_H = \frac{\mathcal{E}_y}{J_x H_z} = \frac{-\mathcal{E}_x}{J_y H_z} = \frac{T_{21}}{H_z} = \frac{-T_{12}}{H_z}$$

indicating that the Hall coefficient is isotropic when the magnetic field is parallel to the trigonal axis.

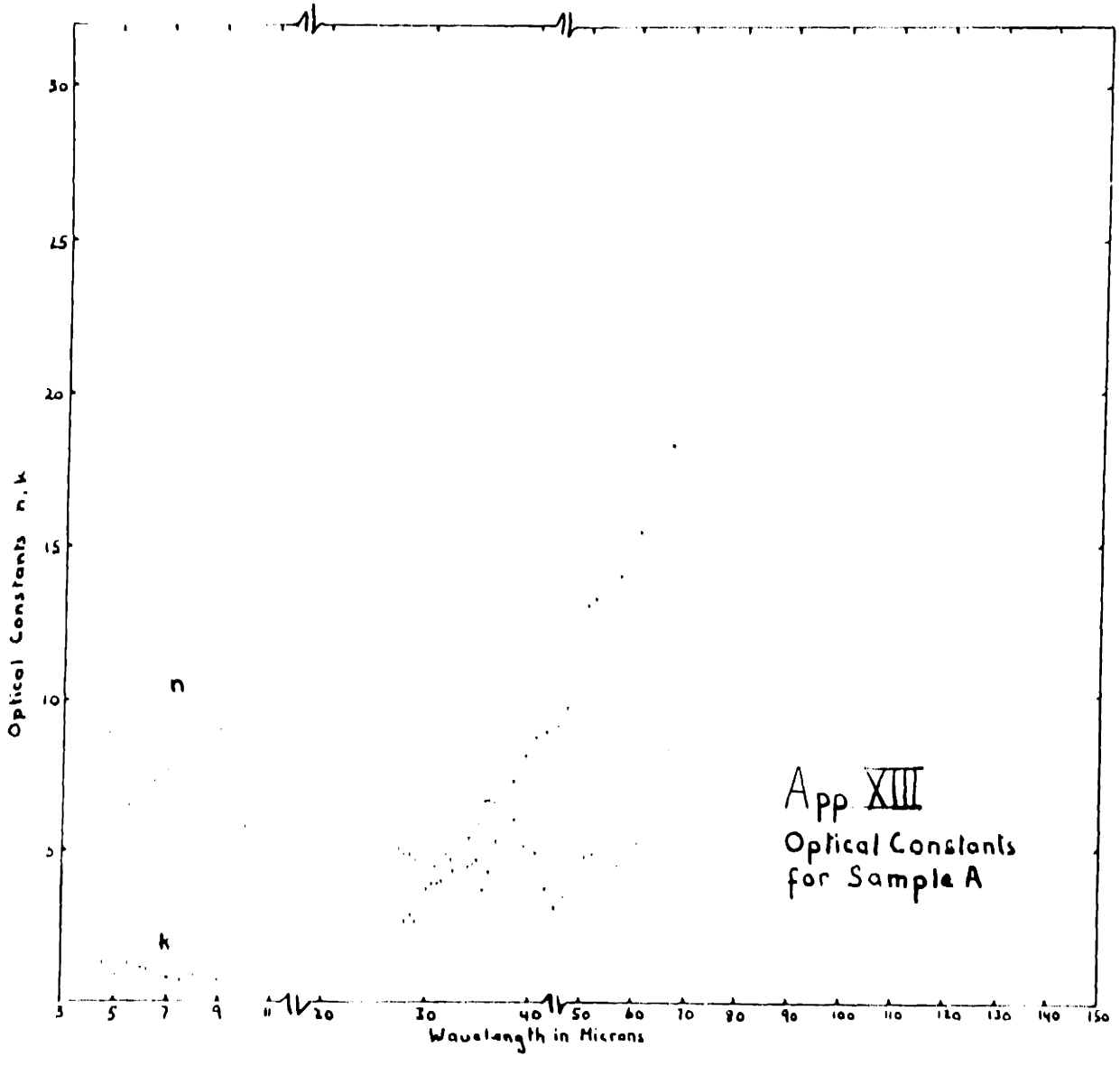

App. XIII
Optical Constants
for Sample A

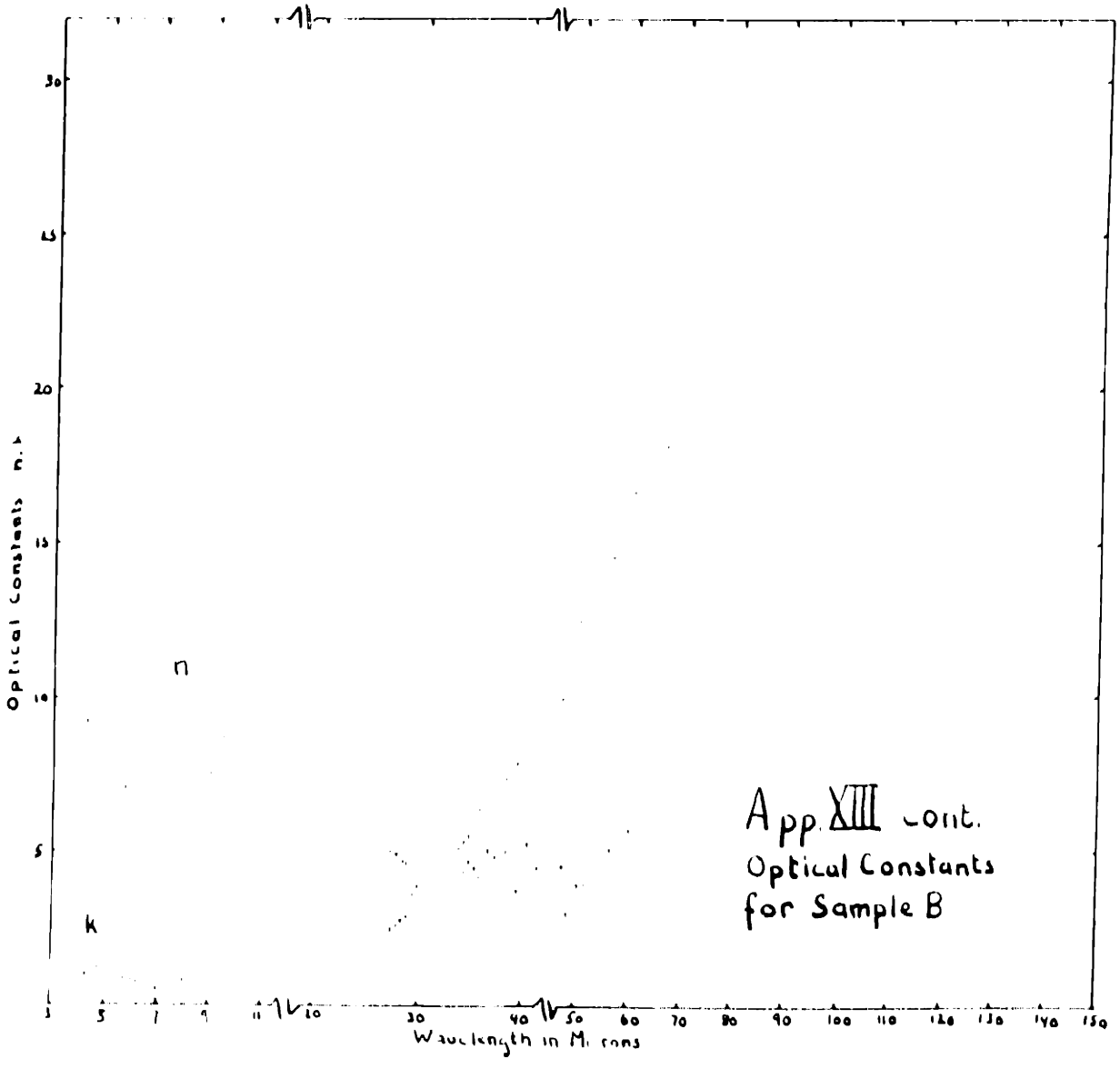

App. XIII cont.
Optical Constants
for Sample B

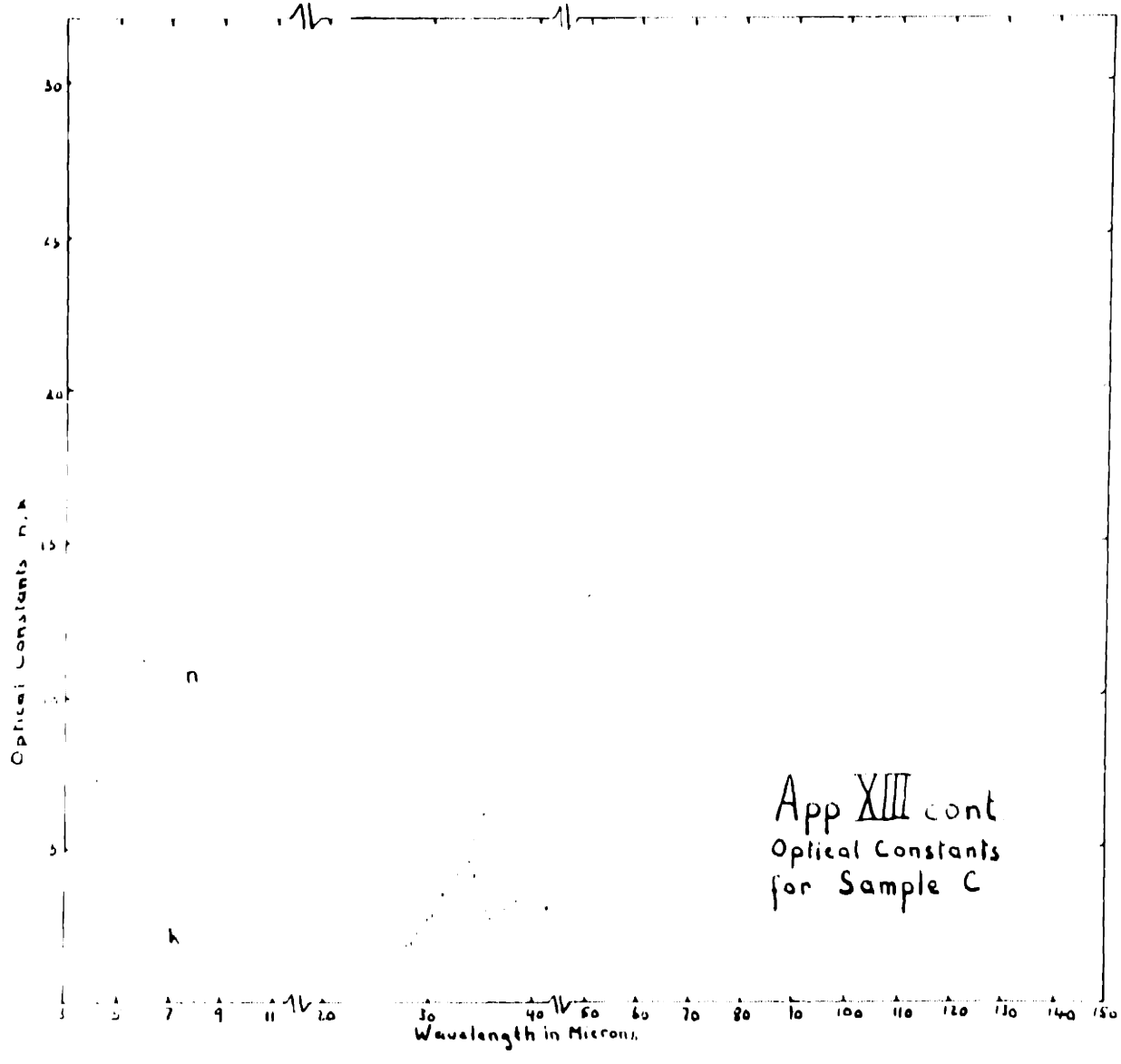
Optical Constants n, k
n
k
Wavelength in Microns
App XIII cont
Optical Constants
for Sample C

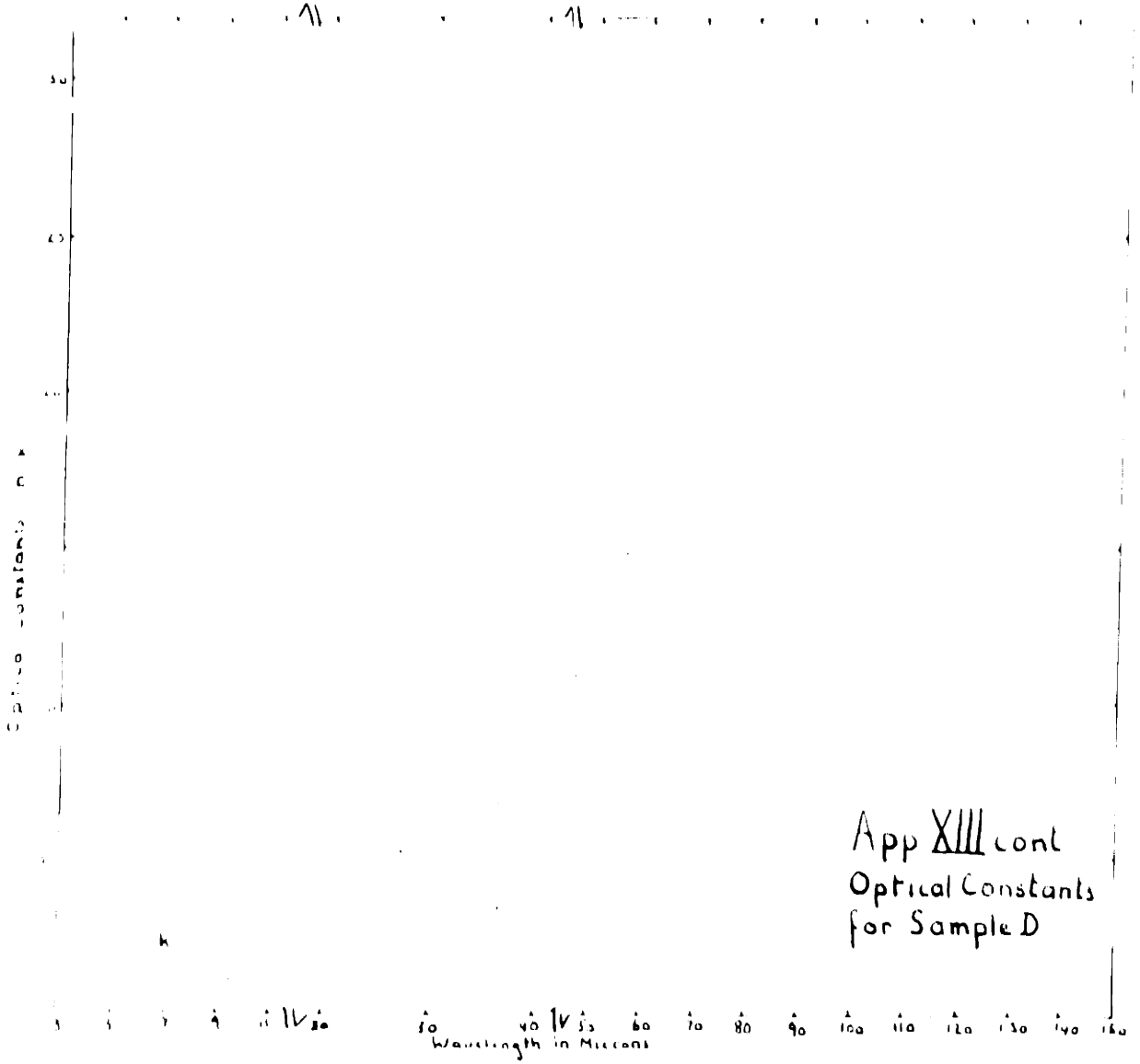

App XIII cont
Optical Constants
for Sample D

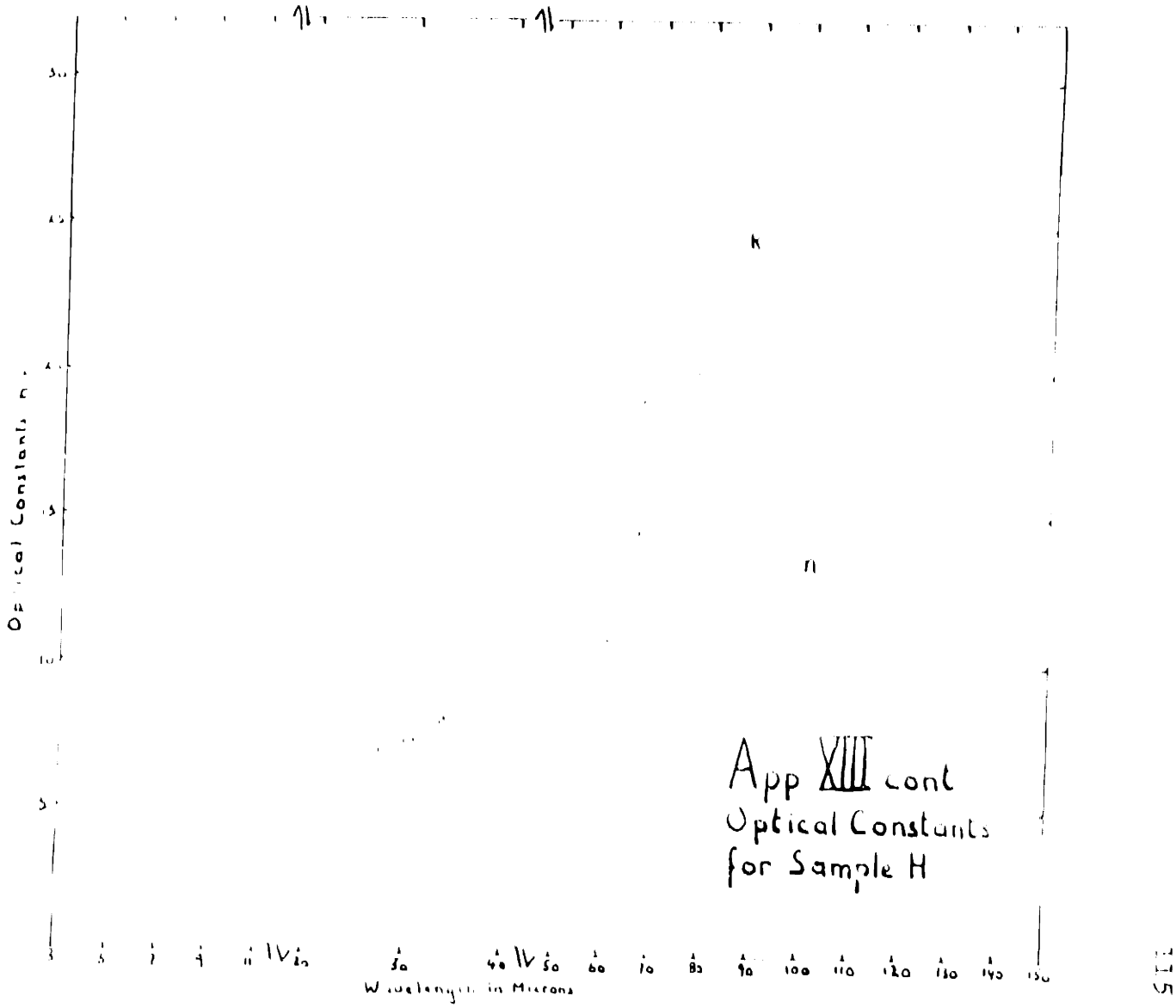

App XIII cont
Optical Constants
for Sample H

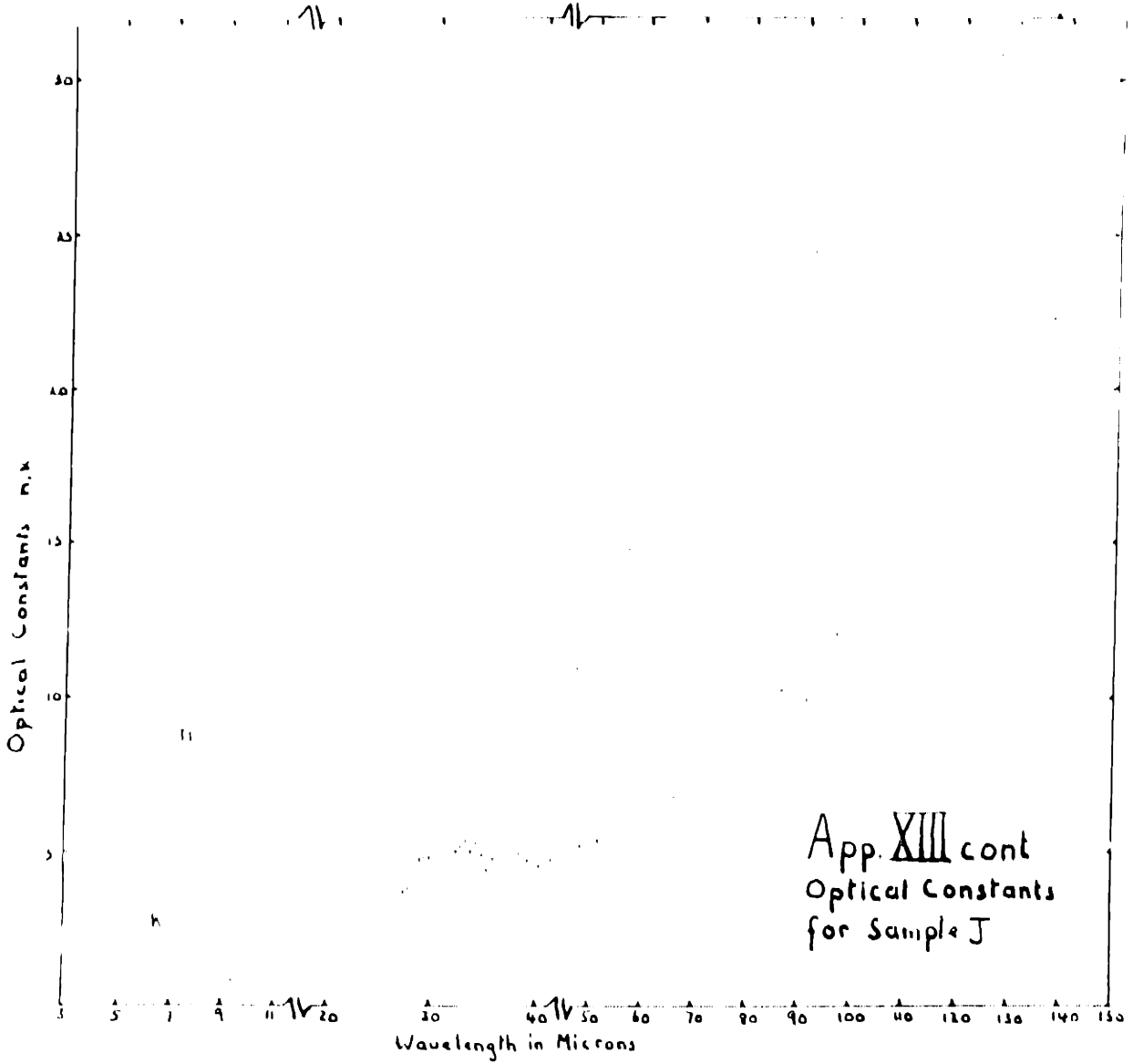

App. XIII cont
Optical Constants
for Sample J

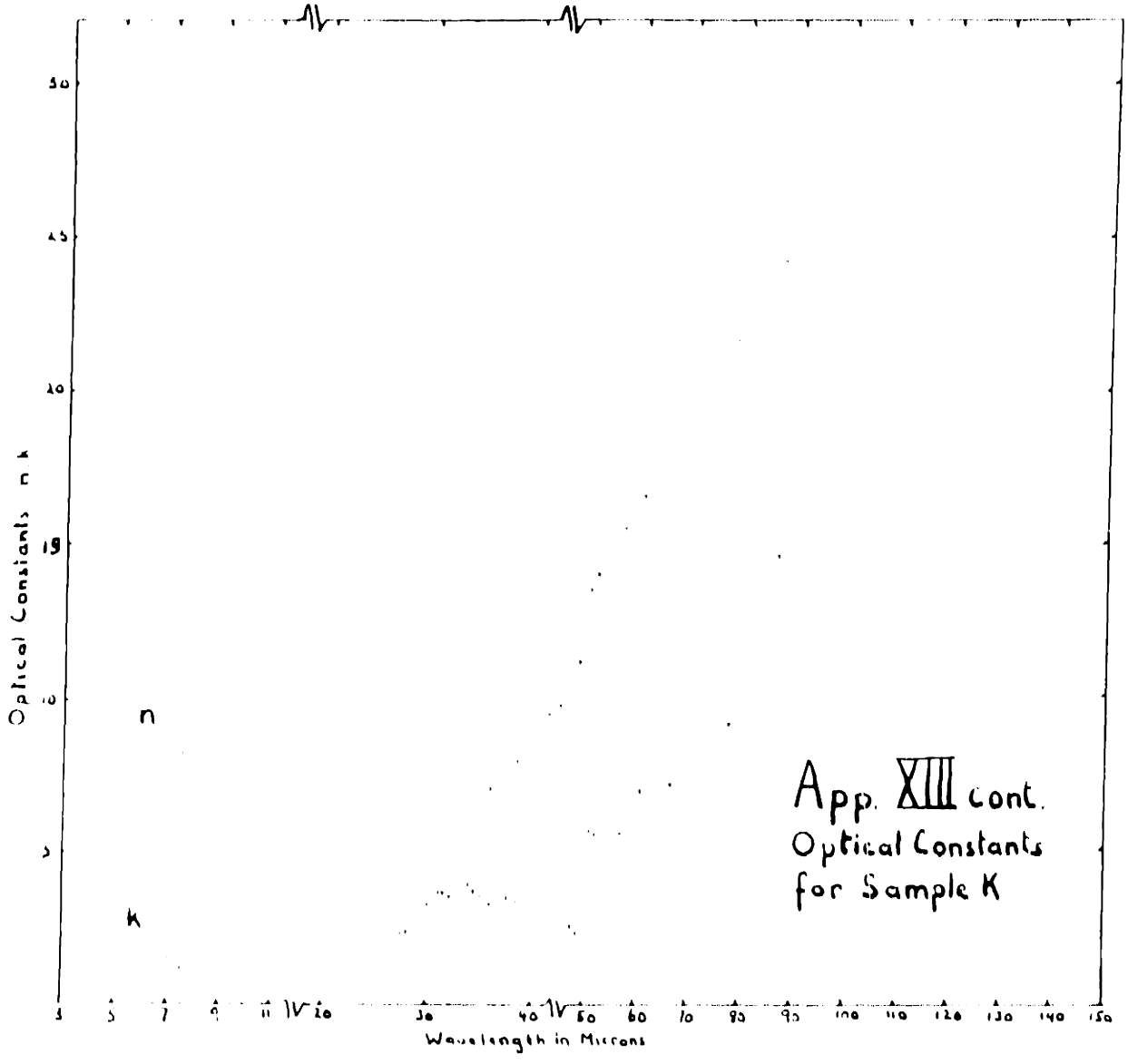

App. XIII cont.
Optical Constants
for Sample K

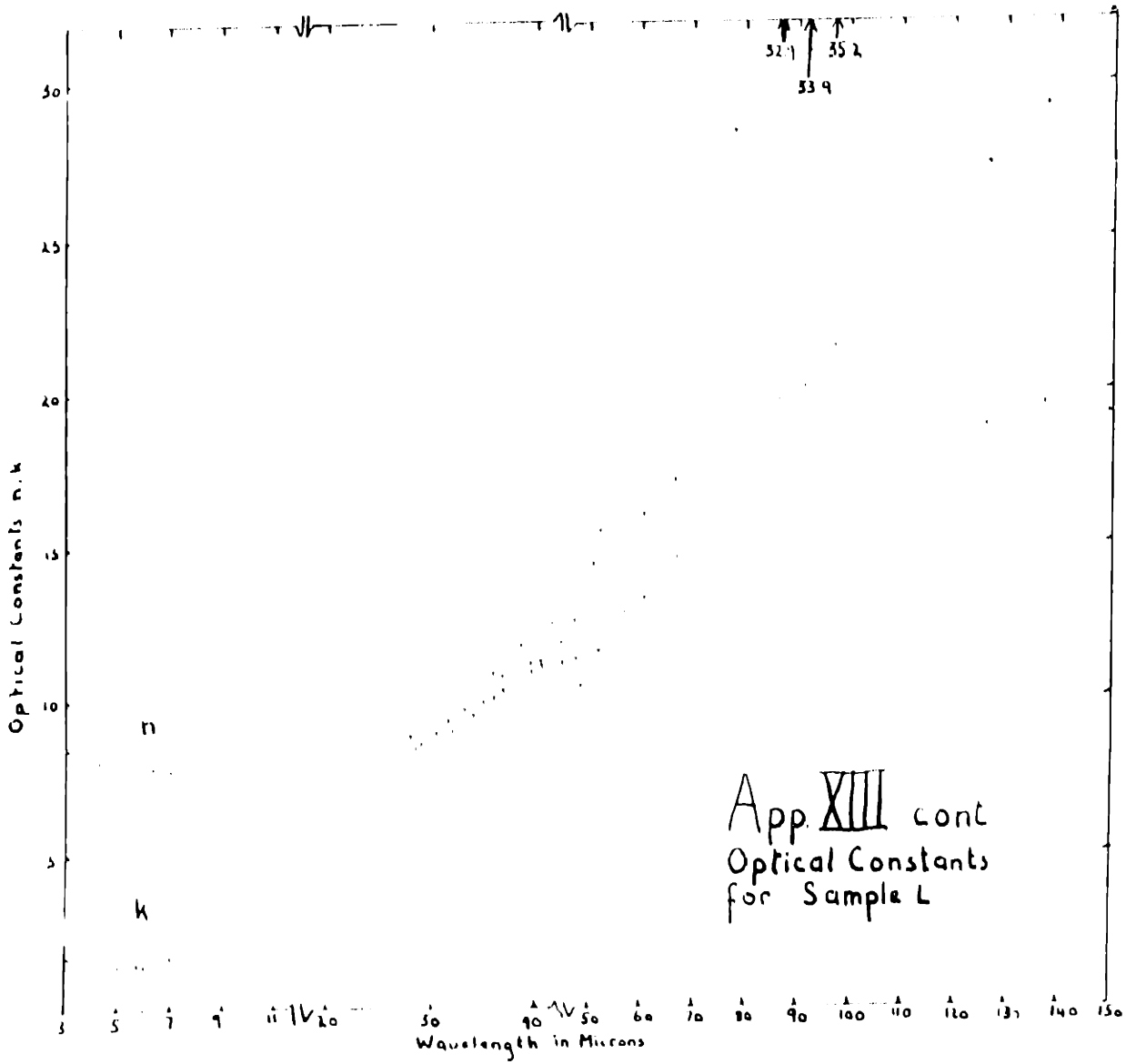

App. XIII cont
Optical Constants
for Sample L

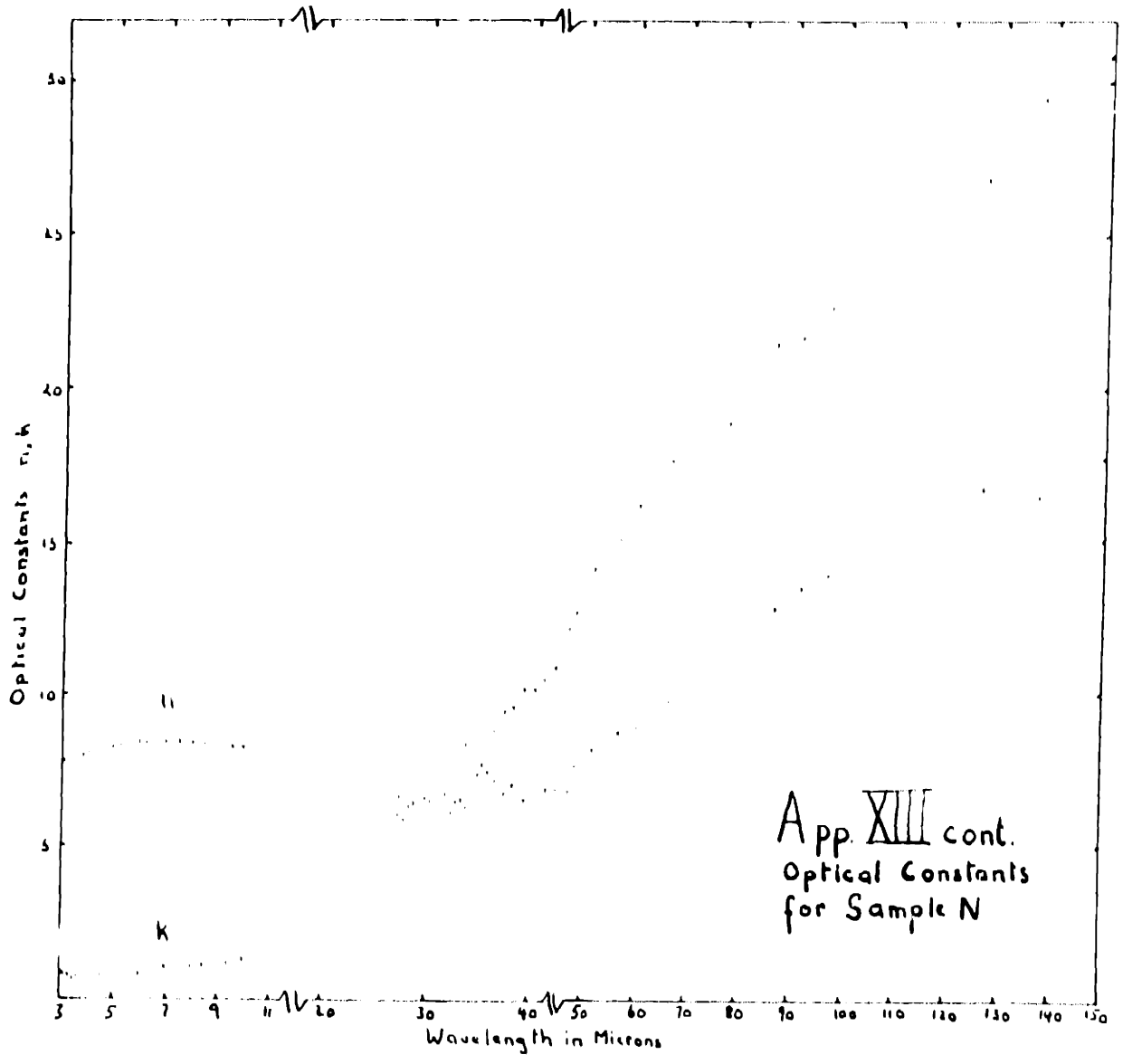
Optical Constants n, k
Wavelength in Microns
n
k
App. XIII cont.
Optical Constants
for Sample N

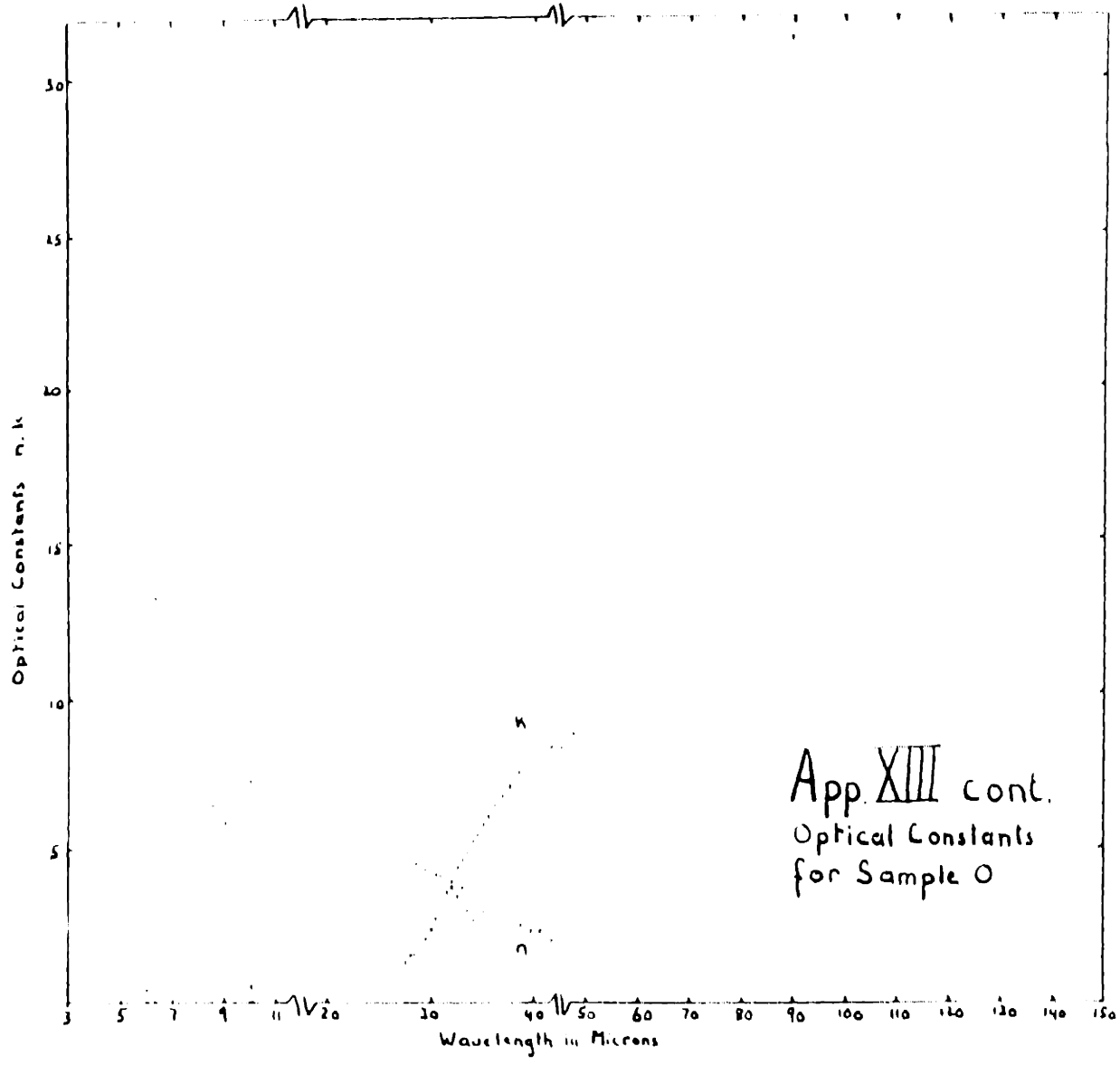

App. XIII cont.
Optical Constants
for Sample O

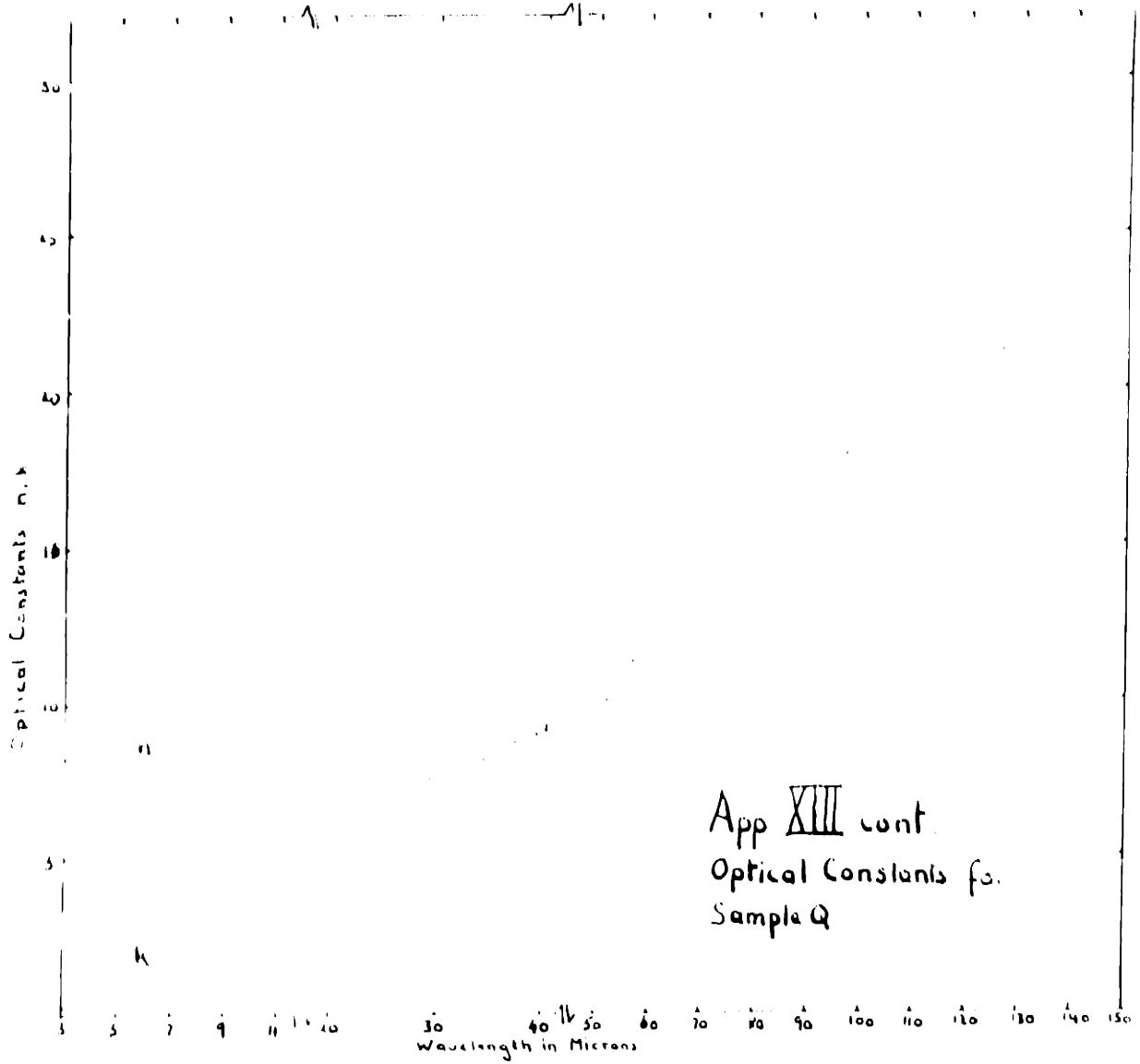

App XIII cont
Optical Constants for
Sample Q

APPENDIX XIV

Calculation - Sample A

The optical conductivity data from Figure VII plotted against the square of the frequency may be fitted with an expression of the form

$$\sigma_\omega = \frac{A}{1+Bx} \qquad \text{(A-32)}$$

where $A = N e \left(\frac{\mu_1+\mu_2}{2}\right)$, $B = 4\pi^2\tau_n^2$, x is the square of the frequency.

The two parameters A and B are varied until a good fit of the data is obtained. The curve given in Figure XII results from setting $A = 21 \times 10^4$ MKS, $B = 0.12 \times 10^{-24}$ sec^2. The points in Figure XII represent the experimental points.

Thus $\tau_n = 5.5 \times 10^{-14}$ sec

$Ne(\mu_1+\mu_2) = 42\times10^4$ $\qquad$ $Pe\nu_1 = \sigma_{dc} - A = 4.5\times10^4$

$R_0\sigma_{dc}^2 = Ne(\nu_1^2 - \mu_1\mu_2)$ $\qquad$ (Equation (26) in text)

With the substitution of $N = 2.2 \times 10^{24}$ per cubic meter

$e = 1.6 \times 10^{-19}$ coulombs

$$NeR_0\sigma_{dc}^2 = 8.13 \times 10^8 = (Ne)^2(\nu_1^2 - \mu_1\mu_2)$$

where R_0, σ dc are the experimental values.

Solving the 3 equations above one obtains

$N e \mu_1 = 41.7 \times 10^4$ MKS

$N e \mu_2 = 0.3 \times 10^4$ MKS

$\frac{\mu_1}{\mu_2} = \frac{\alpha_1}{\alpha_2} = 140$

$\frac{\mu_1+\mu_2}{2\nu_1} = 4.6$

Equations (A-32) may be rewritten in the form

$$\frac{1}{\sigma_\omega} = \frac{1}{A} + \frac{Bx}{A}$$

Appropriate plotting gives the data points in Figure XIII. Two equally good straight lines may be drawn to give

$$A = 19 \text{ or } 21 \times 10^4 \text{ MKS}$$

$$B = 0.11 \text{ or } 0.10 \times 10^{-24} \text{ sec}^2.$$

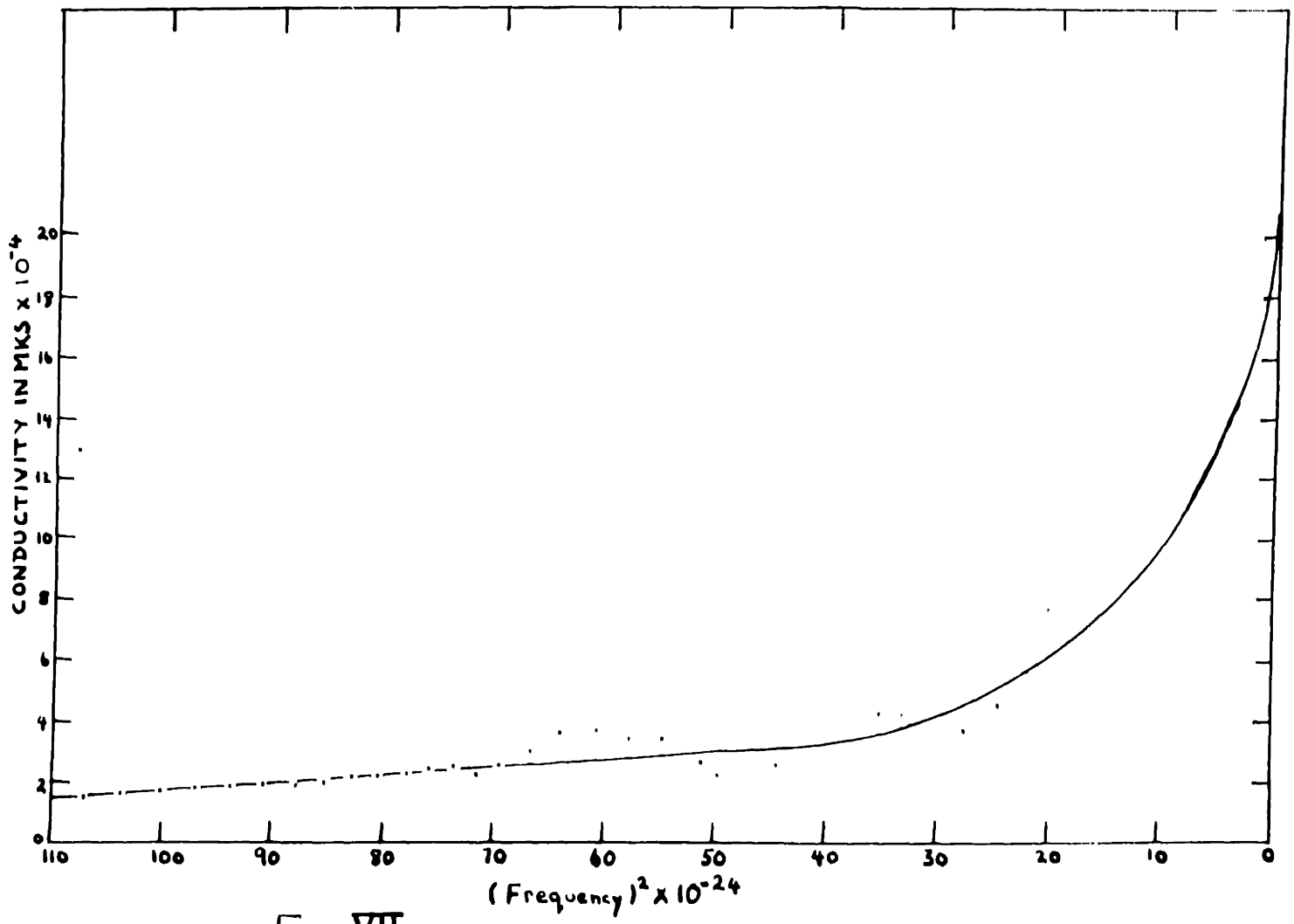

Fig XII Conductivity of Sample A as a function of Frequency

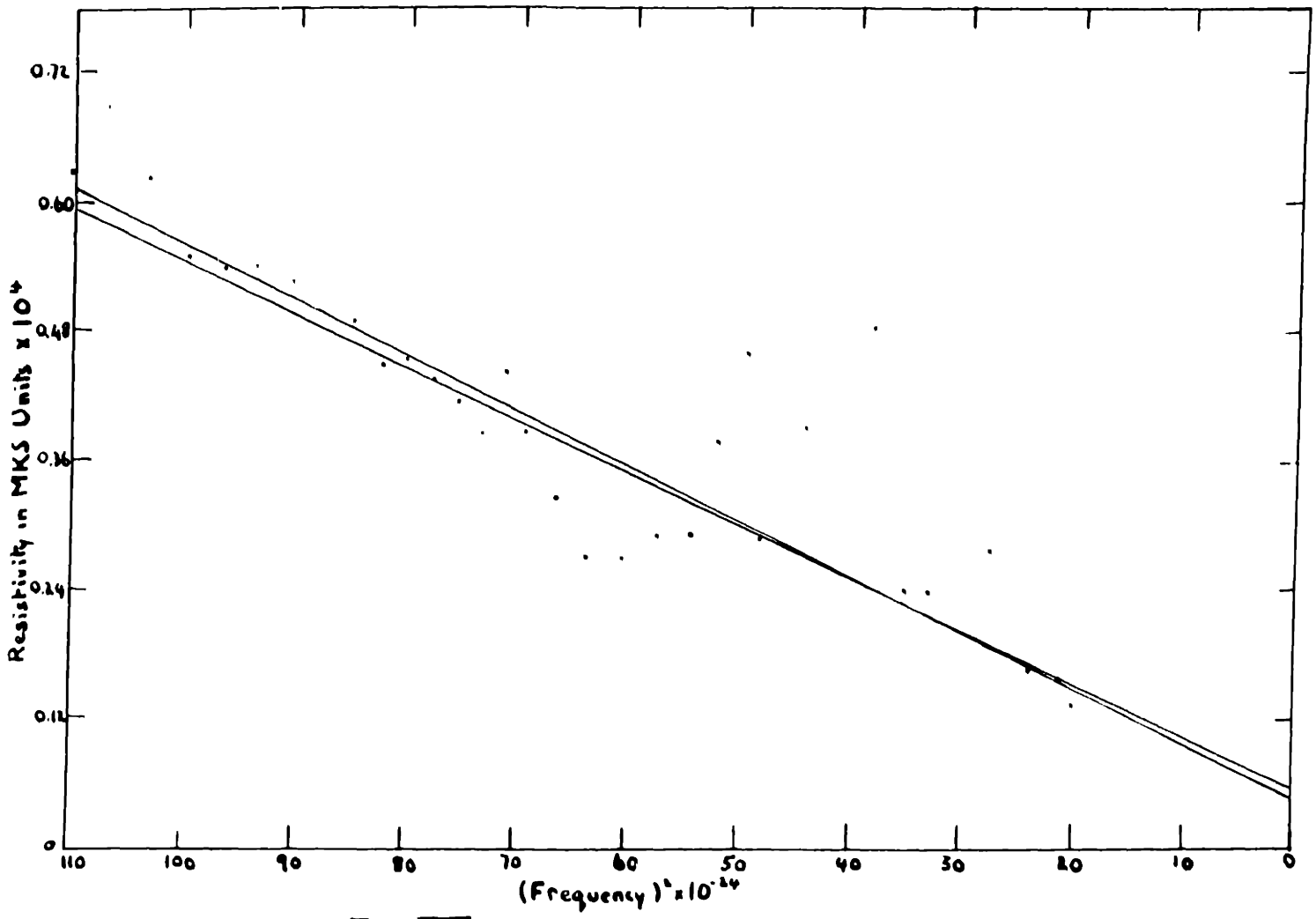

Fig. XIII Resistivity of Sample A as a Function of Frequency

APPENDIX XV.

Parameters Used in Figure VII c.

The solid curves in Figure VIIc are based on equation (28) with the following parameters

Sample	A MKS	B Sec^2
H	17 x 10^4	0.070 x 10^{-24}
L	12	0.034
N	14.3	0.046
Q	9.5	0.020

BIBLIOGRAPHY

1. H. Jones, Proc. Roy. Soc. (Lond.) A155, 653 (36); A147, 396 (34)
2. B. Abeles, S. Meiboom, Phys. Rev. 101, 544 (56)
3. T. Okada, J. Phys. Soc. Japan 12, 1327 (57)
4. H. Hasegawa, S. Nakano, N. Hashitsuma, J. Phys. Soc. Japan 12, 104(57)
5. A. L. Jain, Phys. Rev. 114, 1518 (59)
6. G. W. Kaye, Proc. Roy. Soc. (Lond.) A 170, 561 (39)
7. J. Babiskin, Phys. Rev. 107, 981 (57)
8. P. B. Alers, R. T. Webber, Phys. Rev. 84, 863 (51)
9. P. Kapitza, Proc. Roy. Soc. (Lond.) 119, 358 (28)
10. D. Shoenberg, Proc. Roy. Soc. (Lond.) A 170, 341 (39)
11. D. Shoenberg, "Low Temp. Phys. and Chem. - Proc. 5th Int. Conf. on Low Temp. Phys. and Chem." Ed. by J. R. Dillinger, Madison : Univ. of Wisc. Press, 1958 Page 450
12. M. Tinkham, Phys. Rev. 101, 902 (56)
13. J. K. Galt, W. A. Yager, et al. Phys. Rev. 100,748 (55)
14. B. Lax, K. J. Button, H. J. Zeiger, L. M. Roth, Phys. Rev. 102, 715 (56)
15. R. J. Keyes, S. Zwerdling, et al., Phys. Rev. 104, 1804 (56)
16. J. E. Aubrey, R. G. Chambers, J. Phys. Chem. Solids, 3, 128 (57)
17. A. D. Brailsford, J. K. Galt, Phys. Rev. 109, 1396 (58)
18. R. G. Chambers, "Low Temp. Phys. and Chem. - Proc. 5th Int. Conf. on Low Temp. Phys. and Chem." Ed. by J. R. Dillinger, Madison: Univ. of Wisc. Press, 1958, Page 470
19. V. Heine, Proc. Phys. Soc. (Lond.) A69, 513 (56)
20. M. Blackman, Proc. Roy. Soc. (Lond.) A166, 1 (38)
21. S. Mase, J. Phys. Soc. Japan 13, 434 (58)
22. N. F. Mott, H. Jones "The Theory of the Properties of Metals and Alloys." Oxford: Clarendon Press, 1936 Page 108

23. W. Woltersdorff, Z. Phys. 91, 231 (34)

24. R. A. Oetjen, et al., J. Opt. Soc. Am. 42, 559 (52)

25. R. C. Lord, T. K. McCubbin, J. Opt. Soc. Am. 47, 689 (57)

26. H. Yoshinaga, et al., J. Opt. Soc. Am. 48, 315 (58)

27. A. L. Loeb, H. Denman, J. Soc. Inst. Appl. Math. 3, 1 (55)

28. W. F. Leverton, A. J. Dekker, Phys. Rev. 81, 156 (51)

29. A. Colombani, P. Huet, "Structure and Properties of Thin Films" Ed. by C. A. Neugebauer, J. B. Newkirk, D. A. Vermilyea, N.Y.; John Wiley and Sons, Inc., 1959 Page 253

30. L. Harris, J. Opt. Soc. Am. 45, 27 (55)

31. G. Hass, H. Kehler, Kolloid Zeits 95, 26 (41)

32. G. Hass, Z. anorg. Chem. 254, 96 (47)

33. H. König, G. Helwig, Optik 6, 111 (50)

34. R. W. G Wyckoff, "Crystal Structures" N.Y.: Interscience Publishers, Inc., 1951 Ch II page 16.

35. E. I. Salkovitz, J. Metals (A.I.M.E. Trans.) 206, 176 (56)

36. D. Hubbard, Anal. Chem. 20, 363 (48)

37. W. Shockley, "Electrons and Holes in Semiconductors," N.Y.: D. Van Nostrand and Co., Inc., 1950 Page 205

38. I. Isenberg, et al., Rev. Sci. Inst. 19, 085 (48)

39. F. Seitz, "Modern Theory of Solids," N.Y.: McGraw-Hill Book Co.,Inc. 1940 Page 183

40. D. Metzger, "Process Control for Thin Film Deposition." M. S. Thesis, Dept. of El. Eng. M.I.T., August 1958.

41. A. L. Loeb, Private Communication

42. O. Lindberg, Proc. I.R.E. 40, 1414 (52)

43. W. Benedict, et al., J. Res. N.B.S. 49, 91 (52)

44. H. M. Randall, et al., Phys. Rev. 52, 160 (37)

45. P. Fowler, M. S. Thesis, Dept. of Phys. M.I.T. January 1960

46. L. Harris, J. K. Beasley, A. L. Loeb, J. Opt. Soc. Am. 41, 604(51)

47. O. S. Heavens, "Optical Properties of Thin Solid Films." London: Butterworths Scientific Publications, 1955, Chap. 4.

48. W. K. H. Panofsky, M. Phillips, "Classical Electricity and Magnetism" Reading: Addison-Wesley Publ. Co. Inc., 1955, Chap II.

49. L. Harris, A. L. Loeb, J. Opt. Soc. Am. 45, 179 (55)

50. J. C. Slater, N. H. Frank, "Electromagnetism," N.Y.: McGraw-Hill Book Co. Inc., 1947 Page 112.

51. F. Gross, Z. Phys. 64, 520 (30)

52. A. N. Gerritsen, W. J. DeHaas, Physica 7, 602 (40)

53. G. T. Rado, et al., Phys. Rev. 88, 909 (52)

54. L. Harris, A. L. Loeb, J. Opt. Soc. Am. 43, 1114 (53)

55. J. C. Clater, "Quantum Theory of Matter." N.Y.: McGraw-Hill Book Co., Inc. 1951 Page 352

56. G. E. H. Reuter, E. H. Sondheimer, Proc. Roy. Soc. (Lond.) A195, 336 (48)

57. R. B. Dingle, Physica 19, 311 (53)

58. A. B. Pippard, R. G. Chambers, Proc. Phys. Soc. (Lond.) 65, 955 (52)

59. E. Justi, M. Kohler, G. Lautz, Z. Naturforsch 6a 456 and 544 (51)

60. A. Eucken, F. Förster, Nachr. Ge. Wiss., Göttingen 1, 43 (34)

61. G. E. Smith, Phys. Rev. 115, 1561 (59)

62. A. B. Pippard, Proc. Roy. Soc. (Lond.) A 224, 273 (54)

63. C. T. Lane, Phys. Rev. 48 193 (35)

64. W. Büssem, F. Gross, K. Herrman, Z. f. Phys. 64, 537 (39)

65. V. I. Kaidanov, A. R. Regel' Zh. tech. Fiz. 28, 402 (58)

66. C. E. Drumheller, "1957 Vacuum Symp, Trans.", N.Y.: Perganon Press, 1957 Page 27

67. W. Buckel, "Low Temp. Phys. and Chem. - Proc. 5th Int. Conf. on Low Temp. Phys. and Chem." Ed. by J. R. Dillinger, Madison: Univ. of Wisconsin Press, 1958 Page 326.

68. W. Buckel, "Structure and Properties of Thin Films." Ed. by C. A. Neugebaue J.B.Newkirk, D. A. Vermilyea, N.Y.: John Wiley and Sons, Inc., 1959 Page 26

69. B. Lax, Rev. Mod. Phys. 30, 122 (58)

70. A. H. Kahn, H. P. R. Frederikse "Oscillatory Behavior of Magnetic Susceptibility and Electronic Conductivity," Solid State Physics Vol. 9, Ed. by F. Seitz, D. Turnbull, N.Y.: Acad. Press, 1959.

71. J. C. Slater "Quantum Theory of Matter," N.Y.: McGraw-Hill Book Co.,Inc. 1951, Page 339

72. C. Herring, Bell Tel. Syst. Journ., 34, 237 (55)

73. W. Shockley, "Electrons and Holes in Semiconductors," N.Y.: D. Van Nostrand Co., Inc., 1950 Chap. 11.

74. J. Volger, Phys. Rev. 79, 1023 (50)

75. E. R. Washwell, Private Communication

76. L. Harris, J. Opt. Soc. Am. 36, 597 (46)

77. M. M. Markov, I. S. Lindstrem, Optics and Spectroscopy 7, 228 (59)

78. J. N. Hodgson, Proc. Phys. Soc. (Lond.) B67, 269 (54)

79. L. G. Schulz, J. Opt. Soc. Am. 43, 406 (53)

80. J. K. Galt, et al., Phys. Rev. 114, 1396 (59)

81. A. L. Jain, Phys. Rev. 114, 1518 (59)

82. I. N. Kalinkina, P. G. Strehov, J. E. T. P. 7, 426 (58)

83. R. B. Dingle, Physica 19, 348 (53)

84. W. Shockley, "Electrons and Holes in Semiconductors," N.Y.: D. Van Nostrand Co., Inc. 1950 Page 31

85. E. H. Sondheimer, Phys. Rev. 80, 401 (50)

86. R. B. Dingle, Physica 18, 985 (52)

87. R. A. Oetjen, H. Yoshinaga, Phys. Rev. 101, 526 (56)

88. L. Genzel, H. Happ, R. Weber, Zeit, Phys. 154, 1 (59)

89. E. H. Sondheimer, Proc. Phys. Soc. (Lond.) A65, 561 (52)

90. A. H. Wilson, "The Theory of Metals," Cambridge: Univ. Press, 1953, Page 196.

BIOGRAPHICAL NOTE

The author was born in London, England in November 1934.

After attending the Bedford Modern School and Alleyn's School, Dulwich, England, the author immigrated to the United States in 1950.

Two years were spent in attendance at Wm. Hall High School, West Hartford, before the author entered Trinity College, Hartford, Connecticut.

The author received the degree of Bachelor of Science in Chemistry from Trinity College in 1956 and is at present a candidate for the degree of Doctor of Philosophy in Physical Chemistry at the Massachusetts Institute of Technology.